Title
Elucidating the mechanisms and dynamics of olfactory memory formation in Caenorhabditis elegans

Author
Benedetti, Kelli Leilani

Publication Date
2019

Peer reviewed|Thesis/dissertation

Elucidating the mechanisms and dynamics of olfactory memory formation in Caenorhabditis elegans

by
Kelli Leilani Benedetti

DISSERTATION
Submitted in partial satisfaction of the requirements for degree of
DOCTOR OF PHILOSOPHY

in

Genetics

in the

GRADUATE DIVISION
of the
UNIVERSITY OF CALIFORNIA, SAN FRANCISCO

Approved:

DocuSigned by:
Noelle L'Etoile
54CC7336DCB447E...

Noelle L'Etoile
Chair

DocuSigned by:
Aimee Kao
D6C4[illegible]494...

Aimee Kao

DocuSigned by:
Barbara Panning
D6C4[illegible]4B7...

Barbara Panning

DocuSigned by:
Lily Jan
394456D87457494...

Lily Jan

Committee Members

DEDICATIONS

I dedicate this thesis to my family for their love and support, especially my mom and Will, who are my biggest fans.

ACKNOWLEDGEMENTS

I would like to thank my principal investigator/mentor Dr. Noelle L'Etoile for always trusting me and for giving me the confidence necessary to succeed in the sciences. She has always encouraged me to ask questions and has helped me feel confident enough to ask even what I considered to be dumb questions. She inspires everyone with any type of scientific question to jump in headfirst and try to answer them with rigor. Noelle always helped me with writing and we would often write alongside each other as colleagues, feeding off of each others' ideas, whether it was for grant proposals or scientific manuscripts. She always treats her students as her equal and has us work with her to tackle projects. If you need help, she is always there to even work on a wet lab project with you, even if it is something in which she has no expertise, if just to learn for herself or for moral support. She is quite a unique mentor, and I am grateful for having her as supervisor for my PhD work.

Next, I would like to give my gratitude to my undergraduate/Master's advisor, Dr. Miri VanHoven. I joined her lab during my senior year of undergraduate work and would never have done a PhD if it wasn't for her. Not only did she encourage me to pursue a PhD, but she helped give me the knowledge, lab experience, and presentation skills necessary to succeed. She taught me how to think like a scientist, to perform experiments, to stay organized, to write abstracts, to make manuscript figures, to put together a presentation, to present well during meetings and conferences, and to manage others. She inspired my love for genetics, and I am so grateful for her.

I want to thank my thesis committee members, which includes Dr. Barbara Panning, Dr. Aimee Kao, and Dr. Lily Jan. They took their time out to help me sculpt a

thesis project, whether it was my original or new one, suggested experiments that would help me answer my questions, and they gave me advice on what to do for my future.

I want to express gratitude to the L'Etoile lab, past and present, for all of their help in support of the lab and to me specifically. Katie Mellman orders everything for us and makes sure we are all fully supported in our experiments, Bo Zhang keeps the lab running equipment- and safety approval-wise, Sarah Nordquist helps with daunting experiments to spread out the workload and gives emotional support, even when I was close to combustion, Ray helps with fancy experimental setups and with boosting morale, Veronica Valdez makes all of the reagents to keep our lab running, Nando Muñoz-Lobato started a great project that became my thesis project, but was also such a positive spirit and friend to all, and AJ Ablaza and Mary Futey helped keep the lab operating at a high level. All of their hard work helped the lab run at the best level it could, and are a large reason for why I was able to be successful in the lab.

Lastly, I want to give an immense thanks to my family and friends. My mom, Jessie, taught me to read, helped me with algebra, even after getting home at 11PM from work, and was my biggest cheerleader. My dad, Steven, who served as my therapist, always asking me how things in my life were going, and being there to listen and give advice. My sister, Kristin, for her moral support and for helping me plan a wedding while I was busy writing up a manuscript. My niece, Kaia, for making me want to live up to how great she thinks her Hachi is. My partner, William, for being there for me since literally day one of my lab training, and never leaving my side since. My Auntie Polly and Uncle Tom, who always listened to what I had to say, even as a child, encouraged me to pursue higher education, and remain fans of my career trajectory. To

Evonne, who I met in Biology class freshman year of high school, then went to the same college and majored with me in Biological Sciences, both at the Bachelor's and Master's level. Not only did we work as lab partners who can read each others' minds from high school through our Master's, but who has helped me every time I needed to get my mind off of the sciences for a little while. I cannot thank any of these individuals enough for their support in my life and my studies, but I hope that this is a sufficient start.

CONTRIBUTIONS

Chapter Two of this thesis has been submitted for publication and is in review at the journal Cell (Elsevier) at the time of this thesis submission:

The text of this thesis chapter is reproduced from the material of the following citation: Muñoz-Lobato, F., Benedetti, K.L., Farah, F., Nordquist, S.K., Bokka, A., Brueggemann, C., Li, J., Chang, E., Varshney, A., Andersen, K., Dunn, R.L., Tsujimoto, B., Tran, A., Duong, A., Churgin, M.A., Fang-Yen, C., Kato, S., VanHoven, M.K., and L'Etoile, N.D. (2019). Sleep is required to remodel specific synapses for memory consolidation. Manuscript submitted for publication.

I am a co-first author along with Muñoz-Lobato, F. I designed and conceived the experiments along with Muñoz-Lobato, F., L'Etoile N.D., and VanHoven, M.K. I performed experiments in all of the figures except for Figures 2.5, 2.7, 2.S3, 2.S6, and 2.S7, did the statistical analysis for everything except for Figures 2.7, 2.S3, and 2.S7, and wrote the paper along with L'Etoile N.D. and VanHoven, M.K., with help from Muñoz-Lobato, F. and Nordquist, S.K. The senior author L'Etoile N.D. was my mentor and advised on the whole project.

Chapter Three of this thesis will be submitted for publication at the time of this thesis submission.

The text of this thesis chapter is reproduced from the material of the following citation: Benedetti, K.L., Chen, A., Kaye, J.A., and L'Etoile, N.D. (2019). The TRPV channel

OSM-9 mediates olfactory long-term memory consolidation independent of sleep. Manuscript in preparation.

I am the first author of this paper and designed and performed all of the experiments, with help from Chen A. in producing data for Figure 3.5. Kaye J.A. made a construct used in Figure 3.S4. I wrote the manuscript with advice from L'Etoile, N.D. The senior author L'Etoile N.D. was my mentor and advised on the whole project.

Chapter Four of this thesis has been published in the journal Human Molecular Genetics (Oxford Academic):

The text of this thesis chapter is a reprint of the material as it appears in:

Juang B.T., Ludwig A.L., Benedetti K.L., Gu C., Collins K., Morales C., Asundi A., Wittmann T., L'Etoile N., Hagerman P.J. (2014). Expression of an expanded CGG-repeat RNA in a single pair of primary sensory neurons impairs olfactory adaptation in Caenorhabditis elegans. Hum Mol Genet. *23*, 4945-4959.

I am a co-second author along with Ludwig A.L. I performed the reviewer requested experiments and analysis in Figures 4.4 and 4.S2 and wrote the manuscript along with Juang B.T., L'Etoile N., and Hagerman PJ. The senior author L'Etoile N. was my mentor and advised on the whole project.

ABSTRACT

Elucidating the mechanisms and dynamics of olfactory memory formation in *Caenorhabditis elegans*

By Kelli Leilani Benedetti

Learning and memory are essential for survival—organisms must respond to their environment and update their knowledge accordingly. Memories undergo multiple stages before being stored long term: acquisition, consolidation, and maintenance. Various factors contribute to long-term memory formation, including sleep, synaptic plasticity, and molecular mechanisms. Sleep is thought to drive memory consolidation by promoting synaptic plasticity. However, the exact molecular, cellular, and synaptic mechanisms occurring during sleep to drive memory maintenance are not well known. To achieve single-cell and synaptic resolution of memory in a genetically-amenable organism, I utilized *C. elegans* and an odor spaced-training long-term memory paradigm. I show that sleep post training is required to consolidate the odor memory. I found that one specific interneuron (AIY) is required for long-term odor memory maintenance, and that synapses between that interneuron and one olfactory sensory neuron (AWC) are decreased after the long-term memory is formed, only in animals that slept. In addition, I found that the human transient receptor potential vanilloid (TRPV) channel *osm-9,* an ortholog of human TRPV5 and TRPV6, is required specifically for memory consolidation in order to establish this long-term olfactory memory, independent of sleep. Understanding the mechanisms underlying how learning and memory are mediated is important to understand how organisms learn from their environment to ensure survival, as well as what happens when these processes go

awry, such as in the disease context. Expanded CGG repeat RNAs from the fragile X mental retardation 1 (*FMR1*) gene are present in the brain of patients with fragile X and fragile-X tremor/ataxia syndrome (FXTAS). We show that when human *FMR1* with these expanded RNA repeats is expressed in *C. elegans* olfactory sensory neurons, that it blocks short-term odor memory. Behavioral plasticity perturbations are also observed in FXTAS patients, such as altered prepulse inhibition. We find that this aberrant plasticity requires the miRNA-Argonaute pathway. Thus, these studies may help to understand the molecular and cellular mechanisms and dynamics of how neural plasticity drives learning and memory, and what happens molecularly in diseases that limit plasticity.

TABLE OF CONTENTS

LIST OF FIGURES

Chapter Two:

Chapter Three:

Chapter Four:

LIST OF TABLES

Chapter Four:

CHAPTER ONE: INTRODUCTION

Animals must learn from their environment and keep or update their knowledge accordingly to ensure survival. These memories must be converted from short- to long-term memory through memory consolidation. Decades of studies in *Drosophila, C. elegans, Aplysia,* and mammals have elucidated various requirements for long-term memory formation, such as synaptic plasticity (e.g. synaptic strengthening), sleep, and specific molecular pathways (Kandel et al., 2014). There are two types of synaptic plasticity thought to drive memory consolidation: Hebbian and non-Hebbian (Fox and Stryker, 2014). Hebbian plasticity involves neurons firing together to elicit long-term potentiation (LTP) and firing asynchronously to promote long-term depression (LTD) of synapses. Non-Hebbian plasticity includes homeostatic compensation, such as synaptic scaling, to return neurons to their baseline firing rate after LTP or LTD to reach homeostasis (Turrigiano et al., 1998; Fox and Stryker, 2014). These two types of plasticity have been proposed to work together to drive memory formation, especially in the context of sleep. The synaptic homeostasis (SHY) hypothesis states that sleep is required to allow the brain to reset and allow for the proper synaptic plasticity necessary to reach homeostasis, which may drive long-term memory (Tononi and Cirelli, 2014). Various molecular components for memory have also been well studied, including the cAMP pathway, with emphasis on cAMP response element-binding protein (CREB, Kandel, 2012). With all of this knowledge obtained, we still do not know the exact molecular, cellular, and synaptic resolution of long-term memory and how it is affected by sleep. The *C. elegans* nematode provides a great model to ask these questions to help elucidate long-term memory formation.

C. elegans is an ideal organism to study long-term memory with single circuit and cell resolution because it is the only organism with its entire functional connectome mapped out (White et al., 1986; Cook et al., 2019). There are 302 neurons connected by 7000 synapses and each neuron in the animal has a known function and can be probed with specific promoters. Its optical transparency allows for live imaging of the animal as it behaves, allowing visualization of neural activity occurring in real time. Although *C. elegans* has relatively few neurons, it is able to exhibit short- and long-term memory, including aversive and associative classical conditioning (Colbert and Bargmann, 1995; Kaufmann et al., 2010).

Using this model, we attempted to understand single-cell requirements for long-term memory. Studies in mammals, birds, and insects have elucidated specific requirements for whole brain regions or whole populations of cells for memory acquisition, maintenance and recall (Bushey et al., 2011; Ryan et al., 2015; Cowansage et al., 2015; deVivo et al., 2017; Abdou et al., 2018; Yonelinas et al., 2019). We aimed to study a compact circuit, specifically, the AWC olfactory circuit (White et al., 1986; Cho et al., 2016; Gordus et al., 2015), where every neuron has well-characterized connections and functions, to uncover the exact mechanisms of long-term memory at single-cell resolution, in live animals as a memory is being formed.

In the studies presented in this thesis, the animals are subjected to either a short-term or long-term memory paradigm. For short-term memory, the animals are classically conditioned to an attractive, food-related odor in the presence of starvation for one 80-minute cycle of training (Colbert and Bargmann, 1995). The long-term memory studies involve spaced training of the short-term paradigm where the animals are subjected to

three cycles of odor training with recovery on food in between. In Chapter Two of this thesis, I present the findings that odor spaced-training can induce long-lasting aversive olfactory memory that undergoes a fragility period before being consolidated and thus stably maintained. This finding aligns with previous research in other systems showing that long-term memory requires a consolidation period where the memory is lost before it is stored (Dudai, 1996; Dudai, 2004). I show that sleep directly after spaced training is required for this long-term memory. Although sleep has been a known requirement for long-term memory, this is the first evidence of *C. elegans* sleeping after spaced-training to promote memory formation. I provide evidence that this paradigm may not rely heavily on CREB function, which is interesting since CREB is so widely accepted as a molecular driver of long-term memory. Lastly, I show that a single interneuron, AIY, is required for this memory, and that synapses between AIY and the AWC olfactory sensory neuron are selectively decreased in animals that kept the long-term memory and slept right after training. Although global synaptic downscaling has been reported for animals that undergo long-term memory formation after sleeping, I show that synapses between AWC and AIY decrease, but synapses between other neurons are not affected. I also present the synaptic dynamics in animals that slept versus animals that were prevented from sleeping. I show that during the memory fragility period, synapses decrease in both odor- and buffer-trained animals that slept, but that odor-trained animals still have this decrease in synapses in animals that maintained the long-term memory, but that the synapses in the buffer-trained animals are not altered. We hypothesize that sleep and odor spaced-training mark the AWC-AIY synapses for reduction during the memory fragility period, and that the synapses decrease some time

after consolidation during the period when the odor memory is maintained. In sum, *C. elegans* can maintain a long-term memory after spaced-training with sleep driving a synaptic decrease between a single interneuron-olfactory sensory neuron pair.

To understand the molecular requirements of long-term memory in our aversive olfactory memory paradigm, I performed a candidate approach. One such focus I was interested in is the transient receptor potential vanilloid (TRPV) channel family of proteins. Over twenty years ago, *osm-9,* the ortholog of human TRPV5 and TRPV6, was reported to mediate short-term olfactory memory to food-related odorants (Colbert and Bargmann, 1995; Colbert et al., 1997). TRPV channels have multiple biological functions, but the most well-known and studied TRP channel is TRPV1, the capsaicin receptor. Years of research have established a sensory role for TRP channels, currently with a large emphasis on using TRP agonists to treat chronic pain (Julius, 2013). In recent years, the TRPs have been a focus in the learning and memory field. TRP channels are found throughout the mammalian brain, including the hippocampus and neocortex (Kauer and Gibson, 2009). Pharmacological and genetic knockout studies have shown that the TRP channels, including TRPV1, may play a role in long-term memory formation (Sakai et al., 2013; Genro et al., 2012; Marsch et al., 2007; Li et al., 2008). In Chapter Three, I present my finding that the *osm-9/TRPV5/TRPV6* gene is required specifically for olfactory memory consolidation, even though the mutant animals sleep just like wild-type after training. Interestingly, *osm-9* is required for memory consolidation, but not acquisition. Since TRPV5 and TRPV6 function in calcium homeostasis (Dang et al., 2019), *osm-9* is Ca^{2+}-permeable (Lindy et al., 2014), and since calcium is required for synaptic transmission, it may be that *osm-9* is required to

mediate calcium signaling to drive the synaptic plasticity (e.g. downscaling) necessary for long-term memory formation.

Memory is vital for survival, yet diseases and disorders that perturb memory are common, especially in the aged population, including dementia, Alzheimer's, and Parkinson's. Understanding how memory is mediated will not only provide us with an understanding of an essential component of neurologic function necessary for our everyday lives, but will help us treat disorders in which memory is derailed. In Chapter Four, I present data on how expanded CGG repeat RNAs limit neural plasticity. In patients with fragile X and fragile X tremor/ataxia syndrome (FXTAS), expanded CGG repeats in the 5' UTR of the *FMR1* (fragile X mental retardation 1) gene are expressed in the brain (Hagerman, 2013). FXTAS-affected individuals have problems with balance and cognition, with an irregular startle response, or prepulse inhibition (Schneider et al., 2012). Specifically, in unaffected individuals, the response to a loud noise may initially cause a startle, but subsequent loud noises will not instigate a response since the individual has learned to ignore the sound. However, FXTAS patients are unable to attenuate their startle response with repeated loud noises. I present data showing that expressing the human *FMR1* gene with expanded CGG repeats in the *C. elegans* olfactory sensory neuron AWC blocks short-term aversive olfactory memory (Juang et al., 2014). We were interested in what RNA processing pathways are involved in the expanded CGG expression. I show that siRNA and nuclear endogenous siRNA processing pathways are not involved, but a miRNA pathway is involved in driving this expanded repeat-mediated hindrance on short-term memory. Understanding that the miRNA pathway is involved in the expanded CGG-repeat RNA limitation on plasticity in

FXTAS individuals may allow us to understand the exact molecular mechanisms underlying the disease state and how to potentially treat these disorders.

REFERENCES

Abdou, K., Shehata, M., Choko, K., Nishizono, H., Matsuo, M., Muramatsu, S., and Inokuchi, K. (2018). Synapse-specific representation of the identity of overlapping memory engrams. Science *360*, 1227–1231.

Bushey, D., Tononi, G., and Cirelli, C. (2011). Sleep and Synaptic Homeostasis: Structural Evidence in Drosophila. Science *332*, 1576–1581.

Cho, C.E., Brueggemann, C., L'Etoile, N.D., and Bargmann, C.I. (2016). Parallel encoding of sensory history and behavioral preference during Caenorhabditis elegans olfactory learning. ELife *5*, e14000.

Colbert, H., and Bargmann, C.I. (1995). Odorant-specific adaptation pathways generate olfactory plasticity in C. elegans. Neuron *14*, 803–812.

Colbert, H.A., Smith, T.L., and Bargmann, C.I. (1997). OSM-9, A Novel Protein with Structural Similarity to Channels, Is Required for Olfaction, Mechanosensation, and Olfactory Adaptation in *Caenorhabditis elegans*. J. Neurosci. *17*, 8259–8269.

Cook, S.J., Jarrell, T.A., Brittin, C.A., Wang, Y., Bloniarz, A.E., Yakovlev, M.A., Nguyen, K.C.Q., Tang, L.T.-H., Bayer, E.A., Duerr, J.S., et al. (2019). Whole-animal connectomes of both Caenorhabditis elegans sexes. Nature *571*, 63–71.

Cowansage, K.K., Shuman, T., Dillingham, B.C., Chang, A., Golshani, P., and Mayford, M. (2014). Direct Reactivation of a CoherentNeocortical Memory of Context. Neuron *84*, 432–441.

Dang, S., van Goor, M.K., Asarnow, D., Wang, Y., Julius, D., Cheng, Y., and van der Wijst, J. (2019). Structural insight into TRPV5 channel function and modulation. Proc Natl Acad Sci USA *116*, 8869–8878.

Dudai, Y. (1996). Consolidation: Fragility on the Road to the Engram. Neuron *17*, 367–370.

Dudai, Y. (2004). The Neurobiology of Consolidations, Or, How Stable is the Engram? Annu. Rev. Psychol. *55*, 51–86.

Fox, K., and Stryker, M. (2017). Integrating Hebbian and homeostatic plasticity: introduction. Philosophical Transactions of the Royal Society B *372*.

Genro, B.P., de Oliveira Alvares, L., and Quillfeldt, J.A. (2012). Role of TRPV1 in consolidation of fear memories depends on the averseness of the conditioning procedure. Neurobiology of Learning and Memory *97*, 355–360.

Gordus, A., Pokala, N., Levy, S., Flavell, S.W., and Bargmann, C.I. (2015). Feedback from network states generates variability in a probabilistic olfactory circuit. Cell *161*, 215–227.

Hagerman, P. (2013) Fragile X-associated tremor/ataxia syndrome (FXTAS): pathology and mechanisms. Acta Neuropathol. *126*, 1–19.

Juang B.T., Ludwig A.L., Benedetti K.L., Gu C., Collins K., Morales C., Asundi A., Wittmann T., L'Etoile N., Hagerman P.J. (2014). Expression of an expanded

CGG-repeat RNA in a single pair of primary sensory neurons impairs olfactory adaptation in Caenorhabditis elegans. Hum Mol Genet. *23*, 4945-4959.

Julius, D. (2013). TRP channels and pain. Annual Review of Cell and Developmental Biology *29*, 355—384.

Kandel, E.R. (2012). The molecular biology of memory: cAMP, PKA, CRE, CREB-1, CREB-2, and CPEB. Mol Brain *5*, 14.

Kauer, J.A., and Gibson, H.E. (2009). Hot flash: TRPV channels in the brain. Trends in Neurosciences *32*, 215–224.

Kaufmann, A.L., Ashraf, J.M., Corces-Zimmerman, R., Landis, J.N., and Murphy, C.T. (2010). Insulin Signaling and Dietary Restriction Differentially Influence the Decline of Learning and Memory with Age. PLOS Biology *8*, e1000372.

Li, H.-B., Mao, R.-R., Zhang, J.-C., Yang, Y., Cao, J., and Xu, L. (2008). Antistress Effect of TRPV1 Channel on Synaptic Plasticity and Spatial Memory. Biological Psychiatry *64*, 286–292.

Lindy, A.S., Parekh, P.K., Zhu, R., Kanju, P., Chintapalli, S.V., Tsvilovskyy, V., Patterson, R.L., Anishkin, A., van Rossum, D.B., and Liedtke, W.B. (2014). TRPV channel-mediated calcium transients in nociceptor neurons are dispensable for avoidance behaviour. Nat Commun *5*, 4734.

Marsch, R., Foeller, E., Rammes, G., Bunck, M., Kossl, M., Holsboer, F., Zieglgansberger, W., Landgraf, R., Lutz, B., and Wotjak, C.T. (2007). Reduced Anxiety, Conditioned Fear, and Hippocampal Long-Term Potentiation in Transient Receptor Potential Vanilloid Type 1 Receptor-Deficient Mice. Journal of Neuroscience *27*, 832–839.

Ryan, T.J., Roy, D.S., Pignatelli, M., Arons, A., and Tonegawa, S. (2015). Memory. Engram cells retain memory under retrograde amnesia. Science *348*, 1007–1013.

Sakai, T., Sato, S., Ishimoto, H., and Kitamoto, T. (2012). Significance of the centrally expressed TRP channel painless in Drosophila courtship memory. Learning & Memory *20*, 34–40.

Schneider, A., Ballinger, E., Chavez, A., Tassone, F., Hagerman, R.J. and Hessl, D. (2012) Prepulse inhibition in patients with fragile X-associated tremor ataxia syndrome. Neurobiol. Aging, *33*, 1045–1053.

Tononi, G., and Cirelli, C. (2014). Sleep and the Price of Plasticity: From Synaptic and Cellular Homeostasis to Memory Consolidation and Integration. Neuron *81*, 12–34.

Turrigiano, G., Leslie, K.R., Desai, N.S., Rutherford, L.C., and Nelson, S.B. (1998). Activity-dependent scaling of quantal amplitude in neocortical neurons. Nature *391*, 892–896.

de Vivo, L., Bellesi, M., Marshall, W., Bushong, E.A., Ellisman, M.H., Tononi, G., and Cirelli, C. (2017). Ultrastructural evidence for synaptic scaling across the wake/sleep cycle. Science *355*, 507–510.

White, J.G., Southgate, E., Thomson, J.N., and Brenner, S. (1986). The structure of the nervous system of the nematode C. elegans. Philosophical Transactions of the Royal Society B *314*, 1–340.

Yonelinas, A.P., Ranganath, C., Ekstrom, A.D., and Wiltgen, B.J. (2019). A contextual binding theory of episodic memory: systems consolidation reconsidered. Nature Reviews Neuroscience *20*, 364–375.

CHAPTER TWO: SLEEP IS REQUIRED TO REMODEL SPECIFIC SYNAPSES FOR MEMORY CONSOLIDATION

SUMMARY

Sleep is conserved across phyla and is shown here to be required for memory consolidation in the nematode, C. elegans. However, it is unclear how sleep collaborates with experience to change specific neurons and associated synapses to ultimately affect behavior. C. elegans neurons have defined synaptic connections and described contributions to specific behaviors. We show that spaced odor-training induces long-term memory, which transits a labile period before being stably maintained. This post-training labile period is required for long-term memory. Memory consolidation, but not acquisition, requires a single interneuron, AIY, which plays a role in odor-seeking behavior. We find that sleep and conditioning mark inhibitory synaptic connections between the butanone-sensing AWC neuron and AIY to decrease synapses and it is in the post-sleep wake phase that memory-specific synaptic changes occur. Thus, we demonstrate in the living organism how sleep initiates events lasting beyond the period of sleep to drive memory consolidation.

INTRODUCTION

The benefit of sleep to memory has been appreciated since antiquity. Writing in 95 CE, the Roman rhetorician Quintilian mused "…the interval of a single night will greatly increase the strength of the memory…Whatever the cause, things which could not be recalled on the spot are easily coordinated the next day, and time itself, which is generally accounted one of the causes of forgetfulness, actually serves to strengthen the memory (Quintilian, *Inst. Orat*. 11.2.43, trans. Butler, 1921)." Memory provides a survival benefit: an organism that encounters pathogens emitting an environmental cue such as an odorant, and remembers the odorant is associated with a negative outcome will be more likely to avoid the pathogens and survive to produce progeny. Mammals, birds, and insects all overwrite positive associations with negatives ones and the stability of these newly formed memories depends on sleep. Some of the mystery of why sleep is so widespread across phyla could be answered by its ability to overwrite memories and thus, provide a survival benefit for those organisms that learn to avoid cues that signal death or would reduce their progeny's chances for survival.

Honeybees provide an example of experience-based overwriting of memory. A worker honeybee can be trained by just one pairing of an odorant with sugar to extend her proboscis in response to odor presentation. This positive association does not require sleep. After the bee links odor to the reward, she can be trained to ignore the smell if it is repeatedly paired with water. If she is deprived of sleep, she cannot overwrite her behavior and remains attracted to the fruitless odorant (Hussaini et al., 2009). The consequences of failing to overwrite the positive association is a lower energy yield for the hive (Beyaert et al., 2012). Male starlings also require sleep to

remember a go/no-go task in which they are trained to peck for a reward if they hear a specific song, but not in response to a different one. They cannot learn to update this task if they do not sleep after training (Brawn et al., 2018). Humans also require REM sleep to consolidate memories, especially of complicated tasks, including complex declarative memories (e.g. meaningless sentences and stories, Rasch and Born, 2013). Classical studies have shown that in each example of sleep dependent learning, acquisition, consolidation, and recall depend heavily on different sets of brain regions (Vorster and Born, 2015). We still lack a molecular understanding of how and when different brain regions are recruited for each memory task (Asok et al., 2019), nor do we understand why recruitment requires sleep.

Unraveling how sleep affects cells and circuits to consolidate memory requires knowing what cells to focus on. Optimally, we could identify individual cells with defined connections that play a role in circuits that regulate thought or behavior, and identify how the structure of these circuits are altered by sleep to "hold" memories. A large body of work supports the role of two mechanisms acting together in memory consolidation: systems-level consolidation and synaptic downscaling (Tononi and Cirelli, 2014). Work in mammals, birds, and insects has identified populations of cells within specific brain regions that are essential for memory acquisition, maintenance, and recall (Yonelinas et al., 2019; Ryan et al., 2015; Abdou et al., 2018; Cowansage et al., 2015). By targeting specific brain regions to tag cells that are active during fear conditioning with optically-activated channels, fear-based freezing can be triggered by light. These cells are termed engram cells and they are found to initially connect cortical areas associated with the stimulus to limbic areas connected to the expression of fear (Ryan

et al., 2015; Abdou et al., 2018; Cowansage et al., 2015). Over time, more cortical regions seem to be recruited to a memory trace (Asok et al., 2019). Fly and bee olfactory memories are similarly acquired in one location, the antennal lobes, and stored in the mushroom bodies, while bird song memory and chick imprinting are acquired in the intermediate and medial mesopallium and seem to be stored in the brain region S' (Vorster and Born, 2015; Menzel et al., 2006). The pattern of consolidation shares features across phyla: the memory is initially fragile, it may be maintained remotely from the region in which it is required, and it is bolstered by sleep. However, the identity of cells that participate in the memory trace, whether they are a mix of both excitatory and inhibitory, is not known with enough detail and precision to understand how sleep affects their ability to encode or hold a memory.

The properties of cells whose plasticity is required for learning and memory revolve around their ability to connect to the rest of the circuit and brain. Chemical synapses between these cells have been the focus of study for decades. Sleep may strengthen memory by modifying synaptic structures. How it does this is at present unclear. Across many regions in the mammalian (Diering et al., 2017; Dudai et al., 2015) and fly brains (Tononi and Cirelli, 2014), sleep diminishes synapse size and strength. By contrast, long-term memory (LTM) studies have shown a requirement for synaptic strengthening. The classical view of memory consolidation is that purely synaptic mechanisms such as Hebbian plasticity drive learning. Briefly, Hebbian plasticity has been the focus of long-term memory: synapses are strengthened when the pre- and post-synaptic neuron fire in synchrony and, by contrast, weakened when their firing is asynchronous. More recently, the cellular basis for Hebbian plasticity has

been revealed by the observation that synchronous firing will lead to long term potentiation (LTP) while firing in an asynchronous manner induces long term depression (LTD) of a synapse. These changes lead to increases (LTP) or decreases (LTD) in the gain of the synapse, thus driving learning and memory (Fox and Stryker, 2017). Though LTP and LTD could explain memory, the field was left with a conundrum: LTP would "feed forward" into ever increasing synaptic strength and by contrast, LTD should extinguish neuronal responses. It was found that synapses are scaled such that each neuron maintains its baseline firing rate after LTP or LTD protocol. Thus, this homeostatic mechanism returns a system to its initial set point through compensatory mechanisms (often described by average neuronal firing rate) (Turrigiano et al., 1998; Turrigiano, 2017). Homeostatic plasticity can occur via scaling the synaptic strength, changes in inhibition or in intrinsic membrane properties, and by returning synapse size to baseline (Fox and Stryker, 2017). Memory consolidation at the synaptic level recently has been broadened to account for homeostatic scaling responses and the balance between this and Hebbian plasticity may be how sleep acts on learning and memory. Sleep has been posited to integrate these two forms of plasticity to drive memory formation by differentially affecting (down or upscaling) synapses that were acted upon in the wake state. However, the role of sleep at the synapse that holds the memory remains unknown (Tononi and Cierlli, 2014).

Across phyla, synapses in many regions are increased in the wake state and decreased with sleep. For example, in the rodent, the wake state increased synapses and sleep reduced them in the sensorimotor, primary motor, primary somatosensory, and prefrontal cortices (Maret et al., 2011; De Vivo et al., 2017; Acosta-Peña et al.,

2015), and at the dendritic spines throughout the hippocampus (Kreutzmann et al., 2015; Raven et al., 2018). Structural analysis of dendritic branches in the adolescent mouse cortex have demonstrated a wake-induced increase in number and size of synapses that decreases post sleep. Sleep was shown to be necessary for these changes in synaptic plasticity (Maret et al., 2011). A role for sleep in decreasing synapse size or number has been demonstrated in three *Drosophila* neuron groups (small ventral lateral neurons, gamma neurons of the mushroom bodies, and the first giant tangential neuron of the lobula plate vertical system) (Bushey et al., 2011). Similarly, in mouse motor and sensory cortices, ~80% of synapses were reduced in mice that were allowed to sleep, when compared with animals that were not permitted to sleep (deVivo et al., 2017). Taken together, these studies suggest that the temporal segregation of synapse building during wake via Hebbian plasticity and synapse reduction in sleep by homeostatic means allowed a reconciliation of the conundrum of how these two forms of plasticity may work (Tononi and Cirelli, 2014).

Though memory consolidation requires sleep, the global downscaling of synapses during sleep would seem to negate the effects of learning acquired by the waking animal. The synaptic homeostasis hypothesis (SHY) proposes that sleep restores synaptic homeostasis from the wake state (Born and Feld, 2012; Tononi and Cirelli, 2014; Vyazovskiy and Faraguna, 2014). There is much evidence in support of the SHY hypothesis (Vyazovskiy et al., 2008; Liu et al., 2010; Appelbaum et al., 2010; Gilestro et al., 2009; Donlea et al., 2009), including studies in flies and mouse that showed a requirement for sleep to drive homeostatic plasticity (Bushey et al., 2011; deVivo et al., 2017). The SHY hypothesis originally was evoked to explain how slow-

wave (non-REM) sleep, the sleep cycle required for memory consolidation in humans, induces a global downscaling of synapses in the hippocampus, neocortex, and olfactory cortex after the upscaling of synapses following information acquisition and learning during the wake state (Yamaguchi, 2017; Walker, 2009). The question the SHY hypothesis raises is how does downscaling of synapses during sleep not block learning-dependent changes at the synapse? One answer is that downscaling may act differentially on synapses that have undergone LTP versus synapses that have undergone LTD during wake, thus allowing memories to be retained during sleep. Interestingly, Hengen et al., 2016 found that neuronal firing rate homeostasis was suppressed during sleep and promoted by wake and enhanced by a longer wake state in mouse visual cortical neurons. Thus, the mechanisms by which sleep acts on cells and synapses that store memories are still largely unknown. In order to answer this question, we need cellular and synaptic resolution of memory and how it is affected by sleep.

How sleep affects memory consolidation by targeting specific synapses between individual cells with known functions in a behaviorally-relevant circuit remains unknown in any system. Though invaluable research in sleep and long-term memory has been performed in complex systems, e.g. mouse, humans, and insects, the complexity of these systems has precluded an understanding of the interplay of how sleep drives memory formation with single-cell and synaptic resolution. *Caenorhabditis elegans* (*C. elegans*), with its behavioral robustness and complete connectome description of the circuits that underlie these behaviors, is a more tractable system in which to study how sleep affects synapses. The compact nervous system of the *C.*

elegans hermaphrodite is mapped and invariably has 302 neurons (White et al., 1986; Cook et al., 2019) and functions have been assigned to most of these neurons (Bargmann and Marder, 2013). Despite its simplicity, *C. elegans* displays a wide repertoire of complex behaviors such as associative learning, memory, and sleep (Ardiel and Rankin, 2010; Trojanowski and Raizen, 2016). Moreover, a plethora of powerful tools are available for the study of the nervous system of this nematode: its transparency allows visualization of both the whole brain (Nichols et al., 2017) as well as individual synaptic connections in live animals (Feinberg et al., 2008), monitoring of neuronal activity (Chronis et al., 2007) and optogenetic perturbation of specific neurons (Nagel et al., 2005), along with the study of behavioral outputs to determine causal relationships. Appealingly, since we can visualize specific synaptic connections in live animals, we can study which exact synapses are modulated by experience and sleep.

Importantly, the behavioral properties of sleep: reduced locomotion (Hill et al., 2014; Raizen et al., 2008), stereotypical posture (Schwarz et al., 2012; Tramm et al., 2014), increased arousal threshold (Hill et al., 2014; Raizen et al., 2008), homeostatic response to deprivation (Nagy et al., 2014; Raizen et al., 2008) and the molecular pathways that control sleep are conserved across phyla, including in nematodes and mammals (Trojanowski and Raizen, 2016; Zimmerman et al., 2008). For instance, EGF and GABA promote sleep, Period genes control its timing, PKG activity regulates its intensity, while PDF and dopamine govern waking in all worms, mammals and flies (Van Buskirk and Sternberg, 2007; Choi et al., 2013; Singh et al., 2014; Trojanowski and Raizen, 2016). However, no association between sleep and memory consolidation has been described for *C. elegans* as of yet (Trojanowski and Raizen, 2016).

We examine the well-described olfactory system using a spaced-training paradigm in which the odorant butanone is paired with starvation. The worm goes from seeking out a point source of butanone to avoiding or ignoring it. Butanone is produced both by nutritious and pathogenic strains of bacteria and thus, the worm needs to overwrite its response to this volatile cue as a function of its experience. The paradigm we use to overwrite *C. elegans* attraction to butanone is a repeated spaced training that, remarkably, is followed by sleep. This task is akin to the honeybee extinction training and the go/no-go training of starlings. We adapted this from Kaufmann et al., 2010 by pairing butanone with a negative experience. Here we show that the memory is labile for two hours after training. During this time, sleep is required to consolidate the memory into a stable form. The labile memory requires a dispersed set of at least two interneurons, but is consolidated into long-term memory by the AIY interneuron pair. We show that sleep during this consolidation period is required to reduce inhibitory synaptic connections between AWC and AIY. Thus, the mechanism by which sleep consolidates an overwritten memory is by removing synaptic connections in an odor-seeking circuit. We find that sleep does this by acting on a signal that is established during conditioning. Sleep then initiates processes that continue past the period during which the memory is fragile, to reduce synapses. This provides cell biological insight into how experience, when followed by sleep, triggers physical changes in the circuit hardware at the level of the connections between neurons. Our time course shows that the newly acquired information, specifically, that butanone is deleterious, is held in a dispersed neuronal network where it is dynamic and easily overwritten. If the animal is allowed to sleep, then physical reductions of the synaptic connections commit the circuit to a stable

change. Thus, information is held, manipulated, and stored in an intact nervous system during the memory labile period when the synapses are decreased after training and sleep. This provides a testable hypothesis for why sleep is strongly evolutionarily selected for: if an organism cannot update its response to a cue that could kill it before it reproduces, it will be selected against.

RESULTS

Spaced olfactory conditioning yields long-lasting memory

In order to understand how long-lasting memories are formed and retained, we designed a Pavlovian style conditioning paradigm to quantitate the strength and duration of an olfactory memory. Unconditioned *C. elegans* animals move towards butanone, a volatile component of naturally attractive bacterial food sources (Worthy et al., 2018a; Worthy et al., 2018b), which they sense using their AWC^{ON} olfactory sensory neuron (Wes and Bargmann, Nature 2000). We quantify this attraction by employing the population-based chemotaxis assay developed by Bargmann et al. in 1993. In this assay, animals are placed onto a 10cm petri dish filled with a layer of agar and a point source of diluted butanone is placed opposite a similar source of diluent (ethanol) and animals are introduced at an origin equidistant from each source. Each spot is supplemented with sodium azide to paralyze the animals once they reach it. After at least two hours of roaming, the position of each animal on the plate is scored. The chemotaxis index is calculated by subtracting the number of animals at ethanol from the number at butanone and dividing by the total number on each plate. The bulk of a naïve or buffer-exposed population is attracted to the odor butanone: they move towards the point source of butanone and their chemotaxis index (CI) is usually from 0.6 to 0.9 (**Figure 2.S1**). Of note, each point on the graphs represents the CI resulting from a population of >50 animals. Experience, however, can suppress or even reverse this attraction. Pairing butanone with a single 80-minute period of food removal causes the population to move randomly with respect to the odor and the CI drops to near zero

during subsequent recall tests (Colbert and Bargmann, 1995). This indifference indicates that the animals have acquired the memory that butanone is profitless. We define memory as the response of the odor-trained population (with CI as the readout) being significantly different from the buffer-trained cohort. We use the conditioned response of the unperturbed wild-type to compare with the experimental groups to test if they differ significantly. If they differ, then we deem them memory defective. This memory decays rapidly and, after two hours of recovery on food, the population is once again attracted to butanone and this attraction persists for at least 16 hours (**Figure 2.S2**). Previous studies using other pairings in *C. elegans* and in other organisms have shown that spaced-conditioning paradigms in which the unconditioned and the conditioned stimuli are paired in different intervals separated by resting periods give rise to long-lasting memory (Estes, 1955; McGaugh, 1966; Mauelshagen et al., 1998; Beck et al., 2000; Kauffman et al., 2010). Employing a similar paradigm, we found that three spaced pairings of butanone and the absence of food with recovery periods on food in between the odor conditioning periods (**Figure 2.1A**) stably reduces attraction to butanone. This memory persists for at least 16 hours when animals are allowed to recover with food (**Figure 2.1B**, second pair of bars). The enduring nature of this olfactory memory indicates that the spaced-training paradigm induces a long-lasting memory and thus, we proceeded to ask whether this memory was specific for the training odor, or was a result of generalized inability to respond to odor across all sensory neurons, and whether it requires the cyclic AMP response element binding protein, CREB.

To determine if this conditioning paradigm interfered with odor detection in general, we asked if the butanone conditioning affected the animals' ability to sense and track the food-associated odor, benzaldehyde, which is an odor sensed by both AWC neurons. We found that pairing butanone with the absence of food did not affect attraction to benzaldehyde after 16 hours of recovery (**Figure 2.1C**), confirming that animals specifically remember their aversion of butanone, but keep their attraction to an odor sensed by the AWC^{OFF} neurons. Thus, the training does not impair the animal's general ability to chemotax.

To understand if the long-lasting memories are specific for butanone, or if this is a more generalized property of the olfactory system, we asked if repeated pairings of the AWA olfactory sensory neuron-sensed odor diacetyl (2,3-butanonedione, Sengupta et al., 1996) with the absence of food would also result in long-lasting memory (**Figure 2.S3**). We found that three spaced pairings of diacetyl and the absence of food reduce the chemotaxis response to diacetyl initially after spaced-training and the reduced attraction persists after 16 hours of recovery on food (**Figure 2.S3**). This finding is in agreement with prior studies that showed that training with diacetyl decreases attraction to this odor that is partially retained after 24 hours of recovery, though some of the memory is lost (Hadziselimovic et al., 2014). We observe that butanone memory, likewise, decays between 2 and 16 hours of recovery, albeit more slowly than that of diacetyl.

CREB, the cyclic AMP response element binding protein, is required for memory formation in flies, *Aplysia,* mice (Silva et al., 1998), and more recently, in *C. elegans* appetitive learning (Kaufmann et al., 2010). We tested whether CREB also

plays a role in our negative associative long-term memory paradigm by performing the butanone spaced-training with *crh-1(tz2)/CREB* mutants. Interestingly, we found that though the buffer-trained (control) populations of *crh-1/CREB* mutants show reduced chemotaxis to butanone, they were able to acquire memory as seen in the 0-hour recovery (**Figure 2.S4**). This memory is maintained at 16 hours post recovery as the CI of the wild-type and *crh-1/CREB* butanone-trained populations are not significantly different from each other (**Figure 2.S4**). Though the difference between buffer and butanone-trained animals is less striking than in wild-type populations, we conclude that the long-term training paradigm may not require CREB.

Thus, *C. elegans* can learn in a Pavlovian-style spaced-training paradigm to stably and selectively avoid at least two innately-attractive odors if they are associated repeatedly with the absence of food.

Butanone memory is labile immediately post conditioning

Learning is known to progress through stages, the first of which is labile, and thus we sought to determine the time course for stabilization of the aversive olfactory memory. A single butanone-no food pairing creates a memory that persists for just 30 minutes (**Figure 2.S2**) which is in contrast to the more enduring memory engendered by three-cycle spaced interval conditioning (**Figure 2.1A, 2.1B**). It is of note that three-cycle trained animals strongly ignore and are even averse to butanone as compared to one-cycle trained animals, which show no preference or aversion to the odor (**Figure 2.1B, Figure 2.S2**). To understand the dynamics of LTM decay, we assessed the chemotaxis index (CI) of three-cycle trained populations every 15 minutes following

conditioning (**Figure 2.2A**). To our surprise, we found that animals are attracted to butanone when tested 15 minutes after conditioning. This apparent memory loss persists for up to 60 minutes. Memory, as indicated by Cis close to zero, returns around 75 minutes, after which point, the memory persists with only slight decay until the 16-hour time point. This can perhaps be better appreciated by considering the Learning Index (LI)(LI = $CI_{CTL} – CI_{BTN}$) plotted in **Figure 2.2B** which shows the rapid decline in LI at 15 minutes recovering after two hours. The difference between the LI after two and 16-hour recovery is not as significant or great as between 0 and 15 minutes, which suggests two distinct mechanisms for memory decay. These results indicate that recently acquired memories are labile *in C. elegans.* Memory in insects, mammals and avians, transitions through a labile stage that stabilizes after a sleep bout (reviewed in Vorster and Born, 2015). This prompted us to examine our populations of trained animals more closely in the two hours in which memory was most labile.

C. elegans animals sleep after spaced olfactory conditioning

We noticed that animals appeared lethargic after spaced conditioning, thus we asked whether *C. elegans* sleep after conditioning. Sleep is best defined as a behavioral state in which animals are reversibly quiescent, reduce their feeding rates, take longer to arouse, and exhibit increased quiescence when they are deprived of sleep (sleep homeostasis) (Trojanoswki and Raizen, 2016). Therefore, we quantitated each sleep-related behavior in populations of buffer and butanone-conditioned animals.

We first compared movement of the butanone-trained to untrained animals during the first hour of recovery. We placed animals into the individual wells of a WorMotel

(Churgin et al., 2017), thus keeping animals separated from each other and allowing us to monitor locomotion using an automated imaging system. The output is shown in **Figure 2.3A** where blue sections of a raster plot represent 30 seconds of complete stillness. We quantitated the mean total quiescence for each population within the WorMotel and found that the mean total quiescence of trained populations is increased compared to that of the untrained animals (**Figure 2.3B**; untrained showed 5 minutes quiescence/hour vs. ~10 min/hr in the butanone-trained populations). Further, we found that whether cohorts of animals are conditioned with buffer or butanone, that their mean quiescence increases (**Figure 2.3B**; each population shows between 10 and 20 minutes of quiescence/hour). Thus, spaced training increased quiescence, regardless of whether they were buffer or butanone trained.

When we examined feeding rates, we found that they are significantly decreased in the trained populations (**Figure 2.3C**; 214 pumps/min for untrained vs 198 for trained). In addition, it takes longer for butanone-trained than untrained animals to mount an escape response when stimulated with a blue light pulse (a noxious stimulus) in conjunction with mechanical (1 KHz) vibrations from a piezo buzzer (**Figure 2.3D**; 7 seconds for untrained vs 12 for trained). The trained animals also show fewer sinusoidal waves after the stimulus is removed (**Figure 2.3E**; 7 sinusoidal waves for untrained vs 4 for trained). This reduced movement after arousal may reflect a sleep debt incurred by the stimulation, or could mean that the animals are more tired. Thus, by these criteria, animals that are conditioned with three cycles of butanone or buffer and the absence of food alternating with feeding exhibit the hallmarks of sleep.

Taken together, these findings indicate that spaced training promotes a sleep state subsequent to spaced conditioning with buffer alone or butanone. Finally, we asked if the mean total quiescence of a population immediately after training would correlate with the strength of memory after 16 hours of recovery as assessed by the CI. We found that there is a moderate ($r = -0.3914$), but significant ($P = 0.0394$) correlation between our measures of sleep one-hour post training and memory strength at 16 hours (**Figure 2.S5**). Thus, conditioning induces a sleep state, which correlates with the strength of memory after 16 hours of recovery. We wondered if sleep post training was also necessary for long-lasting memory.

Long-term butanone memory requires sleep

Memory consolidation at both the synapse and systems levels has been reported to require sleep in flies, mice, and humans (Tononi and Cirelli, 2014; Dudai et al., 2015). Thus, we wondered whether post-conditioning sleep is required for long-term 16-hour butanone memory in *C. elegans* as well. Starved *C. elegans* worms roam in search of food and do not sleep (Gallagher et al., 2013; You et al., 2008). We took advantage of this to keep animals from sleeping after conditioning to ask whether sleep is necessary for long-term memory. We disrupted sleep in the first two hours post conditioning, when memory appears most labile, by removing animals from food and then allowing them to recover on food for the remaining 14 hours prior to behavioral testing. We find that the animals off food immediately post conditioning are significantly less quiescent than animals on food (**Figure 2.4A**; on food is 15 min/hr quiescence vs 3 min/hr for off food). These data confirm that removing animals from food keeps them awake after

conditioning. When we assessed memory at 16 hours post conditioning, we found that animals that were initially kept off food do not sleep and they fail to maintain memory (**Figure 2.4B**; last pair of bars, the CTL and BTN mean CIs are not significantly different from each other). This result suggested that sleep might be necessary for memory maintenance. Another interpretation is that our treatment (removal from food) induced changes in metabolism rather than lack of sleep blocking memory stabilization.

In order to rule out the purely metabolic effects of starvation, we decided to induce sleep in animals that were removed from food. We forced animals that were recovered off food to sleep by overexpressing a sleep neuropeptide. Independent neuronal circuits control different types of sleep in *C. elegans* (Trojanowski et al., 2015) and different neuropeptides have been shown to mediate the induction of sleep by these neurons (Nelson et al., 2013, 2014; Turek et al., 2016). The FLP-11 neuropeptide mediates developmentally-timed quiescence and has also been found to induce sleep when overexpressed (Turek et al., 2016). Overexpression of FLP-11 not only induces sleep in animals off food (**Figure 2.4C**) but also restores memory to populations that were off food post conditioning (**Figure 2.4D**; compare the two hours off food, no sleep, and no peptide fifth bar with the off food plus peptide sixth bar). Heat shock induces sleep via the stress pathway and causes the release of somnogenic peptides (Hill et al., 2014), which may explain the small increase in memory of heat-shock treated wild-type animals off food (**Figure 2.4D**). The increase in memory of animals that have been forced into sleep via peptide expression while they are off food suggests that it is not purely the metabolic changes induced by starvation that block memory stabilization; rather, it is the lack of sleep. Further, restoration of sleep by overexpressing peptides

that induce sleep in development or after stress indicates that memory stabilization after sleep is not restricted to a specific type of sleep, but may be a general feature of sleep. Thus, sleep is necessary for memory and restoring sleep to animals off food is sufficient to promote long-lasting memory. The exact cellular mechanism by which sleep acts to consolidate memory is elusive because the field lacks precise cellular resolution of the cells that encode the memory trace.

Long term memory does not result from changes in AWC sensory neuron activity

One advantage of using the transparent *C. elegans* is that we can examine neuronal activity at the single neuron level in live animals at various times points during the sleep-induced memory stabilization. The AWC sensory neuron is the entry gate for butanone detection, thus we used GCaMP3 (Tian et al., 2009) to monitor calcium transients in AWC as memory develops. We imaged animals immediately after conditioning when they are repulsed from butanone, but the memory is labile, and after 16 hours of recovery on food when they are indifferent to the odor, but the memory is stable (**Figure 2.5**).

As previously reported (Chalasani et al., 2007; Cho et al., 2016), AWC calcium levels decrease when animals are exposed to butanone and rise dramatically after odor removal before returning to baseline. However, we find that odor removal triggers a larger increase in calcium in animals immediately after three cycles of butanone training than in the buffer-trained controls (**Figure 2.5A**, P = 0.0264). Odor onset triggers a small, but significant (**Figure 2.5B**, P = 0.0172) silencing of the AWC neuron in butanone-trained animals as compared to the buffer-trained controls. The difference

between AWC activity in buffer and butanone-trained animals is thus seen immediately after training while the animals are repulsed from the odor and the memory is labile (**Figure 2.5A** and **2.5B**, respectively). However, after 16 hours recovery on food when the memory is stabilized and the animals are indifferent to butanone, these differences in the AWC response to butanone disappear (**Figure 2.5C** ($P = 0.316$) and D ($P = 0.521$)). Thus, it is unlikely that the sensory response of AWC is solely responsible for maintaining memory.

The long-lasting memory trace is held in the interneurons AIB and AIY

We reasoned that the cells that hold the memory trace may thus be downstream of AWC. Serial electron micrographs (White et al., 1986; Cook et al., 2019) indicate that the primary postsynaptic partners of AWC chemosensory neurons are the AIY interneurons, which make approximately 8-12 synapses with the AWCs, and the AIA and AIB interneurons, which each make approximately 4-5 synapses with the AWCs (see **Figure 2.6A**). Thus, we killed AIB by expressing the caspase CED-3 from the *odr-2b* promoter specific for the neuron. To inactivate AIY, we employed the *ttx-3(ks5)* mutant allele that prevents the birth of the AIY neurons (Altun-Gultekin et al., 2001). We found that animals that lack either AIB or AIY are still able to acquire memory (**Figure 2.6B**, compare first pair to the second and third pair of bars). However, when AIB and AIY are both missing, memory acquisition is reduced (see **Figure 2.6B**, compare first and fourth pair of bars). This might be explained if another neuron in the circuit is primarily responsible for memory acquisition and AIB and AIY are redundant and less involved. Although animals missing either AIB or AIY are able to acquire the memory,

animals missing AIY lose the memory after 16 hours of recovery on food (compare tenth bar with fourteenth and sixteenth). This demonstrates that the AIY neurons are required for long-lasting memory. Thus, we have identified one specific cell that is required for memory consolidation; this is to our knowledge the highest cellular precision for memory. Having identified the exact cells that hold the memory allows us to now determine the subcellular mechanism by which memory is held and how sleep may affect the memory trace.

Synapses between AWC and AIY neurons are diminished after odor training and sleep

AIY interneurons are the primary postsynaptic partners of the AWC chemosensory neurons, and their ablation causes the most severe defect in memory. To determine if the structure of AWC-AIY synapses are altered by sleep after conditioning, we utilized the split GFP-based trans-synaptic marker Neuroligin-1 mediated GFP Reconstitution Across Synaptic Partners, or NLG-1 GRASP, (**Figure 2.7A** and Feinberg et al., 2008; Park et al., 2011; Varshney et al., 2018) to label synapses between AWC and AIY (**Figure 2.7B**, Feinberg et al., 2008; Park et al., 2011; Varshney et al., 2018). We found that the localization and distribution of AWC-AIY NLG-1 GRASP fluorescent puncta (**Figure 2.7C**) is consistent with EM micrographs, as has been the case for several other neuron pairs visualized with this marker (White et al., 1986; Cook et al., 2019; Park et al., 2011; Varshney et al., 2018; Feinberg et al., 2008), and did not affect the animals' behavior (**Figure 2.S7**).

We subjected AWC-AIY NLG-1 GRASP-labeled animals to three cycles of training, but we recovered half the cohorts without food for two hours. As shown in **Figure 2.4A**, under these conditions, animals fail to sleep during this time and though animals are returned to food for the 14-hour balance of the recovery time, their memory is impaired (**Figure 2.4B**). The other half of the cohort recovered on food for the entire 16 hours, allowing them to sleep in the two hours after training. We then compared AWC-AIY NLG-1 GRASP fluorescence intensity in the butanone-trained populations with the buffer-trained cohorts that either slept or were kept awake post-training (**Figure 2.7D, 2.7E**). The AWC-AIY NLG-1 GRASP fluorescence intensity was assessed on at least four independent days with a total N of greater than 90 animals for each condition. We found that the median synaptic intensity does not significantly differ between buffer-trained animals that are permitted to sleep and those that are not (**Figure 2.7D, 2.7E**, compare first and third boxes). Similarly, the median synaptic intensity does not significantly differ between buffer-trained and butanone-trained animals that are not permitted to sleep (**Figure 2.7D, 2.7E**, compare third and fourth boxes). By contrast, the synaptic signal in animals that were butanone-trained and permitted to sleep post-training is significantly lower than that in the buffer-trained animals permitted to sleep (**Figure 2.7D, 2.7E**, compare first and second boxes). This indicates that odor training and sleep work together to diminish AWC-AIY synapses in animals that retain the memory.

To determine if synaptic changes in response to butanone training are global, we examined the synaptic connections between PHB chemosensory neurons and two of their primary postsynaptic partners, the AVA neurons, using a strain that carries a NLG-

1 GRASP marker that labels connections between this pair of neurons (Park et al., 2011; Varshney et al., 2018). PHB is a chemosensory neuron that senses noxious chemicals including dodecanoic acid (Tran et al., 2017) and sodium dodecyl sulfate (Hilliard et al., 2002). PHB-AVA connections are not significantly altered by training or sleep (**Figure 2.S6**), indicating that the synaptic changes induced by butanone training and sleep are not global.

Given that both training and the two-hour labile period during which the animals sleep are required for alteration of AWC-AIY synaptic structures, synaptic changes could occur with at least three different timelines: A) AWC-AIY synaptic reductions could be specified and take place during training, and be stabilized during post-training sleep, B) synaptic reductions could be specified and occur during training and sleep, or C) synaptic reductions could be specified during training and sleep, but occur later during the 14-hour recovery period. Timelines A-C can be distinguished, as in timeline A, a reduction in AWC-AIY synaptic signal in butanone-trained compared with buffer-trained animals would be observed immediately after training. In timeline B, a difference in synaptic signal would be observed only after the two-hour period of sleep. In timeline C, synaptic changes would be observed only after the 16-hour period of recovery. The timelines would suggest different roles for sleep in memory consolidation. Timeline A would suggest a maintenance role for sleep, while timelines B and C predict that sleep diminishes the synapses of interest or specifies them for subsequent reduction, respectively. To test these hypotheses, we assessed AWC-AIY NLG-1 GRASP

fluorescence directly after training, after the two-hour post-training sleep, and after the subsequent 14-hour recovery period in buffer-trained and butanone-trained animals. When we assessed NLG-1 GRASP fluorescence directly after training, we find that the level of synaptic signal in buffer-trained and butanone-trained animals is not significantly different (**Figure 2.7F**, first and second boxes). Thus, the training itself does not reduce synapses, and timeline A is unlikely to explain the observed plasticity at 16 hours post-training. After the two hour post-training period of sleep, synaptic signal was significantly reduced in both buffer-trained and butanone-trained animals compared to the same cohorts immediately after training (**Figure 2.7F**, compare first to third and second to fourth boxes), however the level of synaptic signal was not significantly different between these two populations at this time point (**Figure 2.7F**, compare third and fourth boxes). This indicates that our system can reveal rapid synaptic dynamics in a physiologically-relevant time period. This is consistent with timeline C, in which butanone-training and sleep-induced AWC-AIY synaptic alterations are specified during training and sleep, but occur later during the 14-hour recovery period.

DISCUSSION

Sleep is highly conserved, indicating evolutionary pressure to be retained. Here we show that *C. elegans*, which diverged from our last common ancestor ~1.18 billion years ago (Wang et al., 1999), is our most distant relative that requires sleep to consolidate memory. The current state of the field of learning and memory is that we have a systems understanding of engrams at the level of cells and synapses (Asok et al., 2019). Having a living, behaving animal that allows the synthesis of these processes in such a way that they can be studied with great resolution would give us insights into the molecular and cellular biology underlying memory. Here, we show that *C. elegans* forms long-lasting aversive memories to the odorant butanone following three spaced-training cycles. This olfactory memory transitions through a two-hour labile period before being stably maintained. During this labile period post training, we find that animals sleep and that sleep is required to stabilize memory. Animals kept off food during the period of time that memory is fragile do not sleep and also fail to maintain the memory. Forcing animals to sleep off food by overexpressing a sleep neuropeptide during this time, however, enables them to keep the memory. In order to understand the circuitry involved in this paradigm, we looked at calcium dynamics in the AWC olfactory sensory neurons in animals subjected to odor training. We found that though there was a difference in response to butanone in the AWC neurons in animals immediately after training while the memory was labile, this difference disappeared by 16 hours, when the memory was stable. To understand how chemotaxis behavior could diminish so profoundly when the olfactory circuit's sensory neurons are apparently still sensitive to odor, we asked if downstream interneurons might underlie changes in behavior. We

found that memory could be acquired in the absence of either AIB or AIY; however, the AIY interneuron was required for long-term memory maintenance. To understand the mechanism by which this neuron might store the olfactory memory, we examined synapses between AWC and AIY. Interestingly, we found that synapses were decreased 16 hours after training, but only in animals that were both conditioned to butanone and had slept. To probe the mechanism behind the collaboration between olfactory conditioning and sleep, we examined the time course for training and sleep-dependent synapse reduction as a function of memory. We found that synapses are reduced in animals after their memory is stable two hours post training, regardless of whether they were trained with buffer alone or buffer and butanone. This reduction occurs in the two hours of recovery on food. The difference between the AWC-AIY synapses in butanone as compared to buffer-trained animals does not become apparent until the animals have recovered for 16 hours on food. This change suggests that odor training marks the synapses between the sensory AWC and AIY interneuron for reduction and that sleep collaborates with these marks to diminish the connection further once the animal reawakens.

Evolutionary selection for memory consolidation

Memory is essential for survival; failure to heed cues associated with harmful infectious agents can be fatal. Odors, universally powerful signals for food and its contaminants, are such salient cues. Butanone is possibly one such cue for *C. elegans*. This volatile chemical, emitted from both nutritious and infectious bacteria (Worthy et al., 2018a; Worthy et al., 2018b), could thus be associated with either positive or negative experiences. For example, the pathogenic *Serratia marcescens* attracts *C. elegans* with

its bouquet of butanone and acetone, is subsequently ingested, and infects the host, killing it in 2-3 days (Worthy et al., 2018a). However, once the bacteria are ingested and if the worm survives, it will have learned to avoid the bacteria's bouquet (Zhang et al., 2005). Thus, the mechanism for learning to ignore butanone could potentially be an evolutionary trait to avoid further ingestion of pathogenic bacteria. This may explain why *C. elegans* can be trained to either seek butanone (Torayama et al., 2007; Kaufmann et al., 2010; Vohra et al., 2017), or avoid it completely (Tsunozaki et al., 2008; Figure 1). In studying this memory, we are tapping into the strongly-conserved function of odor to uniquely signal discreet information about the environment. The synaptic remodeling we observed after sleep may permit increased evolutionary fitness. This refinement may allow the animal to stably and appropriately respond to salient cues such as pathogen-associated odors and be a clue for why sleep is so highly-conserved among animals that have a nervous system.

The aversive memory of butanone is stable and lasts for an ethologically-relevant length of time: 16 hours out of the 18-day lifespan of *C. elegans*, which is proportional to three years of an average 79 year-long human life (Kochanek et al., 2017). Further, this memory is engaged when the animal is in its prime reproductive stage (day-one adult) and accounts for more than half of its five-day reproductive span. The initiation and duration of this memory could thus have profound consequences for the survival of the animals' progeny. This evolutionary argument may explain why stable learning after spaced training is seen across phyla. We posit that the circuit, cellular, and molecular logic underling these processes is also conserved, and that we have developed a

behavioral correlate to memory overwriting in *C. elegans* that has opened up this organism to in-depth understanding of long-term memory driven by sleep.

Memory is consolidated by sleep and its benefit may serve an evolutionarily-conserved function. Individuals that sleep after an adverse encounter with a noxious agent may thus link the negative experience with the salient cue that is removed when they can finally sleep. Though this is the first report of the *C. elegans* nematode sleeping after spaced-training, sleep has been studied for over ten years in *C. elegans*. Developmental sleep, or lethargus (Raizen et al., 2008), was initially discovered, followed by stress-induced sleep in the adults (van Buskirk and Sternberg, 2007). More recent studies found that starvation also induces sleep in worms. Starvation causes a stress-induced sleep that is linked to inhibited insulin signaling and was posited to reflect an energy conservation mechanism (Skora et al., 2018). These prior studies documented in *C. elegans* the hallmarks of sleep that are conserved across the animal kingdom: periods of quickly reversed immobility, increased arousal threshold, homeostatic compensation, and stereotypical posture (Trojanowski and Raizen, 2016). With this report, we show that like other organisms, nematodes require sleep to consolidate memory. This may explain the strong evolutionary conservation of sleep among animals that have a nervous system: to modify their behavior as a function of experience.

Sleep post conditioning

Stress may induce sleep after conditioning. *C. elegans* and other organisms sleep in a variety of circumstances - growth stages are coincident with increased sleep

needs in adolescent mammals as well as before each molt in *C. elegans* larval development. Mammals and nematodes sleep after UV light-induced DNA damage (Trojanowski and Raizen, 2016), prolonged starvation (Skora et al., 2018), re-feeding after starvation (You et al., 2008), and heat shock (Hill et al., 2014). Each trigger engages neurons in a sleep circuit that release somnogenic peptides (Trojanowski and Raizen, 2016). *C. elegans'* ALA interneuron triggers stress-induced sleep by releasing the FMRFamide FLP-13 among other neuropeptides (Nath et al., 2016) and the interneurons RIS and RIA regulate lethargus at least in part by releasing FLP-11 and NLP-22 respectively (Turek et al., 2016; Nelson et al., 2013). These neuropeptides, conserved in fly and fish, engage GABA-ergic pro-sleep circuits (Meeusen et al., 2002; Lenz et al., 2015; Lee et al., 2017 ELife). The present conditioning paradigm involves repeated starvation followed by re-feeding. We have not identified the neuropeptides that control post-conditioning sleep, nor do we know which sleep circuit this paradigm may trigger. However, the circuit is likely to involve a stress-response component. The worms may grow exhausted due to liquid training, or become stressed by starvation. Another possibility is that worms naturally sleep periodically throughout the day and our training keeps them awake such that once they are returned to food, the entire population sleeps, perhaps due to a buildup of sleep pressure.

What is it about the sleep brain state that predisposes memory consolidation?

Changes in the brain state are indicative of sleep. Mammals cycle between rapid-eye-movement (REM) and non-rapid-eye-movement (NREM) sleep in which the neuronal activity in the thalamocortical and hippocampal systems alternates (Weber,

2017). Flies alternate between states of deeper and lighter sleep and these states are homeostatically-regulated as in mammalian sleep (van Alphen et al., 2013). Fly sleep has recently been revealed to have two stages of brain activity. One stage has increased oscillatory activity and the other has decreased activity, with the switch between the two brain states mediated by sleep and arousal-promoting neurons in the dFB, or the dorsal fan-shaped body, in the central brain (Yap et al., 2017). The finding that flies go through a more active state in their sleep patterns means that when worms sleep, they too may have subtle head movements and other neuronal firing patterns. Skora et al., 2018 suggested that a head waving for example may indicate a state of reduced arousal.

C. elegans is no exception to having a brain state specific to sleep. Whole-brain calcium imaging has been reported on wake and sleeping *C. elegans* and this revealed that 40% of the worm's 300 neurons show oscillatory dynamics in the wake state that cycle through firing patterns indicative of different movement regimes (Nichols et al., 2017; Skora et al., 2018). 75% of those neurons become inactive during lethargus. The notable exceptions are GABAergic and peptidergic head neurons, including the sleep-promoting interneuron RIS (Nichols et al., 2017), which have slow, stochastic cycles of calcium waves. In-depth analysis of each neuron's activity in the starvation-induced sleep state revealed that both of the paired AWC neurons are insensitive to sleep (Skora et al., 2018). Thus, AWC is potentially more active than AIY in the post-training animal. The picture that emerges from these observations is that the *C. elegans* brain is mostly quiet during sleep.

CREB and sleep-dependent memory consolidation

Cyclic AMP response element binding protein, or CREB, is part of a highly-conserved process that has been shown to mediate long-term memory formation across phyla, including in flies, mollusks, mice (Silva et al., 1998), and more recently, in *C. elegans* appetitive learning (Lakhina et al., 2015). We found that *crh-1(tz2)/CREB* mutants become less responsive to butanone after 16 hours of recovery from conditioning—buffer-trained *crh-1/CREB* animals show a significantly lower chemotaxis index than wild-type animals (**Figure 2.S4**). When we observed that *crh-1(tz2)/CREB* mutants were able to acquire and retain aversive memory, we examined the olfactory phenotype and molecular nature of this often-used allele more closely.

The *crh-1(tz2)* allele we tested removes the last 60% of the highly-conserved basic leucine zipper (bZIP) domain, which mediates DNA binding and dimerization (Kimura et al., 2002). It has been previously reported that the *crh-1(tz2)* mutant has irregular appetitive long-term memory in *C. elegans* (Lakina et al., 2015) and other abnormal behaviors, including clumping and burrowing in food-rich conditions (Kimura et al., 2002). It could be that for our aversive-learning paradigm, that the first 40% of the bZIP domain retains functionality. Conversely, the kinase inducible domain (KID) may be responsible for long-term negative-associative memory. The *C. elegans* KID contains the Ser 133 residue which is conserved in CREB family proteins in mammals and flies. This residue is recognized by the transcriptional co-activator CREB binding protein (CBP) and subsequently activate gene expression (Kimura et al., 2002; Lonze and Ginty, 2002). Perhaps, the KID domain is required for negative-associative memory and, by contrast, the bZIP domain is required for positive-associative memory. The two

domains may mediate plasticity and memory via distinct downstream mechanisms. On the other hand, even though most forms of long-term memory require CREB, other transcription factors, including SFR, c-fos, EGR-1, and NF-κ B, are also necessary for memory in flies and mammals (Kandel, 2012), and could contribute to *C. elegans* negative associative long-term memory.

Aversive memory transitions from being independent of the AIY interneuron to depending on it

We observed that neither AIB nor AIY (AWC presynaptic ~5 or ~12 synapses) was required for acquisition of the labile aversive memory of butanone, nor were they required for chemotaxis, but AIY is required for long-term memory. The finding that neither AIB nor AIY are required for acquisition, could indicate that another interneuron such as AIA is needed instead. AIA was shown to be required for memory induced by one training session with butanone and starvation (Cho et al., 2016). Memory in response to repeated, spaced-training may, likewise, require this interneuron for its acquisition. Our focus, however, is on long-term memory, thus, we examine cells such as AIB and AIY that are not required for either the primary response or acquisition of initial memory. The transition from short to long-term memory may reflect a sleep-dependent reorganization of the memory for long-term storage, perhaps being handled by mainly AIA to being dependent on both AIB and AIY neurons. In an interesting parallel, distinct brain regions, such as the mammalian hippocampus, the avian intermediate and medial mesopallium, and the insect antennal lobe handle newly acquired, labile memory and transfer this in a sleep-dependent process to ill-defined

regions in the mammalian neocortex, an unidentified cortical region termed S' in birds (Jackson et al., 2008; Vorster and Born, 2015), and the mushroom body in insects (Hussaini et al., 2009) for long-term storage. Since discovering that worms sleep after training and that sleep is required for memory consolidation, it becomes possible to visualize the anatomically-compact nervous system of this transparent organism as memory is consolidated in real time. Thus, using *C. elegans* to understand the transition of memory may be a powerful way to elucidate the mechanisms by which long-term memories are formed.

The AIY interneurons regulate thermotaxis (Mori and Oshima, 1995), locomotion speed, and direction switch, and connect to downstream interneurons and motor command hubs via acetyl cholinergic connections to produce these behaviors (Li et al., 2014). In addition, AIY has been previously found to mediate plasticity to starvation paired with thermo- or chemotactic cues (de Bono and Maricq, 2005; Ishihara et al., 2002). AIY may function as a sensory integrator of information from upstream sensory neurons, including AWC in our paradigm. The butanone-sensing chemotaxis circuit is well characterized. Animals navigate up a gradient of butanone using a well-defined chemosensory circuit. The butanone-sensing AWC chemosensory neuron is silenced by the odor butanone and begins signaling upon butanone removal (Chalasani et al., 2007). Activation of AWC results in glutamate release onto AIY neurons that express glutamate-gated chloride channels (Chalasani et al., 2007). AIY neurons promote smooth, fast runs, and hyperpolarization of AIYs terminates these runs (Li et al., 2014). This results in a system in which animals sensing butanone have silenced AWCs and active AIYs, promoting the smooth, fast runs toward the butanone. When an animal

moves away from the butanone, AWC is stimulated, and AIYs are prevented from stimulating runs. The AWCs also form excitatory synapses with AIB interneurons, which promote turning (Chalasani et al., 2007). Thus, when butanone levels are reduced and AWC becomes active, AIB interneurons promote pirouettes (Pierce-Shimomura et al., 1999). The synapses between AWC and AIY are inhibitory. Reduction of these synapses after butanone training and sleep could decouple AIY from the butanone-responsive AWC neuron, allowing it to promote forward locomotion, regardless of the butanone gradient. Thus, animals 16 hours post training would appear indifferent to the butanone gradient. However, other functions of AIY may not be affected, as they can still climb a benzaldehyde gradient, which is sensed by the non-butanone responsive AWC neuron as well (Wes and Bargmann, 2000). This mechanism of diminishing AWC-AIY synapses in a training and sleep-dependent manner could thus lead to the specific odor memory we observe.

Inhibitory synapses and sleep

The synapses between AWC and AIY are inhibitory through glutamate-gated chloride channels, which are only found in protostome invertebrate phyla (including mollusks, annelids, and arthropods). These glutamate-gated chloride channels mediate locomotion, feeding, and sensory input integration and closely resemble mammalian glycine receptors (Wolstenholme, 2012). Glycine receptors in the mammalian hippocampus also have an inhibitory role and may function in conjunction with excitatory NMDARs, or to inhibit GABAergic inhibition, to regulate hippocampal function, including learning and memory (Xu and Gong, 2010). In addition, α2-glycine receptor knockout mice show defects in spatial memory (Lin et al., 2017).

Not much is known about inhibitory synaptic dynamics. The inhibitory synapses of hippocampal neurons change in size considerably over time as compared to their excitatory counterparts, and their size configurations changed at much slower rates. Suppression of network activity only slightly affected remodeling dynamics, unlike in excitatory synapses (Rubinski and Ziv, 2015). Similar molecular processes may be at play in memory storage within the *C. elegans* olfactory circuit. It could be that these differing dynamics of inhibitory and excitatory synapses lead to homeostatic compensation of the system driven by sleep.

The SHY hypothesis says that the brain needs to reset during sleep to improve cellular health and to promote memory consolidation (Tononi and Cirelli, 2014). One mechanism for memory consolidation during sleep is synaptic homeostasis, where global synaptic strength decreases (Tononi and Cirelli, 2014). Though there is a preponderance of evidence for global synaptic downscaling, an upscaling of excitatory postsynaptic potentials was found to occur during slow-wave sleep (Chauvette et al., 2012). In addition, it was observed that synaptic downscaling in the hippocampus occurs instead during REM sleep (Grosmark et al., 2012). It was also observed that synaptic potentiation occurs in the mouse visual system during sleep after periods of visual experience, regardless of sleep cycle (Durkin and Aton, 2016). Surprisingly, neuronal firing rate homeostasis in mouse visual cortical neurons was suppressed by sleep and promoted by wake, and enhanced by a longer wake state (Hengen et al., 2016). Our paradigm may reveal a similar mechanism, where synapses are not taken down during sleep in the labile period immediately after training, but are instead decreased in awake animals 16 hours after spaced training.

The model posits that during wake, long-term potentiation (LTP) and long-term depression (LTD) modulate synaptic activity, and that during sleep, many synapses are downscaled potentially via a mechanism that differentially affects active and less-active synapses (Tononi and Cirelli, 2014). In our study, we observe significant synaptic reductions in both buffer- and butanone-trained animals during sleep. Interestingly, the two levels diverge later during subsequent wakefulness. We hypothesize that AWC-AIY synapses may be specified during butanone training and subsequent sleep, and the synaptic changes may be completed only after subsequent wakefulness. The training and sleep-dependent reduction in AWC-AIY synapses may be required to form the long-term odor memory. On the other hand, the reduced synapses may only be correlated with memory, but not causative. However, we find that AIY is required for long-term memory, and the observed reduction in AWC-AIY synapses would explain the long-term butanone indifference. Thus, we favor our hypothesis that sleep and training collaborate to produce long-term memory.

ACKNOWLEDGEMENTS

We would like to thank all of the L'Etoile, VanHoven, Kato, and Fang-Yen lab members for all of their helpful discussions, especially Katie Mellman, AJ Ablaza, Mary Futey, Sarah Woldemariam, Bo Zhang, Trang Duong, and Aarati Asundi. We would also like to thank Sara Alladin, Nebat Ali, Anjana Baradwaj, Claudia Echeverria, Jordan Mitchell, and Idan Siman-Tov for help with synapse experiments. We would like to thank Veronica Valdez for making the reagents to support the experiments in this manuscript. We are thankful to Andrei Goga, Maria Gallegos, Torsten Wittmann, Matt Gruner, Stephen Nurrish for all for all of their advice on experiments in this manuscript. We give a big thanks to the *Caenorhabditis* Genetics Center (CGC), supported by the NIH Office of Research Infrastructure Programs (P40 OD010440), for the strains they provided to us and for their support of the greater *C. elegans* community. We would also like to give another big thanks to the Sternberg lab and everyone else behind Wormbase.org (NIH grant #U24 HG002223) and the Hall lab for Wormatlas.org (NIH grant #OD010943 to DHH), both for their immensely helpful resources. Thanks to BioRender for their artwork which was used in **Figure 2.1** and **2.S1**. This work was funded by the NIH, specifically R01DC005991 (N.L.D., M.K.V., C.F.Y.), R15NS109803 (M.K.V.), R01NS087544 (N.L.D., M.K.V.), R35GM124735 (S.K.), F31DC014921 (K.L.B.), and R01NS084835 (M.A.C.).

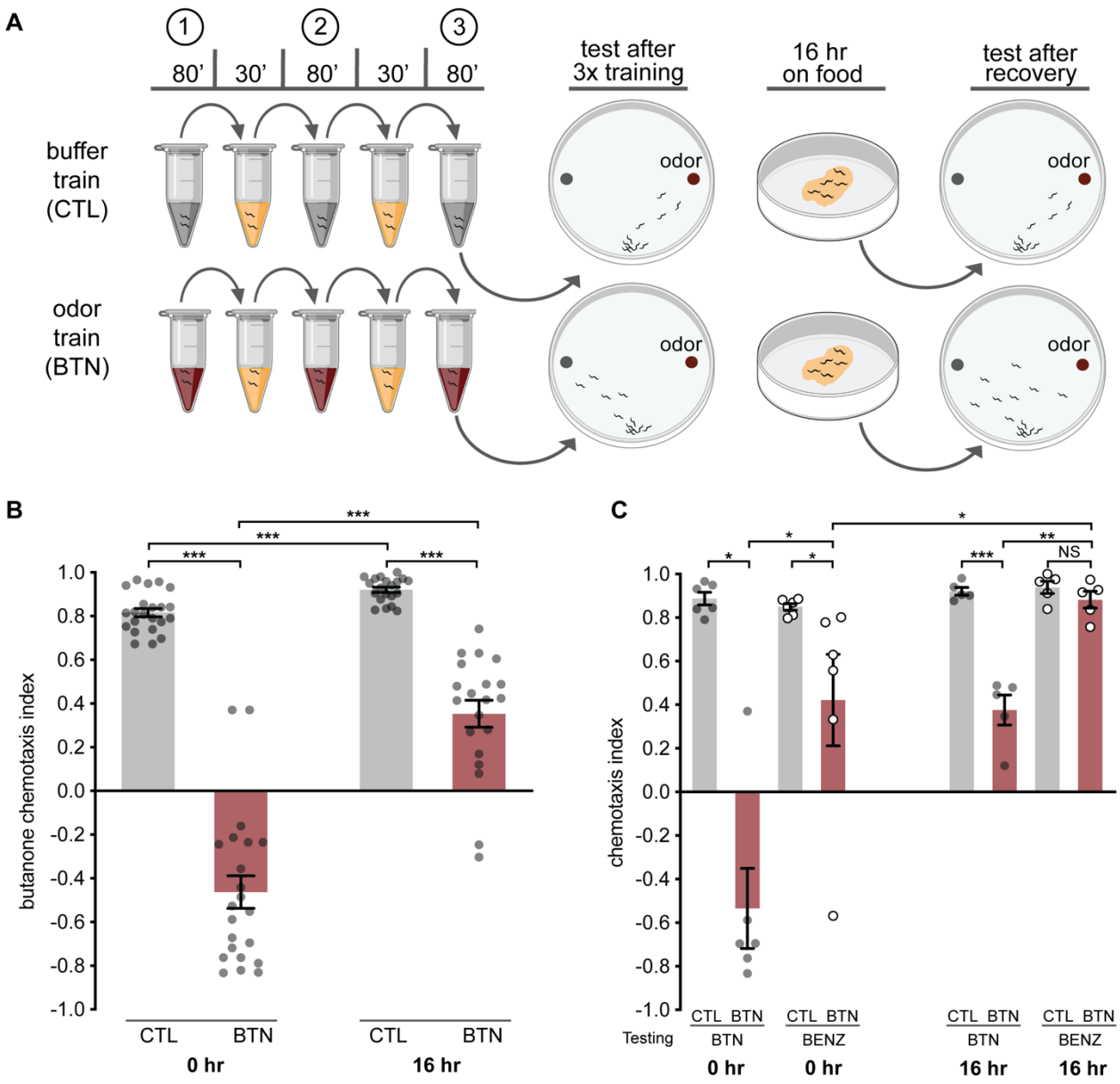

Figure 2.1. Spaced training induces long-lasting memory.

(A) Schematic of aversive olfactory memory assay to induce long-lasting memory. Age-synchronized adult worms are rinsed from food and conditioned to either buffer (CTL, gray) or butanone (BTN, red) for 80 minutes followed by incubation with liquid food (OP50 of OD = 10). After three cycles of conditioning, animals recover on NGM plates seeded with OP50 for either 0 hours or 16 hours before testing their attraction to BTN in a chemotaxis assay (1:1000 BTN dilution). Chemotaxis assay shown in Figure S1.
(B) Three-cycle training induces initial repulsion followed by long lasting memory 16 hours later. Aversive learning and memory in wild-type animals conditioned to either buffer (CTL, gray) or butanone (BTN, red) immediately post training (0 hr) or after 16 hours of recovery on food (16 hr). The Chemotaxis Index (CI) is calculated and is the

number of worms on the control subtracted from the number on butanone, divided by the total number of worms, not including worms at the origin. A positive chemotaxis index (CI) indicates attraction and negative, aversion. N = number of trials where all trials are done on independent days and each grey dot represents an individual assay day, with 50-200 animals/day. Error bars represent S.E.M. Statistical significance was reported as ***P <0.001, ** P < 0.01, *P<0.05, and NS is P>0.05. The Shapiro-Wilk normality test was performed to determine data distribution, followed by the Kruskal-Wallis test, an analysis of variance of multiple comparisons for non-parametric data (***P<0.001). If normally distributed, then P values were generated with a Student's unpaired t-test. If non-parametric, then P values were generated with the Mann-Whitney u-test. Hochberg adjustment for multiple comparisons was performed on all P-values generated from data included in the same graph to control Type I error. The t-test was performed on CTL 0 hr vs CTL 16 hr and CTL 16 hr vs BTN 16 hr. The u-test was performed on CTL 0 hr vs BTN 0 hr and BTN 0hr vs BTN 16 hr. Behavioral data throughout the paper are represented in this same way with the same numbers of animals on independent days. Additionally, throughout the paper, the same statistical analysis was performed on the data unless otherwise noted in the figure legend.
(C) Three cycle butanone training does not affect attraction to benzaldehyde after 16 hours of recovery. Chemotaxis indices of animals trained to buffer (CTL, gray bars, gray dots) or butanone (BTN, red bars, gray dots) and tested for attraction to butanone or of animals trained to buffer (CTL, gray bars, white dots) or benzaldehyde (BENZ, red bars, white dots) and tested to benzaldehyde. The t-test was performed on CTL vs BTN both tested on BTN at 16 hr, CTL vs BTN both tested on BENZ at 16 hr, and BTN 16 hr tested to BTN vs BTN 16 hr tested to BENZ. The u-test was performed on CTL vs BTN 0 hr both tested on BTN, BTN 0 hr tested on BTN vs BTN 0 hr tested on BENZ, CTL vs BTN 0hr both tested on BENZ, and BTN 0 hr test on BENZ vs BTN 16 hr tested on BENZ. For every graph in this paper, the Kruskal-Wallis test was performed and yielded ***P<0.001, unless otherwise noted.

See also **Figures 2.S1, 2.S2, 2.S3,** and **2.S4**.

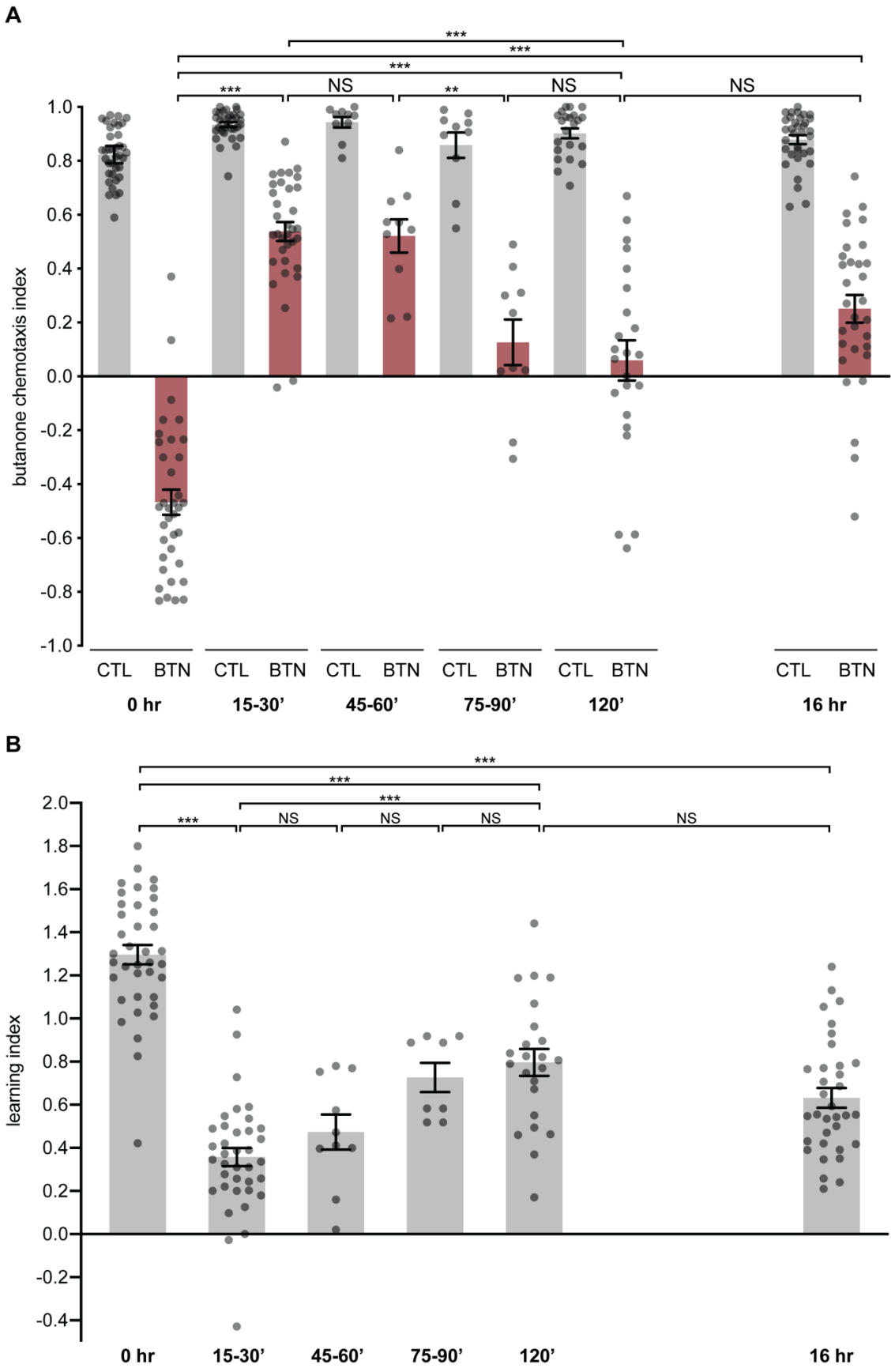
A
butanone chemotaxis index
1.0
0.8
0.6
0.4
0.2
0.0
-0.2
-0.4
-0.6
-0.8
-1.0
***
***
***
***
NS
**
NS
NS
CTL BTN CTL BTN CTL BTN CTL BTN CTL BTN CTL BTN
0 hr
15-30'
45-60'
75-90'
120'
16 hr
B
learning index
2.0
1.8
1.6
1.4
1.2
1.0
0.8
0.6
0.4
0.2
0.0
-0.2
-0.4
***
***
***
***
NS
NS
NS
NS
0 hr
15-30'
45-60'
75-90'
120'
16 hr

Figure 2.2. Memory is labile immediately post training.
(A) Chemotaxis indices of animals conditioned to CTL or BTN. After three cycles of conditioning, animals recover on NGM plates seeded with OP50 for either 0 minutes, 15-30 minutes, 45-60 minutes, 75-90 minutes, 120 minutes, or 16 hours before testing their attraction to BTN in the chemotaxis assay. The P value is ***P<0.001 for all of the comparisons between the CTL and BTN of the same recovery time. The t-test was performed on CTL vs BTN 15-30', BTN 45-60' vs BTN 75-90', BTN 75-90' vs BTN 120', and BTN 120' vs BTN 16 hr. The u-test was performed on CTL vs BTN 0 hr, CTL vs BTN 45-60', CTL vs BTN 75-90', CTL vs BTN 120', CTL vs BTN 16 hr, BTN 0 hr vs BTN 15-30', BTN 15-30' vs BTN 45-60', BTN 0 hr vs BTN 120', BTN 15-30' vs BTN 120', and BTN 0hr vs BTN 16 hr.
(B) Learning indices of spaced-trained animals. The learning index is calculated as the chemotaxis index of the BTN animals subtracted from the chemotaxis index of the CTL animals. The higher the learning index, the more the animals have learned and thus kept the BTN memory. The t-test was performed on 0 hr vs 15-30', 15-30' vs 45-60', 120' vs 16 hr, 0 hr vs 120', 15-30' vs 120', and 0 hr vs 16 hr. The u-test was performed on 45-60' vs 75-90' and 75-90' vs 120'.

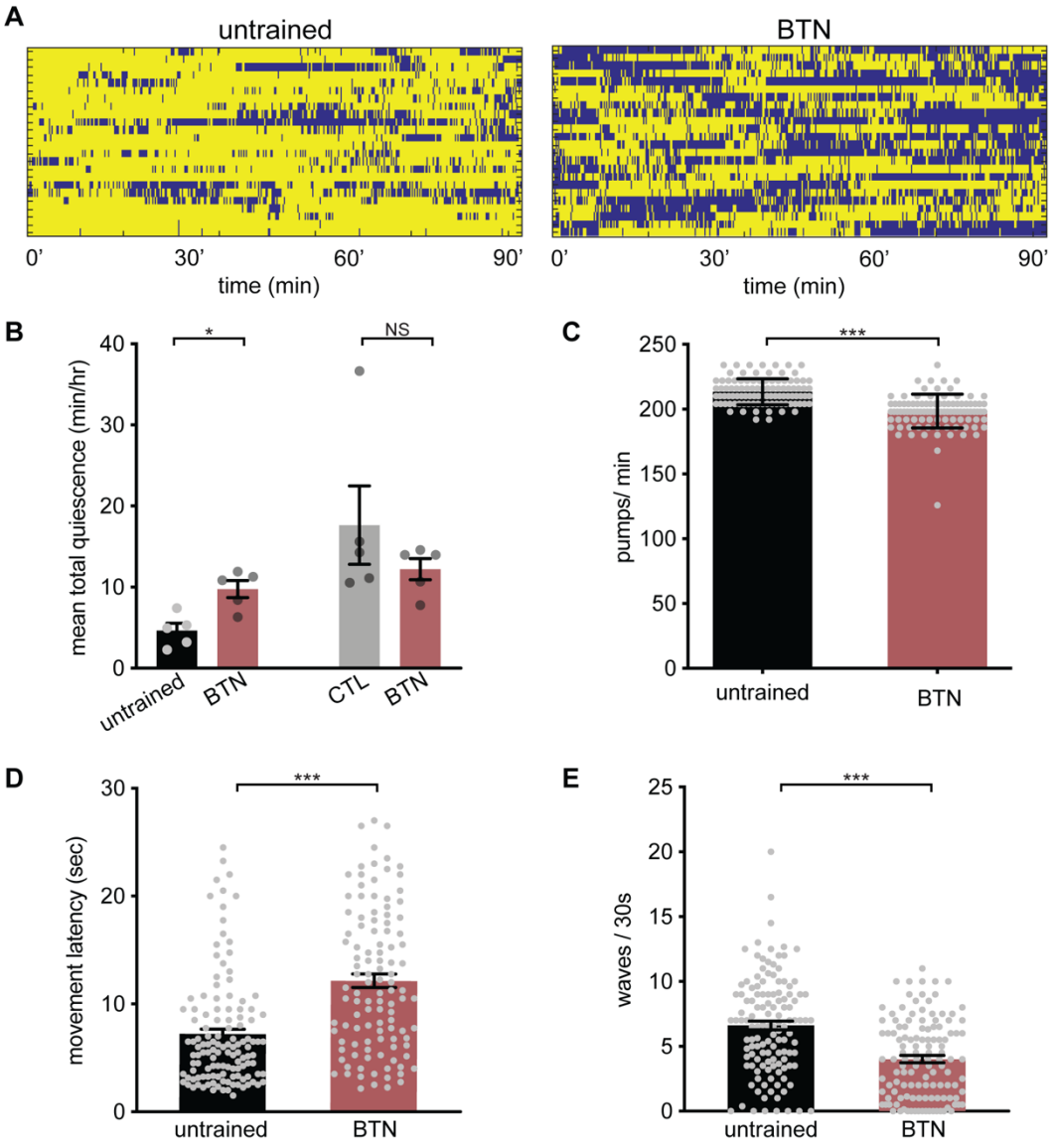

Figure 2.3. *C. elegans* sleeps after spaced-training.
(A) Untrained animals are more active than butanone spaced-trained animals during the 90 minutes after training. Raster plot of activity of untrained (left panel) vs spaced-trained animals to BTN (right panel). Yellow indicates activity and dark blue, quiescence. Individual animals were placed into a PDMS 48-well microtiter plate (WorMotel, Churgin et al. 2017) and their movement was recorded by camera. Movement was analyzed with a custom MatLab script. Each row represents an individual worm's movement over 90 minutes. Quiescence was defined as no movement for >30 seconds and marked with a blue raster.
(B) Untrained animals are less quiescent than BTN animals, and CTL or BTN have no difference in quiescence. Mean total quiescence in total minutes per hour of animals in WorMotel that are untrained (black bars, grey dots) or CTL or BTN animals. Each grey dot represents 24 animals tested per condition on an independent day, and this is the

same for every mean total quiescence graph in this paper. The t-test was performed on untrained vs BTN (first and second bars) and the u-test was performed on CTL vs BTN (third and fourth bars).
(C) Feeding rate is reduced post odor training. Feeding rate is measured as pharyngeal pumps per minute. Each dot represents one animal. Assay was performed on three separate days with animals that were untrained (black bar, grey dots) vs BTN. Pharyngeal pumping was scored manually. Error bars represent S.D. The u-test was performed.
(D) Butanone-trained animals have an arousal delay in compared to untrained animals. Movement response latency was measured as number of seconds until a sinusoidal wave is initiated (an escape response) after exposure to blue LED light and 1.2KHz of vibrations in untrained (black bar, grey dots) or BTN animals. Videos were taken of animals over three days. The u-test was performed.
(E) Butanone-trained animals are less active upon an arousal stimulus than untrained animals. Activity post stimulus was measured by counting how many full sinusoidal wave movements were completed in 30 seconds after exposure to blue LED light and 1.2 KHz vibrations stimuli. Videos were taken of animals over three days. The u-test was performed.

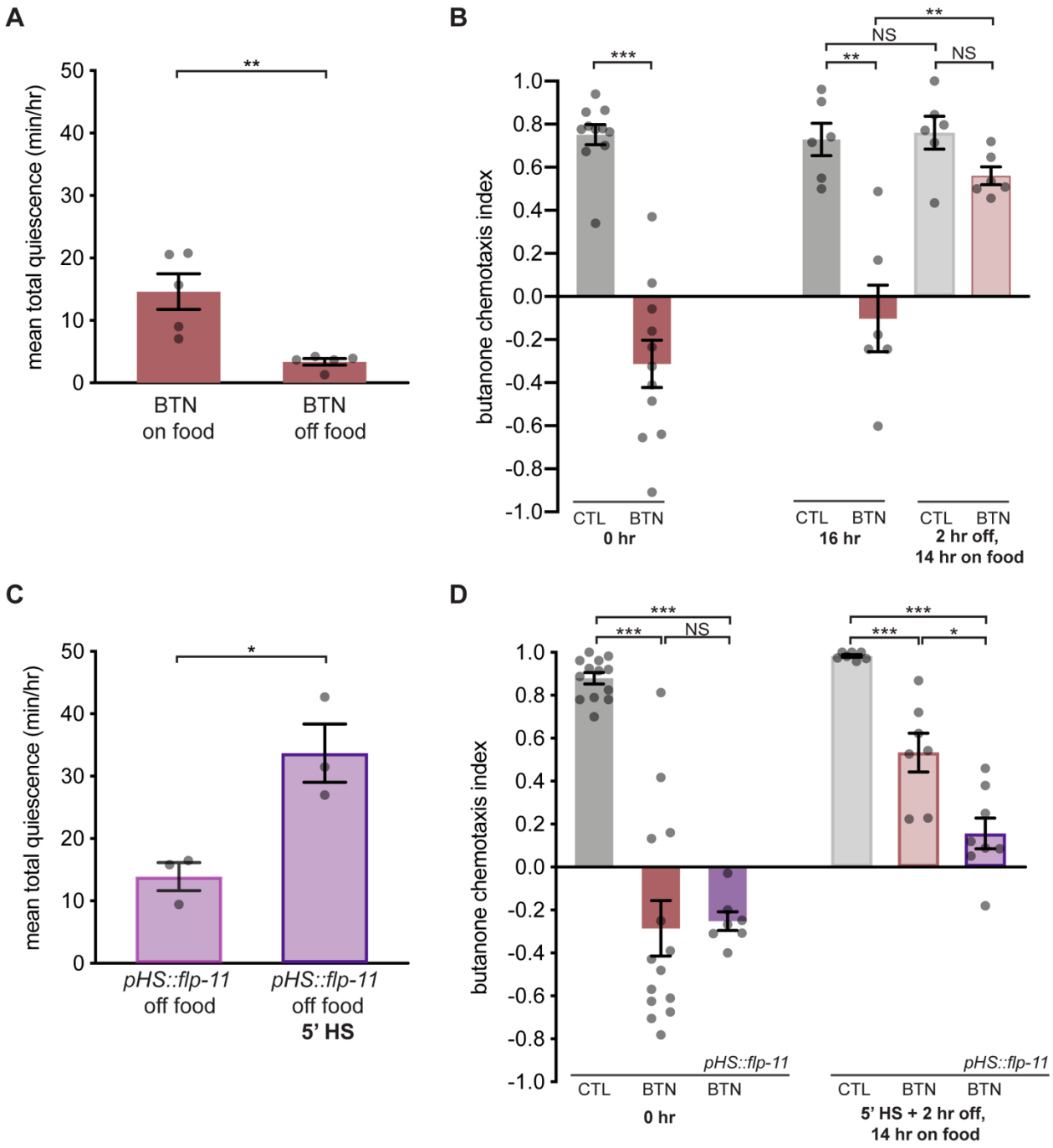

Figure 2.4. Sleep is required post training for long-term memory.
(A). Animals are less quiescent off food than on food in one hour post training. Mean total quiescence was measured in minutes per hour of animals after training either on food (first bar) or off food (second bar). Individual animals were placed into a PDMS 48-well microtiter plate (WorMotel, Churgin et al. 2017) either seeded with food (OP50 in 24 of the wells for the "on food" condition) or without food ("off food"), and animals were recorded with a camera. Movement was analyzed with a custom MatLab script. The u-test was performed.

(B) Animals off food for two hours immediately after training do not maintain the memory 16 hours later. After three cycles of conditioning, animals are immediately tested in a chemotaxis assay or recovered on either unseeded NGM plates or NGM plates seeded with OP50 for 120 minutes before testing 16 hours after the end of the training assay. Chemotaxis indices of animals conditioned to buffer (CTL, gray) or butanone (BTN, red), tested after 0 hr or 16 hr post training, or animals off food for 2 hr and on food for 14 hr (CTL, lighter gray with darker gray outline, fifth bar, or BTN, lighter red with darker red outline, sixth bar). The t-test was performed on CTL 16 hr vs BTN 16 hr, CTL 16 hr vs CTL 2 hr off, 14 hr on food, BTN 16 hr vs BTN 2 hr off, 14 hr on food, and CTL 2 hr off, 14 hr on food vs BTN 2 hr off, 14 hr on food. The u-test was performed on CTL 0 hr vs BTN 0hr.
(C) Animals overexpressing the neuropeptide *flp-11* are more quiescent than control animals. Mean total quiescence was measured in minutes per hour. *Hsp16.2::flp-11* ("*pHS::flp-11"*) animals overexpress the *flp-11* neuropeptide after heat-shocking. The heat shock was performed after spaced training for 5 min at 37°C. The *pHS::flp-11* off food animals (first bar, pink outline) were off food for one hour while filmed in the WorMotel and the *pHS::flp-11* off food 5' HS animals (second bar, purple outline) were heat-shocked for five minutes off food and then put into the WorMotel without food and filmed for one hour. The t-test was performed.
(D) Animals that overexpress *flp-11* via heat-shock keep the memory off food better than heat-shocked wild-type animals off food. Chemotaxis indices measured immediately after training (0 hr) for wild-type animals conditioned to CTL (first bar), BTN (second bar), and of BTN-trained animals expressing the *pHS::flp-11* transgene (purple, third bar), and trained animals heat-shocked for 5' at 37°C, two hours off, 14 hours on food ("2 hr off 14 hr on food") including CTL (lighter gray, fourth bar), BTN (lighter red, fifth bar), and *pHS::flp-11* (lighter purple with dark purple outline, sixth bar). Heat-shocked *pHS::flp-11* animals were confirmed to all be quiescent after the heat pulse. The t-test was performed on CTL 0 hr vs *pHS::flp-11* 0 hr, CTL 5' HS + 2 hr off, 14 hr on food vs BTN 5' HS + 2 hr off, 14 hr on food, BTN 5' HS + 2 hr off, 14 hr on food vs *pHS::flp-11* 5' HS + 2 hr off, 14 hr on food, and CTL 5' HS + 2 hr off, 14 hr on food vs *pHS::flp-11* 5' HS + 2 hr off, 14 hr on food. The u-test was performed on CTL 0 hr vs BTN 0 hr and BTN 0 hr vs *pHS::flp-11* 0 hr.

See also **Figure 2.S5**.

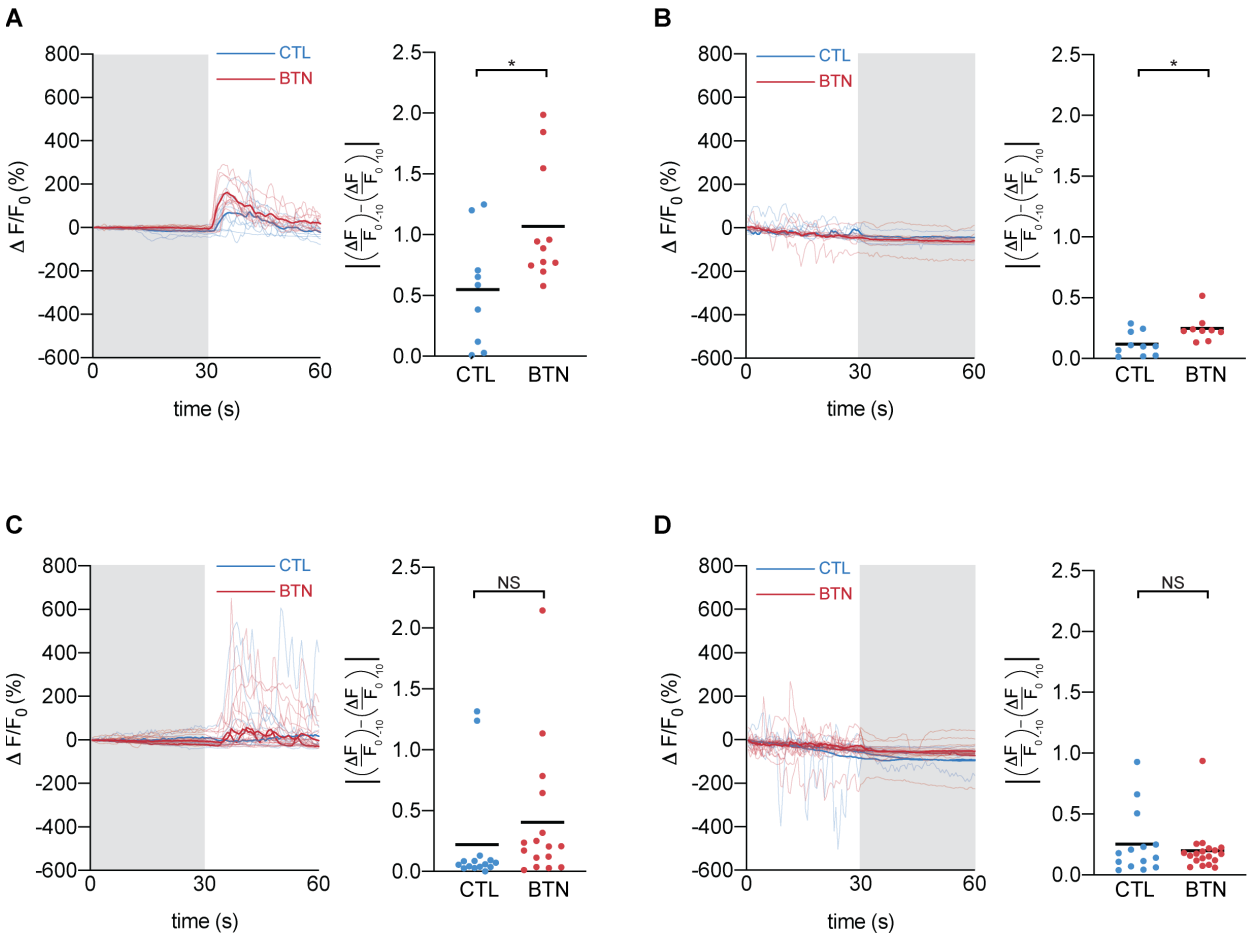

Figure 2.5. AWC sensory activity is slightly altered only immediately after spaced-training. Calcium responses in AWC^{ON} for CTL (blue) or BTN (red) animals to removal (A, C) or addition (B, D) of butanone measured immediately after training (A-B) or after 16 hr of recovery (C-D). Video recordings were taken for 60 seconds and the percent fluorescence intensity of the GCaMP3 fluorophore was measured and graphed as $\Delta F/F_0$ for each animal tested. The worms are immobilized in a PDMS microfluidic chip and the gray shading indicates butanone being flowed over the worm nose via laminar flow for 30 seconds and no shading means that buffer was being flowed. Each line indicates a recording from one worm and the bold lines indicate the means. The CI of the populations that these animals came from showed that the CTL animals were attracted to butanone (mean CI = 0.9) and each population of BTN animals was repulsed (mean CI at 0 hr recovery = -0.01, mean CI for 16 hr recovery = -0.57). The scatter plot panels on the right of each calcium recording panel contain the absolute values of the deltas between the mean $\Delta F/F_0$ (%) values from 10 seconds before stimulus on or offset and the mean $\Delta F/F_0$ (%) values 10 seconds after stimulus on or offset, where each dot signifies one worm. The black bars indicate the means. The t-test was performed on all of the comparisons.

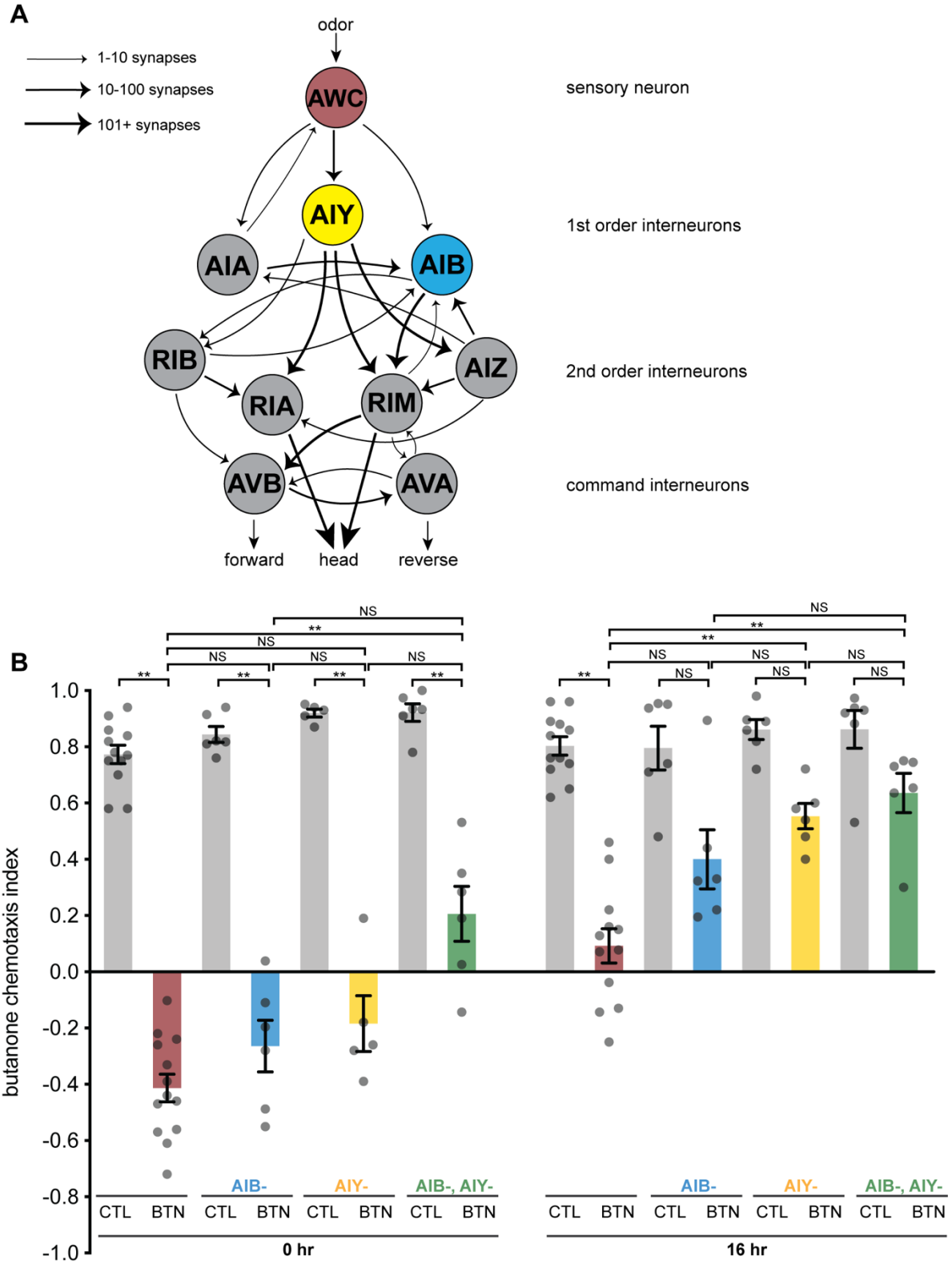
A
1-10 synapses
10-100 synapses
101+ synapses
odor
AWC
AIY
AIA
AIB
RIB
AIZ
RIA
RIM
AVB
AVA
forward
head
reverse
sensory neuron
1st order interneurons
2nd order interneurons
command interneurons
B
butanone chemotaxis index
1.0
0.8
0.6
0.4
0.2
0.0
-0.2
-0.4
-0.6
-0.8
-1.0
NS
**
AIB-
AIY-
AIB-, AIY-
CTL
BTN
0 hr
16 hr

Figure 2.6. Memory acquisition requires AIB or AIY and long-lasting memory requires AIY.
(A) AWC olfactory circuit of *C. elegans*. Sensory neuron AWC (red) is inhibited by odor. The AIY (yellow) interneuron promotes straight runs and is inhibited by AWC while the AIB (blue) interneuron promotes turns and is activated by AWC. Thus, odor activates AIY and inhibits AIB allowing the animal to run up an odor gradient and reorient if going down the gradient. Smallest arrow indicates 1-10 synapses between the two neurons, medium arrow, 10-100 synapses, and largest arrow, more than 100 synapses. Only chemical synapses are indicated in the circuit (gap junctions not shown). Figure adapted from Gordus et al., 2015.
(B) Killing AIB and AIY somewhat inhibits memory acquisition and killing AIY blocks memory maintenance. Chemotaxis indices after 0 or 16 hr of recovery of wild-type vs animals carrying a transgene or mutation to kill specific interneurons including AIB (blue), AIY (yellow) or AIY and AIB (green). The t-test was performed on CTL vs BTN 0 hr, CTL vs BTN AIB- 0 hr, CTL vs BTN AIY- 0 hr, CTL vs BTN AIB-, AIY- 0 hr, BTN vs BTN AIB- 0 hr, BTN AIB- vs BTN AIY- 0 hr, BTN AIY- vs BTN AIB-, AIY- 0 hr, BTN vs BTN AIY- 0 hr, BTN vs BTN AIB-, AIY- 0 hr, BTN AIB- vs BTN AIB-, AIY- 0 hr, CTL vs BTN AIB- 16 hr, CTL vs BTN AIY- 16 hr, CTL vs BTN AIB-, AIY- 16 hr, and BTN 16 hr vs BTN AIY- 16 hr. The u-test was performed on CTL vs BTN AIB- 16 hr, BTN 16 hr vs AIB- 16 hr, BTN AIB- vs BTN AIY- 16 hr, BTN AIY- vs BTN AIB-, AIY- 16 hr, BTN AIB- vs BTN AIB-, AIY- 16 hr, and BTN 16 hr vs BTN AIB-, AIY- 16 hr.

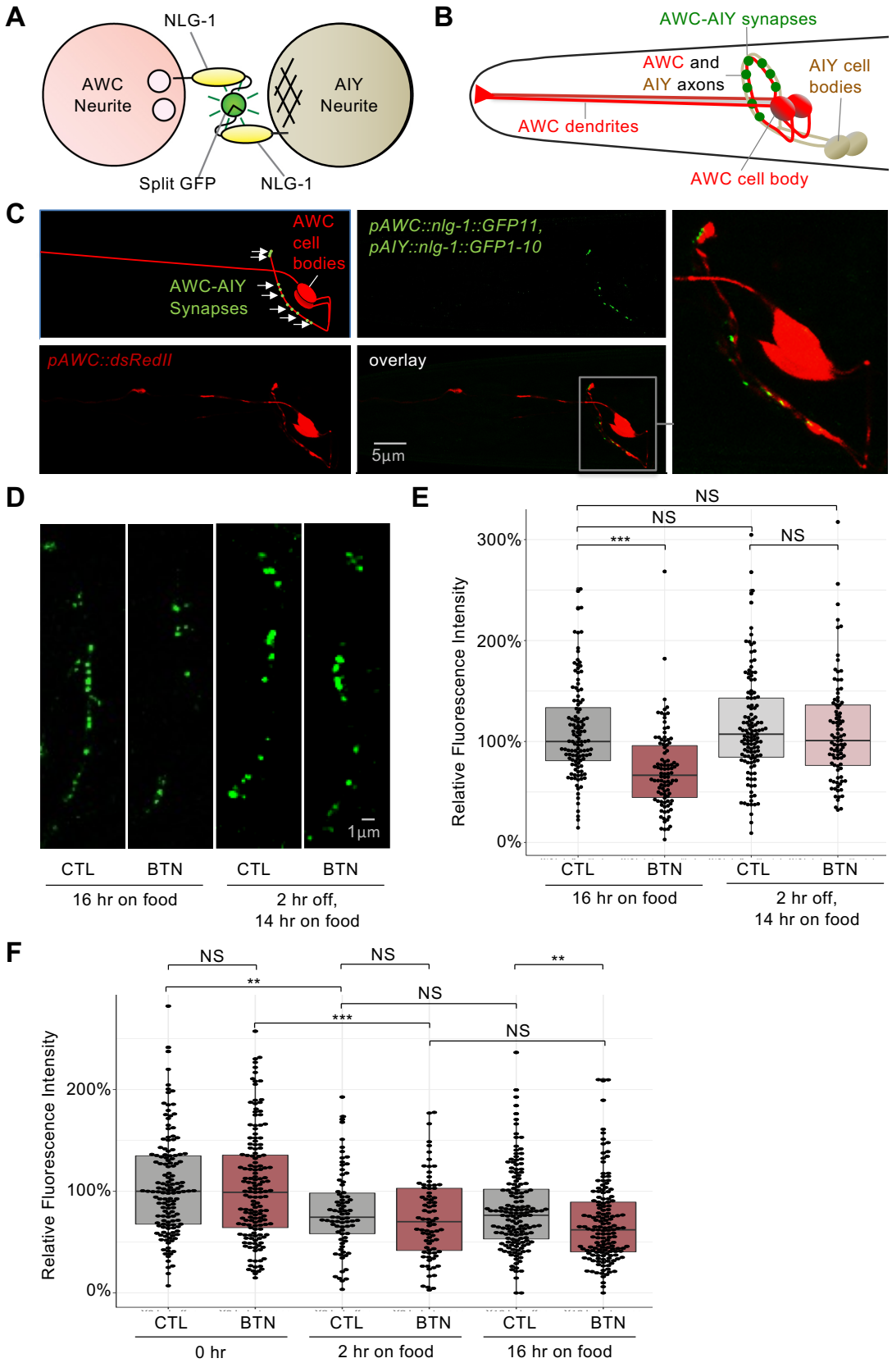
A
NLG-1
AWC Neurite
AIY Neurite
Split GFP
NLG-1
B
AWC-AIY synapses
AWC and AIY axons
AIY cell bodies
AWC dendrites
AWC cell body
C
AWC cell bodies
AWC-AIY Synapses
pAWC::nlg-1::GFP11, pAIY::nlg-1::GFP1-10
pAWC::dsRedII
overlay
5µm
D
1µm
CTL
BTN
CTL
BTN
16 hr on food
2 hr off, 14 hr on food
E
NS
NS
NS
***
300%
200%
100%
0%
Relative Fluorescence Intensity
CTL
BTN
CTL
BTN
16 hr on food
2 hr off, 14 hr on food
F
NS
NS
**
**
NS
***
NS
200%
100%
0%
Relative Fluorescence Intensity
CTL
BTN
CTL
BTN
CTL
BTN
0 hr
2 hr on food
16 hr on food

Figure 2.7. AWC-AIY synapses are diminished in butanone-trained animals allowed to sleep directly after training.
(A) Schematic of split GFP-based AWC-AIY NLG-1 GRASP marker. Circles represent cross-sections of the AWC and AIY neurites, and one of each neurite is represented for simplicity. Fragments of the split GFP are linked to the pre- and postsynaptically localized protein NLG-1 (Neuroligin 1), and expressed in the AWC and AIY neurons with the selective promoters *odr-1* and *ttx-3*. When synapses form between the neurons, the split GFPs reconstitute and fluoresce. Small white circles indicate a presynaptic site, and crosshatching represents a postsynaptic site.
(B) Schematic of the head of an animal in which NLG-1 GRASP labels synapses between the AWC (red) and AIY (beige) neurites.
(C) Schematic and micrographs of a buffer-trained animal carrying the AWC-AIY NLG-1 GRASP marker with the AWC neuron labeled in red with the cytosolic mCherry fluorophore. Synaptic fluorescence is observed in a punctate pattern spread across the arc of the AWC axons. The area in the gray box is expanded in the rightmost image.
(D) Micrographs of AWC-AIY NLG-1 GRASP fluorescence in animals trained with butanone (BTN) or control buffer (CTL), placed on or off food during the first two hours after training, and recovered on food for an additional 14 hours, as described in Figure 4. AWC-AIY NLG-1 GRASP fluorescence is reduced in the animal trained with butanone and recovered on food for the first 2 hours post-training. (E) Quantification of the reduction in AWC-AIY NLG-1 GRASP fluorescence intensity in animals trained with butanone (BTN) and recovered on food for the first two hours post training in comparison to animals trained with a control buffer (CTL), or animals trained with butanone and recovered off food for the first two hours post training. N>90 for each box and includes animals trained on four different days. *** $P<0.001$, NS $P>0.05$, Mann-Whitney u-test. P values were adjusted for multiple comparisons using the Hochberg procedure. (**F**) Quantification of AWC-AIY NLG-1 GRASP fluorescence intensity at 0 hours, 2 hours and 16 hours post-training in buffer-trained (CTL) and butanone-trained (BTN) animals allowed to sleep for the two hours post-training. N>75 for each box and includes animals trained on four different days. *** $P<0.001$, ** $P<0.01$, NS $P>0.05$, Mann-Whitney u-test. P values were adjusted for multiple comparisons using the Hochberg procedure.

See also **Figures 2.S6** and **2.S7**.

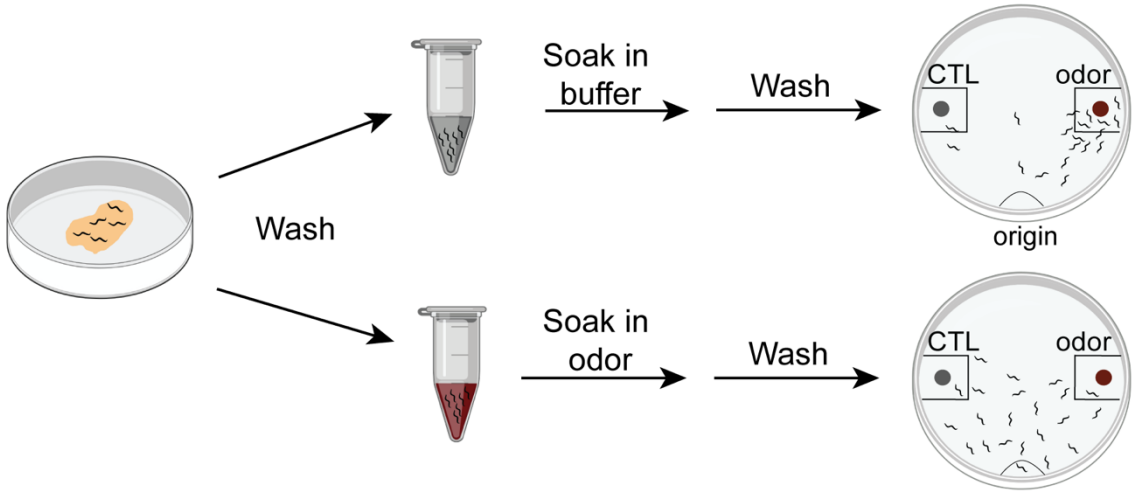

$$\text{Chemotaxis index} = \frac{\text{(worms at odor) - (worms at control)}}{\text{(total worms on plate not at origin)}}$$

Figure 2.S1. Related to Figure 2.1. Schematic for assessing the chemotaxis assay. One-day old adults are washed from NGM plates into two different tubes, where one population will be soaked in buffer and the second will be soaked in butanone diluted in buffer (1:10,000) for 80 minutes. The animals are then washed with buffer two times, with a third wash in ddH_2O, and are subsequently plated on chemotaxis plates with two odor point sources, where CTL is the diluent and odor is butanone at a 1:1000 dilution. Each odor point source has NaAz as a paralytic. Animals are plated at the origin. After roaming for at least two hours, the chemotaxis index (CI) can be calculated, which is the number of animals at the CTL arena (indicated by a black box on the left) subtracted from the number at the odor arena (black box on the right), divided by the total number of worms, not counting any worms at the origin. The higher the CI, the more attracted the worms are to the butanone.

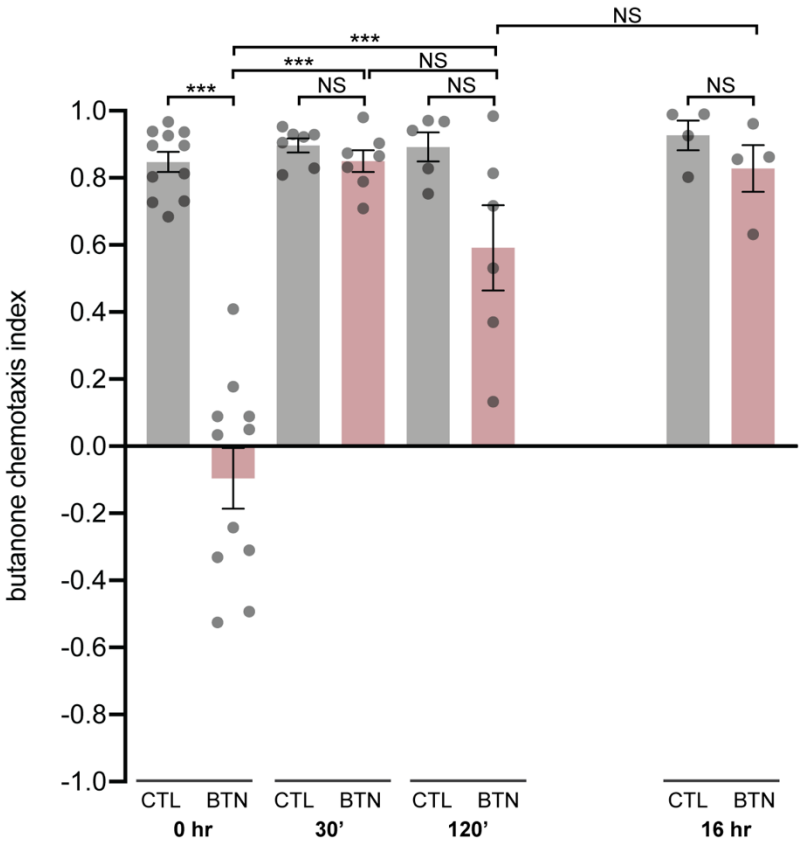

Figure 2.S2. Related to Figure 2.1. One cycle of butanone training induces memory that is lost only after 30 minutes of recovery on food.
Chemotaxis indices of animals conditioned for 80 minutes to CTL (light gray bars with gray dots) or BTN (light red bars with gray dots) after 0 hr, 30', 120', or 16 hr of recovery on food. One-way ANOVA was performed ($P<0.0001$), followed by the Bonferroni correction for multiple comparisons for CTL vs BTN 0 hr, CTL vs BTN 30', CTL vs BTN 120', CTL vs BTN 16 hr, BTN 0 hr vs BTN 30', BTN 0 hr vs BTN 120', BTN 30' vs BTN 120', and BTN 120' vs BTN 16 hr.

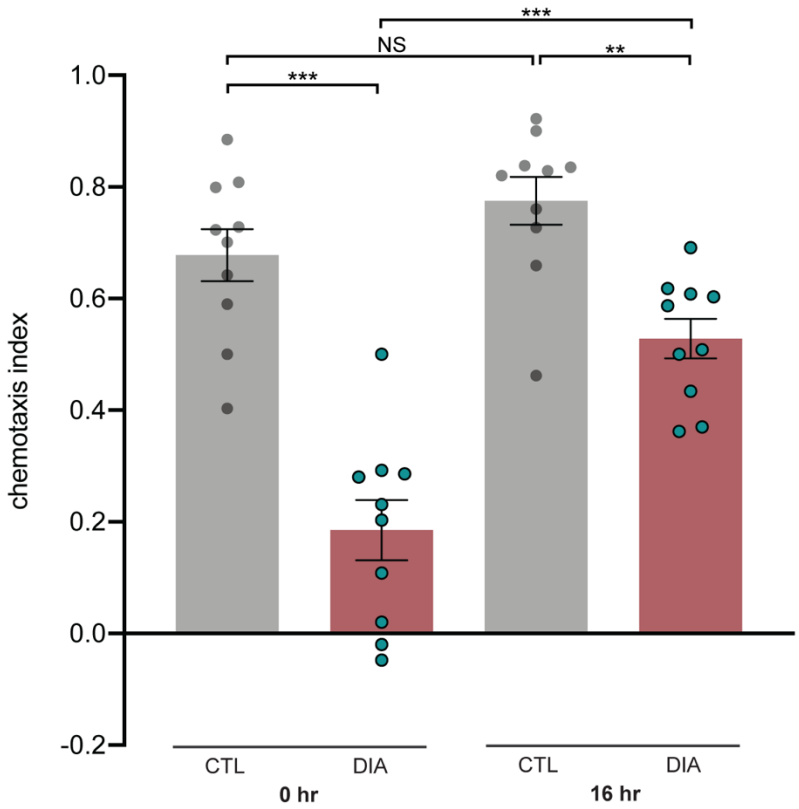

Figure 2.S3. Related to Figure 2.1. *C. elegans* can acquire and maintain memory of the AWA-sensed odorant diacetyl. Chemotaxis indices of animals spaced-trained to CTL or diacetyl (DIA, red bars with teal dots) after 0 hr or 16 hr of recovery on food. One-way ANOVA was performed ($P<0.0001$), followed by the Bonferroni correction for multiple comparisons for CTL vs DIA 0 hr, CTL 0 hr vs CTL 16 hr, DIA 0 hr vs DIA 16 hr, and CTL vs DIA 16 hr.

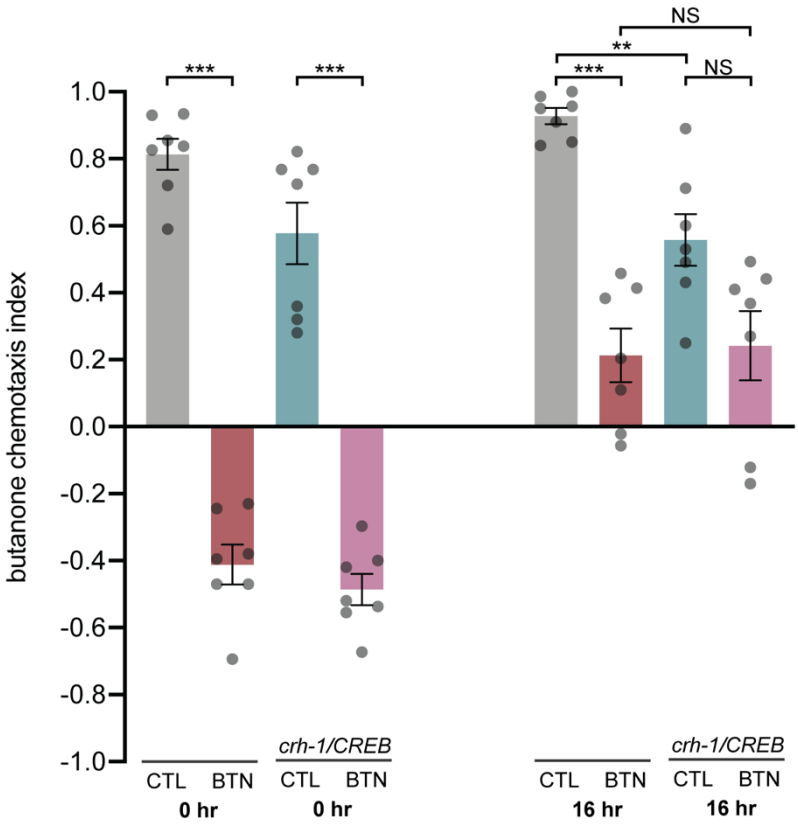

Figure 2.S4. Related to Figure 2.1. CREB mutants acquire butanone memory, but may not maintain it 16 hours post recovery on food.
Chemotaxis indices of wild-type or *crh-1(tz2)/CREB* animals spaced-trained to CTL or BTN (where teal bars with gray dots are CTL *crh-1/CREB* and pink bars with gray dots are BTN *crh-1/CREB*) after 0 hr and 16 hr of recovery on food. The t-test was performed on CTL vs BTN 0 hr, *crh-1/CREB* CTL vs *crh-1/CREB* BTN 0 hr, CTL vs BTN 16 hr, and BTN vs *crh-1/CREB* BTN 16 hr. The u-test was performed on *crh-1/CREB* CTL vs *crh-1/CREB* BTN 16 hr, and CTL vs *crh-1/CREB* CTL 16 hr.

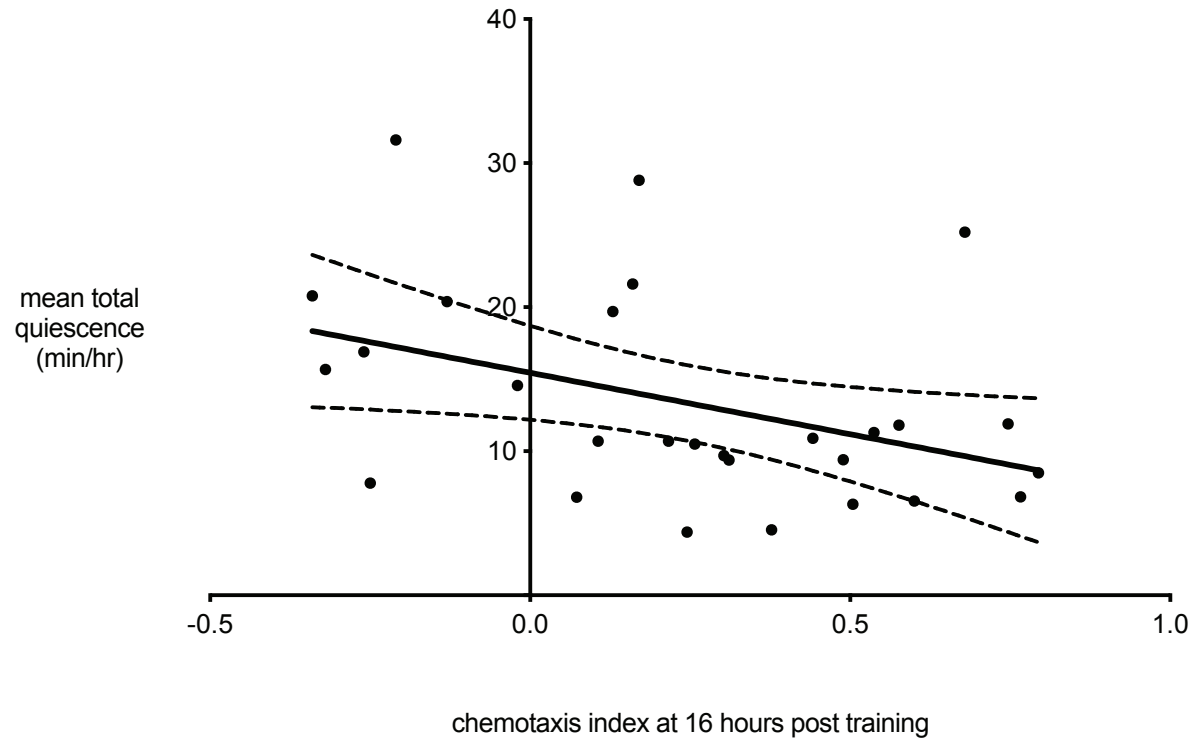

Figure 2.S5. Related to Figure 2.4. Mean total quiescence post training slightly correlates with maintaining the butanone memory 16 hours later.
Correlation analysis was performed between the percentage of animals in a population that sleep during the hour post training and their odor memory 16 hours after training. Sleep was assessed by the high throughput WorMotel analysis as mean total quiescence in minutes per hour, and the memory was assessed by the chemotaxis index of worms trained the same day as the WorMotel analysis after 16 hours of recovery on food. Populations of animals were assayed on independent days. Each dot represents N = 24 animals for mean total quiescence and 400>N>50 for chemotaxis index assays. The Spearman's correlation test was performed (for non-normally distributed data), with r = -0.3914 and *P<0.05.

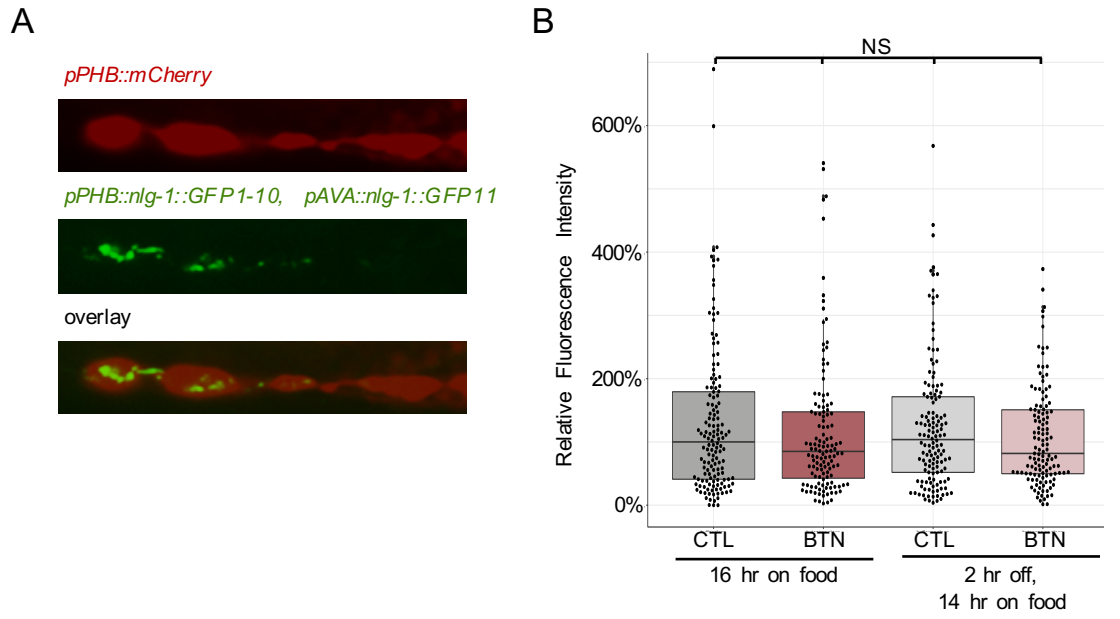

Figure 2.S6. Related to Figure 2.7. PHB-AVA synapses are not significantly different among butanone-trained and buffer-trained animals whether or not they are allowed to sleep.
(A) Schematic and micrographs of a buffer-trained animal carrying the PHB-AVA NLG-1 GRASP marker with the PHB neurons labeled with the red cytosolic mCherry fluorophore. Synaptic fluorescence is observed in a punctate pattern across the region of PHB-AVA axon overlap.
(B) Quantification of PHB-AVA NLG-1 GRASP fluorescence intensity in animals trained with buffer (CTL) or butanone (BTN) and recovered on food for 16 hours, or trained with buffer or butanone and recovered off food for the first two hours, then transferred to plates with food for the following 14 hours. NS, not significant, $p>0.05$, Kruskal-Wallis test.

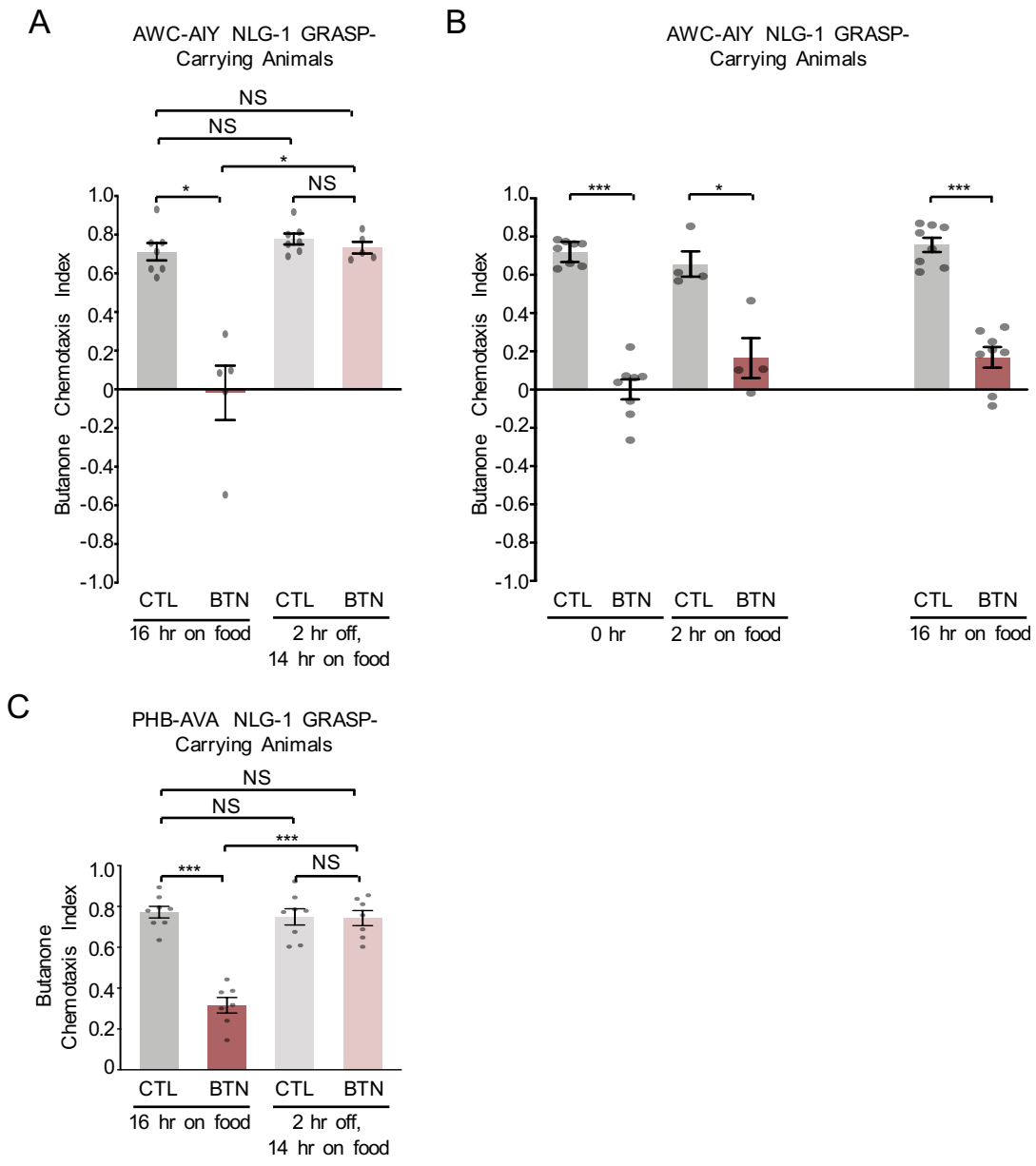

Figure 2.S7. Related to Figure 2.7. Chemotaxis indices for animals carrying NLG-1 GRASP markers.

(A) Chemotaxis indices of AWC-AIY NLG-1 GRASP-carrying animals trained for Figure 7E. Butanone-trained animals that recovered on food for 16 hours have significantly lower chemotaxis indices than similarly treated buffer-trained animals.

(B) Chemotaxis indices of AWC-AIY NLG-1 GRASP-carrying animals trained for Figure 7F. Butanone-trained animals at each timepoint have significantly lower chemotaxis indices than similarly treated buffer-trained animals.

(C) Chemotaxis indices of PHB-AVA NLG-1 GRASP-carrying animals trained for Figure S7. Butanone-trained animals that recovered on food for 16 hours have significantly lower chemotaxis indices than similarly treated buffer-trained animals. *** $P<0.001$, * $P<0.05$, NS not significant $P>0.05$, t-test, followed by the Hochberg method.

KEY RESOURCES TABLE

REAGENT or RESOURCE	SOURCE	IDENTIFIER
Bacterial and Virus Strains		
OP50 *E. coli*	Caenorhabditis Genetics Center	OP50
Chemicals, Peptides, and Recombinant Proteins		
2-butanone	Sigma-Aldrich	360473
Sodium azide 99%	Fisher Scientific, Sigma-Aldrich	ICN10289180, S2002
Benzaldehyde	Sigma-Aldrich	B1334
Diacetyl/2,3-butanedione	Sigma-Aldrich	B85307
Levamisole	Acros Organics	AC187870100
BDM	Fluka Analytical	31550/2003485
Tween 20 detergent	Millipore	655204
NaCl	Fisher Chemical	S671-10
Potassium phosphate dibasic	Fisher Scientific	S375-500
Potassium phosphate monobasic	Sigma-Aldrich	P285
Bacto agar	Difco	90000-762
Calcium chloride	Sigma-Aldrich	C8106
Magnesium sulfate	Sigma-Aldrich	M7506
Low melting point agarose	Apex Chemicals and Reagents/Genesee	20-104
Bacto peptone	Difco	DF0118-07-2
Cholesterol	Sigma-Aldrich	C3045
PDMS/ Dow Corning Sylgard 184 Silicone Encapsulant	Ellsworth Adhesives	4019862
Soil Moist granules	JRM Chemical Inc.	N/A
95% Ethanol	Fisher Scientific	A405P-4
Agarose	Fisher Scientific	BP1356-500
Experimental Models: Organisms/Strains		
wild-type Bristol N2 var.	Caenorhabditis Genetics Center (CGC)	N2
unc-119; goeIs240 [$_p$hsp-16.2::flp-11::SL2::mKate2::unc-54 3'UTR + unc-119 (+)]	CGC	*$_p$HS::flp-11;* strain name: HBR1021
peIs578 ($_p$npr-9::casp1; $_p$unc-122::mCherry; $_p$npr-9::venus)	Iino lab	AIB kill; strain name: JN578
ttx-3(ks5) X	CGC	AIY kill strain

KEY RESOURCES TABLE

REAGENT or RESOURCE	SOURCE	IDENTIFIER
Experimental Models: Organisms/Strains		
ttx-3(ks5) X; peIs578 ($_p$npr-9::casp1; $_p$unc-122::mCherry; $_p$npr-9::venus)	This study	AIB, AIY double kill; strain name: JZ2008
crh-1(tz2) III	CGC	*crh-1/CREB*; strain name: YT17
wyIs155 ($_p$gpa-6::nlg-1::GFP1-10; $_p$flp-18::nlg-1::GFP11; $_p$nlp-1::mCherry; $_p$flp-18::mCherry; $_p$odr-1::DsRedII) X	This study	PHB-AVA NLG-1 GRASP; strain name: MKV1058
iyIs35 ($_p$ttx-3::nlg-1::GFP1-10; $_p$odr-1::nlg-1::GFP11; $_p$odr-1::DsRedII; $_p$unc-122::RFP) III	This study	AWC-AIY NLG-1 GRASP; strain name: MKV1022
pyIs701($_p$str-2::GCaMP3; $_p$ofm-1::GFP; $_p$ceh-36::mCherry)	This study	$_p$*AWC^{ON}::GCaMP3*; strain name: JZ1795
Oligonucleotides		
MVP578: TTGCATGCCTGCAGGTCG	This study	Forward primer used to generate $_p$*odr-1::nlg-1::GFP11*
MVP581: GACTGGCGCGCCTACCTTTGGGTCCTTTGGC	This study	Reverse primer used to generate $_p$*odr-1::nlg-1::GFP11*
Recombinant DNA		
$_p$*ttx-3::nlg-1::GFP1-10*	Feinberg et al., 2008	Used to generate *iyIs35*
$_p$*odr-1::nlg-1::GFP11*	This study	Used to generate *iyIs35*
$_p$*odr-1::DsRedII*	(L'Etoile and Bargmann, 2000)	Used to generate *iyIs35*
$_p$*unc-122::RFP*	(Loria et al., 2004)	Used to generate *iyIs35* and *wyIs155*
$_p$*gpa-6::nlg-1::GFP1-10*	(Park et al., 2011)	Used to generate *wyIs155*
$_p$*flp-18::nlg-1::GFP11*	(Park et al., 2011)	Used to generate *wyIs155*
$_p$*nlp-1::mCherry*	(Park et al., 2011)	Used to generate *wyIs155*

KEY RESOURCES TABLE

REAGENT or RESOURCE	SOURCE	IDENTIFIER
Recombinant DNA		
$_{p}$*flp-18::mCherry*	(Park et al., 2011)	Used to generate *wyIs155*
Software and Algorithms		
Prism 8	Graphpad	https://www.graphpad.com/scientificsoftware/prism/
ImageJ	NIH	https://imagej.nih.gov/ij/download.html
Fiji	Fiji contributors	https://imagej.net/Fiji
RStudio	RStudio	https://www.rstudio.com/products/rstudio/#Desktop
Axiovision	Zeiss	https://www.zeiss.com/microscopy/us/products/microscope-software/axiovision.html
Multi-Worm Tracker	Rex Kerr	https://sourceforge.net/projects/mwt/
Matlab	MathWorks	https://www.mathworks.com/products/matlab.html
μmanager	Ron Vale lab	https://micro-manager.org/wiki/Download%20Micro-Manager_Latest%20Release
Irfanview	Irfan Škiljan	https://download.cnet.com/IrfanView/
ARDUINO 1.8.9	Arduino	https://www.arduino.cc/en/Main/Software
Arduino_blink_buzz	This study	www.GitHub.com/letoilelab
KS_analysis_CFY_Jan2019.m	This study	https://github.com/cfangyen/LEtoile_WorMotel
MC_QuiescenceActivity_v1202.fig	This study	https://github.com/cfangyen/LEtoile_WorMotel

MATERIALS AND METHODS

Experimental model and subject details

C. elegans strain cultivation

All *C. elegans* worms were reared according to standard protocols (Stiernagle, 2006). All strains were raised and tested at 20°C. Animals were raised on 10 cm NGM plates seeded with OP50 *E. coli.* All assays were conducted with one-day old adult worms, unless noted as two day-old adults in the figure legends. All strains used in this study are listed in the Key Resources Table. The JZ2008 AIB and AIY double kill strain (*ttx-3(ks5) X; peIs578(*$_p$*npr-9::casp1;* $_p$*unc-122::mCherry;* $_p$*npr-9::venus)* was made by mating the *FK134/ttx-3(ks5) X* strain with the *; peIs578(*$_p$*npr-9::casp1;* $_p$*unc-122::mCherry;* $_p$*npr-9::venus)* strain from the CGC and the Iino lab, respectively. Other transgenic strains generated for this study are *iyIs35 (*$_p$*ttx-3::nlg-1::GFP1-10* (Feinberg et al., 2008) (70ng/µl)*,* $_p$*odr-1::nlg-1::GFP11* (see below for generation) (40ng/µl)*,* $_p$*odr-1::DsRedII* (L'Etoile and Bargmann, 2000) (5ng/µl) and $_p$*unc-122::RFP* (Loria et al., 2004) (20ng/µl)) and *wyIs155 (*$_p$*gpa-6::nlg-1::GFP1-10* (Park et al., 2011) (60 ng/µl), $_p$*flp-18::nlg-1::GFP11* (Park et al., 2011) (30 ng/µl)*,* $_p$*nlp-1::mCherry* (Park et al., 2011) (10 ng/µl), $_p$*flp-18::mCherry* (Park et al., 2011) (5 ng/µl) and $_p$*odr-1::DsRedII* (20 ng/µl))*.* Constructs were generated using standard molecular techniques. To generate $_p$*odr-1::nlg-1::GFP11,* the *odr-1* promoter was amplified from $_p$*odr-1::DsRedII* (L'Etoile and Bargmann, 2000) using $_p$*odr-1*-specific primers (MVP578: TTGCATGCCTGCAGGTCG, which has an internal SphI site and MVP581: GACTGGCGCGCCTACCTTTGGGTCCTTTGGC, which introduces an AscI site)*.* Then,

the $_p$*odr-1* fragment was subcloned into the SphI-AscI fragment from *nlg-1::GFP11* (Park et al., 2011).

Method Details

Chemotaxis assay

To prep worms for behavior, we picked 4-5 larval stage 4 (L4) animals onto 10cm NGM plates seeded with OP50 *E. coli* and grew them up for 5 days at 20°C when worms were one-day old adults. It is critical that the strains be completely clean with no fungal and bacterial contamination of any kind.

For single-cycle odor training (performed in Figure 2.S2), the adult worms were washed with S. basal buffer (0.1M NaCl, 0.05M K_3PO_4, pH 6.0) off of 10 cm NGM plates and into tubes, where they were washed three times with S. basal buffer. The animal population was split in half where one half was soaked in S. basal and the other half was soaked in a 1:10,000 dilution of butanone or diacetyl in S. basal buffer. Animals were rotated in tubes on a rotisserie for 80 minutes, where they were then washed an additional three times in S. basal.

Chemotaxis plates were made as following: for 100 mL of media, we added 100 mL ddH_2O into a flask with 1.6 g of Difco agar, agar agar, or bacto agar, boiled it in the microwave until dissolved, added a magnetic stir bar and stirred until cooled to 50-55°C, then added 500 uL of 1M K_3PO_4, 100 uL 1M $CaCl_2$ and 100 uL 1M $MgSO_4$. We Pipetted 10 mL of media into 10 cm plastic petri dishes and let it cool to solidify. We drew assay plate guides as shown in Figure S1. We put 1 uL of (M) NaN_3 onto the middle of the

odor and diluent arenas, let it dry, and then added 1 uL of 200 proof ethanol to the diluent (control) arena and for the odor point sources, added 1 uL:1000 uL butanone to ethanol, or 1 uL:1000 uL diacetyl to ethanol, or 1 uL:200 uL benzaldehyde to ethanol, to the odor arena. When plating animals after three cycles of training, we did two washes with S. basal and then a third wash with ddH_2O (to prevent worms from staying at the origin of the chemotaxis plate, since they are attracted to the salt in S. basal). We plated animals at the origin of the plate (bottom) and wicked away any excess moisture with a Kim Wipe, being careful not to cause any gouges in the agar to prevent burrowing. We put 50-400 worms on the origin and wicked up any moisture, and then let them roam at least 2 hours and calculated chemotaxis indices.

To calculate a chemotaxis index, after at least two hours of roaming on the plate, we counted how many worms were within the odor arena, subtracted from that number the number of worms at the diluent (200 proof ethanol) arena, and then divided that by the total number of worms on the plate that were not at the origin.

LTM chemotaxis assay

The single-worm odor training protocol from above was used, but there are three x 80-minute buffer or odor treatment cycles with two x 30-minute bacteria recovery periods in between. After the first 80-minute training cycle, the bacteria recovery period was performed. First, to make the concentrated bacteria, 100 mL of LB was seeded with OP50 and was shaken overnight at 37°C at 250 RPM until it reached an OD of 10 and then centrifuged at 4000 RPM for 15-30 minutes and then the pellet(s) was resuspended in 37-38 mL of S. basal buffer. Next, 1000 uL of concentrated OP50 was

added to the tubes and rotated for 30 minutes, which completes one cycle of recovery post one cycle of buffer or odor treatment. We repeated the buffer or odor treatment cycle, followed by one more cycle of recovery with OP50, then a third treatment cycle, and then washed and put worms on chemotaxis plates as described under the chemotaxis plates protocol above.

For overnight recovery animals, we washed part of the population onto 5.5 cm OP50-seeded NGM plates and kept them at 20°C for 16 hours, before washing three times and plating. For recovery periods different from 16 hours, we washed them onto seeded (or unseeded for the sleep assay) plates for whatever time was desired (e.g. 30 minutes or 2 hours).

LTM NLG-1 GRASP assays

The training paradigm described above was modified to accommodate NLG-1 GRASP imaging. Approximately 30 plates of worms were prepared to allow enough worms for multiple batches and imaging. Worms were divided into four batches that began training 40 minutes apart. Batches 1 and 3 were given the buffer treatment, while batches 2 and 4 were trained in the odor solution.

LTM NLG-1 GRASP 16-hour assay: After three cycles of training (described above), half the worms from each batch were placed on seeded plates, and half were placed on unseeded plates, then transferred to seeded plates after two hours. All plates were incubated at 20°C until 16 hours post-training, when worms were washed (as described above). 20 worms from each of the 8 batches were anesthetized and imaged using a Zeiss Axio Imager.A1 compound fluorescent microscope and Axiovision

software (see “Synapse Imaging and Analysis” below), and 50-400 worms from each of the 8 batches underwent the butanone chemotaxis assay.

LTM NLG-1 GRASP 0-hour, 2-hour, and 16-hour assay: After three cycles of training, worms from batches 1-4 were each divided into three groups so that imaging and chemotaxis experiments could be performed at three timepoints: 0 hours post-training, 2-hours post-training, and 16-hours post-training.

0-Hour Imaging and Chemotaxis: After training, worms from all four batches were washed (as described above). From each batch, ~20 worms were separated, anesthetized, and imaged under the Zeiss Axio Imager.A1 compound fluorescent microscope and Axiovision software (see “Synapse Imaging and Analysis” below), and 50 to 400 worms were assessed for butanone chemotaxis.

Two-Hour Imaging and Chemotaxis: After training, worms from batches one and two were each placed on seeded NGM plates. After two hours, animals were washed as described above. 20 animals from each of these batches were anesthetized and imaged (see “Synapse Imaging and Analysis” below), and 50 to 400 worms from each of these batches were assessed for butanone chemotaxis.

16-Hour Imaging and Chemotaxis: After training, worms from batches one, two, three, and four were each placed on seeded NGM plates. After 16 hours, animals were washed as described above. 20 animals from each of these batches were anesthetized and imaged (see “Synapse Imaging and Analysis” below), and 50 to 400 worms from each of these batches were assessed for butanone chemotaxis.

WorMotel making and analysis

To make the WorMotel (Churgin et al., 2017), we used a PDMS chip with 48 total wells made according to the paper or the online resource (http://fangyenlab.seas.upenn.edu/links.html). Next, we made 100 mL NGM by adding together 2.1 g low melting-point agarose, 0.3 g NaCl, 0.25 g bacto peptone, and 3 uL tween 20 (to keep a flat agar surface). We boiled the media in the microwave, cooled it down to ~50-58°C, then added 100 uL $CaCl_2$, 100 uL cholesterol dissolved in EtOH, 100 ul $MgSO_4$, and 2.5 mL K_3PO_4. We next added 10 uL/well of chip, putting the pipet tip inside the well to avoid bubbles. We did this fast because the chip may dry and crack. About 10-30 minutes after adding the agarose, we added 5 uL of OP50 (same as the concentrated bacteria used for recovery in the training paradigm). It takes about 1-2 hours for the bacteria to dry at room temp, depending on the humidity. We made a humidity chamber for the WorMotel by adding 0.1 g of gel soil (we used Soil Moist granules) with 15 mL water to a 10 cm plastic Petri dish (it takes about 30 min until the soil is properly hydrated). You can re-use the humidity chamber by adding the correct amount of water to come back up to the right weight as before.

We picked one worm per well onto the WorMotel. We used the left 4 x 6 wells loaded with our control worms and the right 4 x 6 wells loaded with our experimental group for ease of analysis. We waited 15 min after picking worms on to the WorMotel for them to settle. The lid was kept on the chamber whenever possible to prevent the agarose from cracking to prevent worms from burrowing. Fogging often occurs, so we would rub either Tween 20 or anti-fog lens cleaner for eyeglasses (we like Cat Crap brand) on the dish lid before imaging.

The camera we used to acquire images was a Teledyne Dalsa PT-21-04M30 Camera Link Camera (Dalsa Proprietary Sensor 2352x1728 Resolution Area Scan Camera) attached with a Linos Rodagon Modular-Focus lens (f = 60mm) attached. We used a four-piece metal post imaging stand with a plastic stage, but any imaging stand will do as long as the imaging distance allows you to see the whole WorMotel with the camera. We used a red LED light stand to illuminate all around the WorMotel for imaging (we specifically used 2-inch long 4 x 6 LED strips and 5-inch long 4 x 12 LED strips (from www.Oznium.com) in a two-concentric square formation. We used a T175 tissue culture flask filled entirely with water added to as the cooling chamber as a buffer against the heat generated by the red LED lights. We put the flask on top of LED stand. We had an imaging setup closed off from any light interruptions (we used black curtains).

We used the Multiple-Worm Tracker (MWT 1.3.0r1041) made by Rex Kerr. Hit “use selected import source,” go to “Raw Image” in pull-down menu, change “experiment duration” to 3600 seconds (1hr) or whatever time is desired. We would make a new folder in icon below “experiment duration” and name files in box below (e.g. name and date). Then, we put 3 as “raw image save interval” (1 image every 3 sec). Next, you would hit the green “Go” button. PNG files were then generated.

We renumbered the PNG files (we used Irfanview for Windows developed by Irfan Škiljan to rename our files “image####” to use with our Matlab script). We analyzed images with Matlab script “KS_analysis_CFY_Jan2019.m” and used the GUI “MC_QuiescenceActivity_v1202.fig,” which are available online at https://github.com/cfangyen/LEtoile_WorMotel.

Once images were renumbered, we used Matlab and typed “guide” into the command window to launch the GUI “MC_QuiescenceActivity_v1202.fig” to open GUI (to segment images into one file). Next, we pressed the “play” button and then pressed “load images” and then “process images.” We opened the first image (e.g. “image0001”) into the GUI. We followed the GUI listed instructions, which tells you to click in the middle of the well/room on the top left, then the top right, then the bottom left, and then the bottom right (in a “Z” pattern) to define the motel size and position. Then, clicked on one representative well at the top left and the top right to define the well/room sizes. We edited the parameters by putting image 1 to the last number minus 1 (e.g. if 1181 images, we had it go from 1 to 1180). We set the threshold (we used about 0.25-0.3, but check if it looks good (should see worms marked in white with not too much background white noise). We then saved the file and then ran it.

Once finished processing, we saved the file as the same file name we created before running it and replaced it with the new one (if desired to avoid confusion, but you can also keep them as separate files). We then opened the script “KS_analysis_CFY_Jan2019.m” in Matlab. We clicked in the first cell and ran it and then opened the processed type file we just created. Next, we clicked in the second cell and ran it to run the analysis and produce the raster map figures. The output gives you the KS analysis graphs for total quiescence on top and the longest quiescence graph on the bottom, with the KS test P value reported at the top of each graph. It will also output Excel files with Group 1 being the control worm quiescence (in minutes) values (assuming your control group was loaded to the left 4 x 6 wells), with the left column as total quiescence and the right column being longest quiescence bout (in minutes) and

Group 2 being the experimental group (assuming the experimental group was loaded to the right 4 x 6 wells). The Group 1 quiescence map is on top and the Group 2 (experimental group) map is on the bottom, where blue marks quiescence over time and yellow marks movement (movement in 30 seconds). You will also get the blue heatmaps and the yellow and blue raster plots (without the graphs in the same figures) as output. We saved these as .fig files to open in Matlab and also as .png files to open it with any picture preview program

Pharyngeal Pumping Assay

This assay was performed by standard methods (Raizen et al., 2012). To perform the assay, we watched the pharynx of a worm under a stereomicroscope at 40-50X magnification and once the grinder in the terminal bulb does one complete contraction and relaxation, or "pump," we counted that as one pump, using a counter to count every time they complete a full pump for 10 seconds. Then, we disposed of the worm to prevent re-counting of the same animal. We took the number of pumps completed and multiplied that by 6 to find the pharyngeal pumping rate in pumps per minute.

Quiescence disruption

We assessed animal responsiveness to a stimulus which has been previously shown to disrupt quiescence in *C. elegans* (Nagy et al., 2014). Specifically, 3.5 or 5.5cm NGM plates seeded with OP50 with 20-30 worms were placed on a 50mm piezo 1.2KHZ piezo buzzer elements (Digikey #668-1190-ND). Piezo elements were supplied

with 5V with a 50% pulse-width modulated duty cycle using an Arduino-style microcontroller and its accompanying software, using the code named "Arduino_blink_buzz" accessible at www.GitHub.com/letoilelab. Stimulus onset was synchronized with video recording by flashing a blue LED, used at the maximum light intensity (we used Digikey #1528-2334-ND) at a distance of about 10 cm during video recording. In cases where animals were exposed to prolonged stimulation, animals were subjected to blocks of stimulation for 5 minutes with the blue light flashing for 1 second every 20 seconds, followed by no stimulation for 5 minutes. Videos were recorded on an Imaging Source DMK 23GP031 camera using Micromanager software (Edelstein et al., 2014).

Heat-shock assay

C. elegans animals were heat shocked at 37°C for 5 minutes in a water bath while on 5.5 cm unseeded NGM plates covered in parafilm. After the heat shock, animals were put at 20°C until behavior was assessed by the chemotaxis assay.

Calcium imaging

Calcium imaging of the AWC^{ON} neuron was performed on lines expressing the genetically-encoded calcium indicator GCaMP3 (Tian et al., 2009) under the *str-2* promoter (*JZ1795/pyIs701(*$_p$*str-2::GCaMP3;* $_p$*ofm-1::GFP;* $_p$*ceh-36::mCherry)*). One-day-old adult worms were conditioned to either buffer or 1.23 mM butanone diluted in S-basal buffer (the same concentration as used for the butanone conditioning mentioned in "Chemotaxis assay") during three, 80-minute training cycles (interspersed) with

feeding (described in “LTM chemotaxis assay”). Immediately after the end of the third training cycle or after a 16-hour overnight recovery on food, worms were rinsed three times in S-basal buffer and loaded into a custom, polymer polydimethylsiloxane (PDMS) microfluidic device (Chronis et al., 2007). The nose of the animal was exposed to liquid streams of either S-basal buffer or 1.23 mM butanone. A manual switch attached to a solenoid valve was used to direct the buffer or odor stream across the nose of the worm. The stimulation protocol consisted of exposing worms to S-basal buffer for 30 seconds followed by a 30 second exposure to 1.23 mM butanone (odor on) or by exposing worms to 1.23 mM butanone for 30 seconds followed by a 30 second exposure to S-basal buffer (odor off). Fluorescence was monitored with a Zeiss 40X air objective on an inverted microscope (Zeiss Axiovert 200). Images were taken at rate of 2Hz with a blue light exposure time of 100 ms using an ORCA-Flash 2.8 camera (Hamamatsu).

Synapse imaging

A Zeiss Axio Imager.A1 compound fluorescent microscope (Figures 2.7E and 2.7F, and Figure 2.S6) and a Zeiss LSM710 confocal microscope (Figure 2.7C and 2.7D) were used to capture images of live *C. elegans* under 630X magnification. Worms were anesthetized on 2% agarose pads using a 2:1 ratio of 0.3 M 2,3-butanedione monoxime (BDM) and 10 mM levamisole in M9 buffer. All micrographs taken were of one-day old and two-day old gravid adults.

Quantification and statistical analysis

Behavioral analysis

Statistics were performed using Graphpad Prism 8 and RStudio. P values are used for the statistical readouts, with the following notations: NS is $P>0.05$, $*P<0.05$, $**P<0.01$, and $***P<0.001$. All data included in the same graph were analyzed for type of data distribution with the Shapiro-Wilk normality test. If datasets were normally distributed, then one-way ANOVA was used for multiple comparisons, followed by Bonferroni correction. If the datasets were non-parametric, then the Kruskal-Wallis test was used to analyze variance, followed by pairwise comparisons using the Student's unpaired two-tailed t-test for normally distributed datasets or the Mann-Whitney two-tailed u-test for non-normally distributed data. Then, to correct for Type I error, the Hochberg test was run on P values compared in the same graph to adjust the P values for multiple comparisons, which often conservatively increases P values to avoid incorrectly rejecting the null hypothesis. For graphs with only two datasets to compare, the Shapiro-Wilk test was performed, followed by the t-test or u-test, depending on the distribution of the datasets. For correlation data, the Shapiro-Wilk normality test was run, followed by the Spearman's correlation test. S.E.M. was calculated and shown on each graph, except in Figure 2.4C where S.D. was used and in Figure 2.5 where none was shown. The total number of trials is represented by dots on every graph. Specific statistical tests used for each graph in the manuscript are included in the figure legends.

Mean total quiescence analysis

For analyzing quiescence, the total quiescence in minutes was taken from each data set (analyzed with our Matlab script) and the mean was taken for each data set.

Quiescence disruption analysis

Videos were scored manually and blinded to experimental treatment. At least two individuals scored each video. After scoring, the measured variables were ranked and averaged across rank to derive a population of scores per video. Specifically, we looked at how many frames passed until the animal completed its first complete sinusoidal bend and how many sinusoidal bends were completed within a set number of frames, both post one second of blue light with constant buzzing treatment. We did not distinguish between forward or backward crawling.

Calcium imaging analysis

Fiji software was used with the Multi Measure plugin to analyze the images. In animals expressing the GCaMP3 reporter in the AWC^{ON} neuron (*JZ1795/pyIs701(*$_p$*str-2::GCaMP3;* $_p$*ofm-1::GFP;* $_p$*ceh-36::mCherry)*), the ROI was established at the center of the AWC cell body. A background ROI was also taken, just outside of the animals. Then, the mean fluorescence intensity at the background ROI was subtracted from the mean fluorescence intensity at the cell body ROI and that serves as the "F" values. The fluorescence intensity of the GCaMP3 reporter in the first three images is defined as F_0. Delta F is the F_0 value subtracted from each F value. For every worm imaged, the mean of the delta F_0/F (%) values is taken from the 10 seconds before and after the BTN is

turned on or off (i.e. the means at 20-30 seconds and 30.5-40.5 seconds are taken). The delta is then taken between the two means and the absolute value is taken of that number for comparisons between the datasets (e.g. buffer vs butanone-trained cohorts) taken on the same day.

Synapse imaging analysis

NIH ImageJ software (Abràmoff et al., 2004) was used to analyze all micrographs taken for AWC-AIY NLG-1 GRASP phenotypic quantification, as previously described (Park et al., 2011; Varshney et al., 2018). In brief, AWC-AIY NLG-1 GRASP intensity was quantified by measuring fluorescence intensity through circling punctal clusters. In Figure 7E, median intensity values for each treatment were normalized to fluorescence intensity levels for buffer-trained animals that recovered on food for 16 hours. For Figure 7F, median intensity values were normalized to buffer-trained levels taken immediately after training.

PHB-AVA NLG-1 GRASP intensity was also measured through outlining clusters of puncta. Background fluorescence intensity was also taken into account by calculating the value of minimum intensity in the area directly surrounding the puncta. This background intensity value was subtracted from the intensity for each pixel in the punctal cluster, and the adjusted values were added.

NLG-1 GRASP analysis was conducted on all buffer-trained batches that had chemotaxis indices above 0.5 after training. The same criteria were used for butanone-trained batches that recovered off food for two hours. Analysis was also conducted on butanone-trained worms with chemotaxis indices of less than 0.5. Micrographs were

not analyzed if the animals moved during imaging or were damaged in the process of making the slide.

For synapse statistical analysis, the Kruskal-Wallis test was used to analyze variance between treatments, If the P value was less than 0.05, then the Mann-Whitney u-test was used to compare the medians of each pair of groups, followed by the Hochberg multiple comparison procedure.

Data and code availability

The code generated during this study is available at www.github.com/letoilelab for the quiescence disruption protocol and https://github.com/cfangyen/LEtoile_WorMotel for the WorMotel quiescence analysis.

Additional resources

Link to download WorMotel detailed protocol:

http://fangyenlab.seas.upenn.edu/links.html

REFERENCES

Abdou, K., Shehata, M., Choko, K., Nishizono, H., Matsuo, M., Muramatsu, S., and Inokuchi, K. (2018). Synapse-specific representation of the identity of overlapping memory engrams. Science *360*, 1227–1231.

Abràmoff, M.D., Magelhaes, P.J., and Ram, S.J. (2004). Image Processing with ImageJ. Biophotonics International *11*, 36–42.

Acosta-peña, E., Camacho-Abrego, I., Melgarejo-Gutierrez, M., Flores, G., Drucker-Colin, R., and Garcia-Garcia, F. (2015). Sleep deprivation induces differential morphological changes in the hippocampus and prefrontal cortex in young and old rats. Synapse *69*, 15–25.

van Alphen, B., Yap, M.H.W., Kirszenblat, L., Kottler, B., and van Swinderen, B. (2013). A Dynamic Deep Sleep Stage in Drosophila. Journal of Neuroscience *33*, 6917–6927.

Altun-Gultekin, Z., Andachi, Y., Tsalik, E.L., Pilgrim, D., Kohara, Y., and Hobert, O. (2001). A regulatory cascade of three homeobox genes, ceh-10, ttx-3 and ceh-23, controls cell fate specification of a defined interneuron class in C. elegans. Development *128*, 1951–1969.

Appelbaum, L., Wang, G., Yokogawa, T., Skariah, G.M., Smith, S.J., Mourrain, P., and Mignot, E. (2010). Circadian and Homeostatic Regulation of Structural Synaptic Plasticity in Hypocretin Neurons. Neuron *68*, 87–98.

Ardiel, E.L., and Rankin, C.H. (2010). An elegant mind: learning and memory in Caenorhabditis elegans. Learning and Memory *17*, 191–201.

Arun Asok, Leroy, F., Rayman, J.B., and Kandel, E.R. (2019). Molecular Mechanisms of the Memory Trace. Trends in Neurosciences *42*, 14–22.

Bargmann, C.I., and Marder, E. (2013). From the connectome to brain function. Nature Methods *10*, 483–490.

Bargmann, C.I., Hartweig, E., and Horvitz, H.R. (1993). Odorant-selective genes and neurons mediate olfaction in C. elegans. Cell *74*, 515–527.

Beck, C.D.O., Schroeder, B., and Davis, R.L. (2000). Learning Performance of Normal and Mutant *Drosophila* after Repeated Conditioning Trials with Discrete Stimuli. J. Neurosci. *20*, 2944–2953.

Beyaert, L., Greggers, U., and Menzel, R. (2012). Honeybees consolidate navigation memory during sleep. Journal of Experimental Biology *215*, 3981–3988.

Bono, M. de, and Villu Maricq, A. (2005). Neuronal Substrates of Complex Behaviors in C. elegans. Annu. Rev. Neurosci. *28*, 451–501.

de Bono, M., and Maricq, A.V. (2005). Neuronal Substrates of Complex Behaviors in C. elegans. Annual Review of Neuroscience *28*, 451–501.

Brawn, T.P., Nusbaum, H.C., and Margoliash, D. (2018). Sleep-dependent reconsolidation after memory destabilization in starlings. Nature Communications *9*, 3093.

Bushey, D., Tononi, G., and Cirelli, C. (2011). Sleep and Synaptic Homeostasis: Structural Evidence in Drosophila. Science *332*, 1576–1581.

Chalasani, S.H., Chronis, N., Tsunozaki, M., Gray, J.M., Ramot, D., Goodman, M.B., and Bargmann, C.I. (2007). Dissecting a circuit for olfactory behaviour in Caenorhabditis elegans. Nature *450*, 63–70.

Chauvette, S., Seigneur, J., and Timofeev, I. (2012). Sleep oscillations in the thalamocortical system induce long-term neuronal plasticity. Neuron *75*, 1105–1113.

Cho, C.E., Brueggemann, C., L'Etoile, N.D., and Bargmann, C.I. (2016). Parallel encoding of sensory history and behavioral preference during Caenorhabditis elegans olfactory learning. ELife *5*, e14000.

Choi, S., Chatzigeorgiou, M., Taylor, K.P., Schafer, W.R., and Kaplan, J.M. (2013). Analysis of NPR-1 reveals a circuit mechanism for behavioral quiescence in C. elegans. Neuron *78*, 869–880.

Chronis, N., Zimmer, M., and Bargmann, C.I. (2007). Microfluidics for in vivo imaging of neuronal and behavioral activity in Caenorhabditis elegans. Nature Methods *4*, 727–731.

Churgin, M.A., Jung, S.-K., Yu, C.-C., Chen, X., Raizen, D.M., and Fang-Yen, C. (2017). Longitudinal imaging of Caenorhabditis elegans in a microfabricated device reveals variation in behavioral decline during aging. ELife *6*, e26652.

Colbert, H., and Bargmann, C.I. (1995). Odorant-specific adaptation pathways generate olfactory plasticity in C. elegans. Neuron *14*, 803–812.

Cook, S.J., Jarrell, T.A., Brittin, C.A., Wang, Y., Bloniarz, A.E., Yakovlev, M.A., Nguyen, K.C.Q., Tang, L.T.-H., Bayer, E.A., Duerr, J.S., et al. (2019). Whole-animal connectomes of both Caenorhabditis elegans sexes. Nature *571*, 63–71.

Cowansage, K.K., Shuman, T., Dillingham, B.C., Chang, A., Golshani, P., and Mayford, M. (2014). Direct Reactivation of a CoherentNeocortical Memory of Context. Neuron *84*, 432–441.

Diering, G.H., Nirujogi, R.S., Roth, R.R., Worley, P.F., Pandey, A., and Huganir, R.L. (2017). Homer1a drives homeostatic scaling-down of excitatory synapses during sleep. Science *355*, 511–515.

Donlea, J.M., Ramanan, N., and Shaw, P.J. (2009). Use-dependent plasticity in clock neurons regulates sleep need in Drosophila. Science *324*, 105–108.

Dudai, Y., Karni, A., and Born, J. (2015). The Consolidation and Transformation of Memory. Neuron *88*, 20–32.

Durkin, J., and Aton, S.J. (2016). Sleep-Dependent Potentiation in the Visual System Is at Odds with the Synaptic Homeostasis Hypothesis. Sleep *39*, 155–159.

Edelstein, A.D., Tsuchida, M.A., Amodaj, N., Pinkard, H., and Vale, R.D. (2014). Advanced methods of microscope control using μManager software. Journal of Biological Methods *1*, e10.

Estes, W.K. (1955). Statistical theory of distributional phenomena in learning. Psychological Review *62*, 369–377.

Feinberg, E., VanHoven, M.K., Bendesky, A., Wang, G., Fetter, R.D., Shen, K., and Bargmann, C.I. (2008). GFP Reconstitution Across Synaptic Partners (GRASP) Defines Cell Contacts and Synapses in Living Nervous Systems. Neuron *57*, 353–363.

Fox, K., and Stryker, M. (2017). Integrating Hebbian and homeostatic plasticity: introduction. Philosophical Transactions of the Royal Society B *372*.

Gallagher, T., Kim, J., Oldenbroek, M., Kerr, R., and You, Y. (2013). ASI regulates satiety quiescence in C. elegans. The Journal of Neuroscience *33*, 9716–9724.

Gilestro, G.F., Tononi, G., and Cirelli, C. (2009). Widespread changes in synaptic markers as a function of sleep and wakefulness in Drosophila. Science *324*, 109–112.

Gordus, A., Pokala, N., Levy, S., Flavell, S.W., and Bargmann, C.I. (2015). Feedback from network states generates variability in a probabilistic olfactory circuit. Cell *161*, 215–227.

Grosmark, A.D., Mizuseki, K., Pastalkova, E., Diba, K., and Buzsáki, G. (2012). REM Sleep Reorganizes Hippocampal Excitability. Neuron *75*, 1001–1007.

Hadziselimovic, N., Vukojevic, V., Peter, F., Milnik, A., Fastenrath, M., Gabor Fenyes, B., Hieber, P., Fastenrath, P., Vogler, C., de Quervain, D.J.-F., et al. (2014). Forgetting is regulated via Musashi-mediated translational control of the Arp2/3 complex. Cell *156*, 1153–1166.

Hengen, K.B., Torrado Pacheco, A., McGregor, J.N., Van Hooser, S.D., and Turrigiano, G.G. (2016). Neuronal Firing Rate Homeostasis Is Inhibited by Sleep and Promoted by Wake. Cell *165*, 180–191.

Hill, A.J., Mansfield, R., Lopez, J.M.N.G., Raizen, D.M., and Van Buskirk, C. (2014). Cellular stress induces a protective sleep-like state in C. elegans. Current Biology *24*, 2399–2405.

Hilliard, M.A., Bargmann, C.I., and Bazzicalupo, P. (2002). C. elegans Responds to Chemical Repellents by Integrating Sensory Inputs from the Head and the Tail. Current Biology *12*, 730–734.

Hussaini, S.A., Bogusch, L., Landgraf, T., and Menzel, R. (2009). Sleep deprivation affects extinction but not acquisition memory in honeybees. Learning and Memory *16*, 698–705.

Ishihara, T., Iino, Y., Mohri, A., Mori, I., Gengyo-Ando, K., Mitani, S., and Katsura, I. (2002). HEN-1, a Secretory Protein with an LDL Receptor Motif, Regulates Sensory Integration and Learning in Caenorhabditis elegans. Cell *109*, 639–649.

Jackson, C., McCabe, B.J., Nicol, A.U., Grout, A.S., Brown, M.W., and Horn, G. (2008). Dynamics of a Memory Trace: Effects of Sleep on Consolidation. Current Biology *18*, 393–400.

Jan Born, and Feld, G.B. (2012). Sleep to Upscale, Sleep to Downscale: Balancing Homeostasis and Plasticity. Neuron *75*, 933–935.

Kandel, E.R. (2012). The molecular biology of memory: cAMP, PKA, CRE, CREB-1, CREB-2, and CPEB. Mol Brain *5*, 14.

Kaufmann, A.L., Ashraf, J.M., Corces-Zimmerman, R., Landis, J.N., and Murphy, C.T. (2010). Insulin Signaling and Dietary Restriction Differentially Influence the Decline of Learning and Memory with Age. PLOS Biology *8*, e1000372.

Kimura, Y., Corcoran, E.E., Eto, K., Gengyo-Ando, K., Muramatsu, M. -a., Kobayashi, R., Freedman, J.H., Mitani, S., Hagiwara, M., Means, A.R., et al. (2002). A CaMK cascade activates CRE-mediated transcription in neurons of Caenorhabditis elegans. EMBO Reports *3*, 962–966.

Kochanek, K.D., Murphy, S.L., Xu, J., and Arias, E. (2017). Mortality in the United States, 2016. NCHS Data Brief (CDC) 8.

Kreutzmann, J.C., Havekes, R., Abel, T., and Meerlo, P. (2015). Sleep deprivation and hippocampal vulnerability: changes in neuronal plasticity, neurogenesis and cognitive function. Neuroscience *309*, 173–190.

Lakhina, V., Arey, R.N., Kaletsky, R., Kauffman, A., Stein, G., Keyes, W., Xu, D., and Murphy, C.T. (2015). Genome-wide Functional Analysis of CREB/Long-Term Memory-Dependent Transcription Reveals Distinct Basal and Memory Gene Expression Programs. Neuron *85*, 330–345.

Lee, D.A., Andreev, A., Truong, T.V., Chen, A., Hill, A.J., Oikonomou, G., Pham, U., Hong, Y.K., Tran, S., Glass, L., et al. (2017). Genetic and neuronal regulation of sleep by neuropeptide VF. ELife *6*, e25727.

Lenz, O., Xiong, J., Nelson, M.D., Raizen, D.M., and Williams, J.A. (2015). FMRFamide signaling promotes stress-induced sleep in Drosophila. Brain, Behavior, and Immunity *47*, 141–148.

L'Etoile, N.D., and Bargmann, C.I. (2000). Olfaction and Odor Discrimination Are Mediated by the C. elegans Guanylyl Cyclase ODR-1. Neuron *25*, 575–586.

Li, Z., Liu, J., Zheng, M., and Xu, X.Z.S. (2014). Encoding of Both Analog- and Digital-like Behavioral Outputs by One C. elegans Interneuron. Cell *159*, 751–765.

Lin, M.-S., Xiong, W.-C., Li, S.-J., Gong, Z., Cao, X., Kuang, X.-J., Zhang, Y., Gao, T.-M., Mechawar, N., Liu, C., et al. (2017). α2-glycine receptors modulate adult

hippocampal neurogenesis and spatial memory: α2-GlyRs Modulate Adult Hippocampal Neurogenesis. Devel Neurobio *77*, 1430–1441.

Liu, Z.-W., Faraguna, U., Cirelli, C., Tononi, G., and Gao, X.-B. (2010). Direct evidence for wake-related increases and sleep-related decreases in synaptic strength in rodent cortex. JNeurosci *30*, 8671–8675.

Lonze, B.E., and Ginty, D.D. (2002). Function and Regulation of CREB Family Transcription Factors in the Nervous System. Neuron *35*, 605–623.

Loria, P.M. (2004). A Conserved Postsynaptic Transmembrane Protein Affecting Neuromuscular Signaling in Caenorhabditis elegans. Journal of Neuroscience *24*, 2191–2201.

Maret, S., Faraguna, U., Nelson, A.B., Cirelli, C., and Tononi, G. (2011). Sleep and wake modulate spine turnover in the adolescent mouse cortex. Nature Neuroscience *14*, 1418–1420.

Mauelshagen, J., Sherff, C.M., and Carew, T.J. (1998). Differential Induction of Long-Term Synaptic Facilitation by Spaced and Massed Applications of Serotonin at Sensory Neuron Synapses of Aplysia californica. Learning and Memory *5*, 246–256.

McGaugh, J.L. (1966). Time-Dependent Processes in Memory Storage. Science *153*, 1351–1358.

Meeusen, T., Mertens, I., Clynen, E., Baggerman, G., Nichols, R., Nachman, R.J., Huybrechts, R., Loof, A.D., and Schoofs, L. (2002). Identification in Drosophila melanogaster of the invertebrate G protein-coupled FMRFamide receptor. 6.

Menzel, R., Leboulle, G., and Eisenhardt, D. (2006). Small brains, bright minds. Cell *124*, 237–239.

Mori, I., and Oshima, Y. (1995). Neural regulation of thermotaxis in Caenorhabditis elegans. Nature *376*, 344–376.

Nagel, G., Brauner, M., Liewald, J.F., Adeishvili, N., Bamberg, E., and Gottschalk, A. (2005). Light activation of channelrhodopsin-2 in excitable cells of Caenorhabditis elegans triggers rapid behavioral responses. Current Biology *15*, 2279–2284.

Nagy, S., Tramm, N., Sanders, J., Iwanir, S., Shirley, I.A., Levine, E., and Biron, D. (2014). Homeostasis in C. elegans sleep is characterized by two behaviorally and genetically distinct mechanisms. ELife *3*.

Nath, R.D., Chow, E.S., Wang, H., Schwarz, E.M., and Sternberg, P.W. (2016). C. elegans Stress-Induced Sleep Emerges from the Collective Action of Multiple Neuropeptides. Current Biology *26*, 2446–2455.

Nelson, M.D., Trojanowski, N.F., George-Raizen, J.B., Smith, C.J., Yu, C.-C., Fang-Yen, C., and Raizen, D.M. (2013). The neuropeptide NLP-22 regulates a sleep-likestate in Caenorhabditis elegans. Nature Communications *4*, Article 2846.

Nelson, M.D., Lee, K.H., Churgin, M.A., Hill, A.J., Van Buskirk, C., Fang-Yen, C., and Raizen, D.M. (2014). FMRFamide-like FLP-13 neuropeptides promote quiescence following heat stress in Caenorhabditis elegans. Current Biology *24*, 2406–2410.

Nichols, A.L.A., Eichler, T., Latham, R., and Zimmer, M. (2017). A global brain state underlies C. elegans sleep behavior. Science *356*, eaam6851.

Park, J., Knezevich, P.L., Wung, W., O'Hanlon, S.N., Goyal, A., Benedetti, K.L., Barsi-Rhyne, B.J., Raman, M., Mock, N., Bremer, M., et al. (2011). A conserved juxtacrine signal regulates synaptic partner recognition in C. elegans. Neural Development *6*, 28.

Pierce-Shimomura, J.T., Morse, T.M., and Lockery, S.R. (1999). The Fundamental Role of Pirouettes in *Caenorhabditis elegans* Chemotaxis. J. Neurosci. *19*, 9557–9569.

Quintilian (1921). Quintilian's Institutio Oratoria, Loeb Classical Library (Harvard University Press).

Raizen, D.M., Zimmerman, J.E., Maycock, M.H., Ta, U.D., You, Y., Sundaram, M.V., and Pack, A.I. (2008). Lethargus is a Caenorhabditis elegans sleep-like state. Nature *451*, 569–572.

Raizen, D.M., Song, B., Trojanowski, N.F., and You, Y. (2012). Methods for measuring pharyngeal behaviors. WormBook.

Rasch, B., and Born, J. (2013). About Sleep's Role in Memory. Physiological Reviews *93*, 681–766.

Raven, F., Van der Zee, E.A., Meerlo, P., and Havekes, R. (2018). The role of sleep in regulating structural plasticity and synaptic strength: Implications for memory and cognitive function. Sleep Medicine Reviews *39*, 3–11.

Rubinski, A., and Ziv, N.E. (2015). Remodeling and Tenacity of Inhibitory Synapses: Relationships with Network Activity and Neighboring Excitatory Synapses. PLOS Computational Biology *11*, e1004632.

Ryan, T.J., Roy, D.S., Pignatelli, M., Arons, A., and Tonegawa, S. (2015). Memory. Engram cells retain memory under retrograde amnesia. Science *348*, 1007–1013.

Schwarz, J., Spies, J.-P., and Bringmann, H. (2012). Reduced muscle contraction and a relaxed posture during sleep-like Lethargus. Worm *1*, 12–14.

Sengupta, P., Chou, J.H., and Bargmann, C.I. (1996). odr-10 encodes a seven transmembrane domain olfactory receptor required for responses to the odorant diacetyl. Cell *84*, 899–909.

Silva, A.J., Kogan, J.H., Frankland, P.W., and Kida, S. (1998). CREB and Memory. Annual Review of Neuroscience *21*, 127–148.

Singh, K., Ju, J.Y., Walsh, M.B., and Dilorio, M.A. (2014). Deep conservation of genes required for both Drosphila melanogaster and Caenorhabditis elegans sleep includes a role for dopaminergic signaling. Sleep *37*, 1439–1451.

Skora, S., Mende, F., and Zimmer, M. (2018). Energy Scarcity Promotes a Brain-wide Sleep State Modulated by Insulin Signaling in C. elegans. Cell Reports *22*, 953–966.

Stiernagle, T. (2006). Maintenance of C. elegans. WormBook.

Tian, L., Hires, S.A., Mao, T., Chiappe, M.E., Chalasani, S.H., Petreanu, L., Akerboom, J., McKinney, S.A., Schreiter, E.R., Bargmann, C.I., et al. (2009). Imaging neural activity in worms, flies and mice with improved GCaMP calcium indicators. Nature Methods *6*, 875–881.

Tononi, G., and Cirelli, C. (2014). Sleep and the Price of Plasticity: From Synaptic and Cellular Homeostasis to Memory Consolidation and Integration. Neuron *81*, 12–34.

Torayama, I., Ishihara, T., and Katsura, I. (2007). Caenorhabditis elegans Integrates the Signals of Butanone and Food to Enhance Chemotaxis to Butanone. Journal of Neuroscience *27*, 741–750.

Tramm, N., Oppenheimer, N., Nagy, S., Efrati, E., and Biron, D. (2014). Why Do Sleeping Nematodes Adopt a Hockey-Stick-Like Posture? PLOS ONE *9*, e101162.

Tran, A., Tang, A., O'Loughlin, C.T., Balistreri, A., Chang, E., Coto Villa, D., Li, J., Varshney, A., Jimenez, V., Pyle, J., et al. (2017). C. elegans avoids toxin-producing Streptomyces using a seven transmembrane domain chemosensory receptor. ELife *6*, e23770.

Trojanowski, N.F., and Raizen, D.M. (2016). Call it Worm Sleep. Trends in Neurosciences *39*, 54–62.

Trojanowski, N.F., Nelson, M.D., Flavell, S.W., Fang-Yen, C., and Raizen, D.M. (2015). Distinct Mechanisms Underlie Quiescence during Two Caenorhabditis elegans Sleep-Like States. The Journal of Neuroscience *35*, 14571–14584.

Tsunozaki, M., Chalasani, S.H., and Bargmann, C.I. (2008). A Behavioral Switch: cGMP and PKC Signaling in Olfactory Neurons Reverses Odor Preference in C. elegans. Neuron *59*, 959–971.

Turek, M., Besseling, J., Spies, J.-P., Konig, S., and Bringmann, H. (2016). Sleep-active neuron specification and sleep induction require FLP-11 neuropeptides to systemically induce sleep. ELife *5*, e12499.

Turrigiano, G. (2017). The Dialectic of Hebb and Homeostasis. Philosophical Transactions of the Royal Society B *372*.

Turrigiano, G., Leslie, K.R., Desai, N.S., Rutherford, L.C., and Nelson, S.B. (1998). Activity-dependent scaling of quantal amplitude in neocortical neurons. Nature *391*, 892–896.

Van Buskirk, C., and Sternberg, P.W. (2007). Epidermal growth factor signaling induces behavioral quiescence in Caenorhabditis elegans. Nature Neuroscience *10*, 1300–1307.

Varshney, A., Benedetti, K., Watters, K., Shankar, R., Tatarakis, D., Coto Villa, D., Magallanes, K., Agenor, V., Wung, W., Farah, F., et al. (2018). The receptor protein tyrosine phosphatase CLR-1 is required for synaptic partner recognition. PLOS Genetics *14*, e1007312.

de Vivo, L., Bellesi, M., Marshall, W., Bushong, E.A., Ellisman, M.H., Tononi, G., and Cirelli, C. (2017). Ultrastructural evidence for synaptic scaling across the wake/sleep cycle. Science *355*, 507–510.

Vohra, M., Lemieux, G.A., Lin, L., and Ashrafi, K. (2017). The beneficial effects of dietary restriction on learning are distinct from its effects on longevity and mediated by depletion of a neuroinhibitory metabolite. PLoS Biol *15*, e2002032.

Vorster, A.P., and Born, J. (2015). Sleep and memory in mammals, birds and invertebrates. Neuroscience and Biobehavioral Reviews *50*, 103–119.

Vyazovskiy, V.V., and Faraguna, U. (2014). Sleep and Synaptic Homeostasis. In Sleep, Neuronal Plasticity and Brain Function, (Springer-Verlag Berlin Heidelberg), pp. 91–121.

Vyazovskiy, V.V., Cirelli, C., Pfister-Genskow, M., Faraguna, U., and Tononi, G. (2008). Molecular and electrophysiological evidence for net synaptic potentiation in wake and depression in sleep. Nature Neuroscience *11*, 200–208.

Walker, M.P. (2009). The Role of Sleep in Cognition and Emotion. The Year in Cognitive Neuroscience 2009: Ann. N.Y. Acad. Sc *1156*, 168–197.

Wang, D.Y.-C., Kumar, S., and Hedges, S.B. (1999). Divergence time estimates for the early history of animal phyla and the origin of plants, animals and fungi. Proceedings of the Royal Society of London. Series B: Biological Sciences *266*, 163–171.

Weber, F. (2017). Modeling the mammalian sleep cycle. Current Opinion in Neurobiology *46*, 68–75.

Wes, P.D., and Bargmann, C.I. (2001). C. elegans odour discrimination requires asymmetric diversity in olfactory neurons. Nature *410*, 698–701.

White, J.G., Southgate, E., Thomson, J.N., and Brenner, S. (1986). The structure of the nervous system of the nematode C. elegans. Philosophical Transactions of the Royal Society B *314*, 1–340.

Wolstenholme, A.J. (2012). Glutamate-gated Chloride Channels. The Journal of Biological Chemistry *287*, 40232–40238.

Worthy, S.E., Haynes, L., Chambers, M., Bethune, D., Kan, E., Chung, K., Ota, R., Taylor, C.J., and Glater, E.E. (2018a). Identification of attractive odorants

released by preferred bacterial food found in the natural habitats of C. elegans. PLoS One *13*, e0201158.

Worthy, S.E., Rojas, G.L., Taylor, C.J., and Glater, E.E. (2018b). Identification of Odor Blend Used by Caenorhabditis elegans for Pathogen Recognition. Chemical Senses *43*, 169–180.

Xu, T.-L., and Gong, N. (2010). Glycine and glycine receptor signaling in hippocampal neurons: Diversity, function and regulation. Progress in Neurobiology *91*, 349–361.

Yamaguchi, M. (2017). The role of sleep in the plasticity of the olfactory system. Neuroscience Research *118*, 21–29.

Yap, M.H.W., Grabowska, M.J., Rohrscheib, C., Jeans, R., Troup, M., Paulk, A.C., van Alphen, B., Shaw, P.J., and van Swinderen, B. (2017). Oscillatory brain activity in spontaneous and induced sleep stages in flies. Nat Commun *8*, 1815.

Yonelinas, A.P., Ranganath, C., Ekstrom, A.D., and Wiltgen, B.J. (2019). A contextual binding theory of episodic memory: systems consolidation reconsidered. Nature Reviews Neuroscience *20*, 364–375.

You, Y., Kim, J., Raizen, D.M., and Avery, L. (2008). Insulin, cGMP, and TGF-β Signals Regulate Food Intake and Quiescence in C. elegans: A Model for Satiety. Cell Metabolism *7*, 249–257.

Zhang, Y., Lu, H., and Bargmann, C.I. (2005). Pathogenic bacteria induce aversive olfactory learning in Caenorhabditis elegans. Nature *438*, 179–184.

Zimmerman, J.E., Naidoo, N., Raizen, D.M., and Pack, A.I. (2008). Conservation of sleep: insights from non-mammalian model systems. Trends in Neurosciences *31*, 371–376.

CHAPTER THREE: THE TRPV CHANNEL OSM-9 MEDIATES OLFACTORY LONG-TERM MEMORY CONSOLIDATION INDEPENDENT OF SLEEP

SUMMARY

Memory is one of the most important abilities of the brain. It is defined as an alteration in behavior from an experience. For example, the *C. elegans* nematode will downregulate its chemotactic response to an innately attractive odor if it is not paired with food. This process is an example of olfactory classical conditioning. Through spaced training with this odor in the absence of food, *C. elegans* will maintain this memory of the odor for a prolonged period of time, akin to long-term memory formation. Although TRP channels are classically thought of as primary sensory receptors, intriguingly, it has been reported that the OSM-9/TRPV5/TRPV6 (TRP vanilloid) channel is required for odor short-term memory. We have discovered a new role for *osm-9/TRPV* in long-term olfactory memory formation (LTM). The *osm-9* mutant animals can acquire memory of the conditioned stimulus (odor) just like wild-type, but are unable to consolidate the memory for long-term maintenance. Interestingly, this TRPV-mediated long-term memory does not require sleep to form the long-lasting memory. Additionally, we found that genomic DNA and not cDNA is able to rescue the short-term odor memory defects seen in the null mutants. TRP channels are well studied in their ability to sense noxious stimuli, yet they are also implicated in memory and many diseases and disorders that limit neural plasticity, including Parkinson's disease, Alzheimer's disease, stroke, and sense disorders including anosmia. Our studies uncovered a role of TRP channels in neural plasticity, specifically, in olfactory long-term memory formation. These findings will broaden our knowledge of TRP channel function as a mediator of plasticity and memory, which could also potentially aid in understanding and treating the many diseases and disorders caused by TRP channel dysfunction.

INTRODUCTION

Transient receptor potential (TRP) ion channels were first discovered in the *Drosophila* eye photoreceptor cells (Cosens and Manning, 1969; Montel and Rubin, 1989; Minke, 2010), but have since been found in mammals and even in the single-celled yeast. Classically, TRP channels have been well established as magnesium-, sodium-, and calcium-permeable cation channels that can be activated by and simultaneously integrate multiple intracellular or extracellular stimuli to drive downstream signaling and membrane depolarization. These stimuli include, but are not limited to, pain, temperature, pH, injury, osmolarity, and cytokines (Yizheng Wang, 2017). There are seven TRP channel families, all sharing a similar topology, with six transmembrane helices, a short pore helix, and a cation-permeable pore loop region. The variability between the TRP families depends on the number of N-terminal ankyrin repeat domains and the presence of a C-terminal TRP box helix, which is a long helix parallel to the membrane (Muller et al., 2019). One TRP protein family is the TRP vanilloid-type (TRPV). TRPV proteins are generally considered as first-line nociceptive sensory receptors and include TRPV1-6, where TRPV1 is the canonical protein. TRPV1 is stimulated by vanillin, vanillic, endogenous lipids like the *N*-acylamides (e.g. endocannabinoids such as anandamide), high temperature (≥43°C), pain, ethanol, low pH, black pepper, garlic (allicin), cannabidiol (CBD), arachidonic acid, resiniferatoxin, and spicy foods, driven by the agonist capsaicin (De Petrocellis et al., 2011; Wang, 2017; De Petrocellis et al., 2017; Muller et al., 2019). The six ankyrin repeats in TRPV1 each contain two short anti-parallel helices and a finger loop and have been shown to interact with the proteins calmodulin and PI3K (Hellmich and Gaudet, 2014; Muller et

al., 2019). Upon activation, the TRPV1 channel allows calcium ions to enter the cell at the plasma membrane through the pore loop region, ultimately leading to desensitization of the channel and a subsequent refractory period (Muller et al., 2019). This desensitization is a large focus in the pain field with research focusing on alleviating acute and chronic pain. Although the sensory role of TRPV proteins has been well established, other roles of the TRPV channels, including the promotion of neural plasticity required for memory formation, are much less known.

Learning and memory are vital to survival. Organisms must update their knowledge of their surroundings based on environmental cues. One such way to promote learning and memory is through neural plasticity, which involves changes at the structural, molecular, and functional levels. Pioneering studies on the *Aplysia* gill-withdrawal reflex demonstrated the importance of synaptic plasticity on learning and memory through *in vitro* pharmacology and physiology experiments (Lent, 1976). Learning and memory are thought to be driven by two types of synaptic plasticity: the first is Hebbian, which includes synaptic long-term potentiation (LTP) and long-term depression (LTD; Fox and Stryker, 2017), and the second is non-Hebbian homeostatic compensation, which includes synaptic scaling (Turrigiano et al., 1998; Fox and Stryker, 2017). A large number of molecules implicated in these processes include factors that reorganize the actin cytoskeleton, affect trafficking, insertion and localization of receptors and cell adhesion molecules, localization of newly translated products, kinase function, and transcription of new genes (Bailey et al., 2015). As deep as, our understanding of these synaptic processes may be, we are still missing the roles of

some molecular players for memory in any intact organism. One protein type that is gaining new evidence for its role in memory is the TRP channel.

Although TRP channels have been studied thoroughly for their roles in sensation in the peripheral nervous system (Julius, 2013), they have more recently been studied for roles in the central nervous system, including neural plasticity (Sawamura et al., 2017). For example, TRPV channels have hippocampal expression and have been implicated in slow synaptic transmission (Eguchi et al., 2016), LTP (Marsch et al., 2007), and LTD of excitatory synapses on the interneurons (Gibson et al., 2008). Neural plasticity underlies learning and memory formation, e.g. through long-term potentiation and depression (LTP and LTD, respectively) of synapses in the mammalian hippocampus. Synaptic plasticity has been shown to underlie learning and memory, and TRP channels have recently been studied for a role in these processes. A TRPA channel (painless) has been observed to play a role in fly courtship associative long-term memory (Sakai et al., 2013). In the mammalian brain, the TRPCs function in the hippocampus to drive synaptic transmission and plasticity, and subsequent spatial working memory (Tai et al., 2008; Zhou et al, 2008). In addition to the hippocampus, expression of TRPCs has been uncovered in the temporal lobe, suggesting a role in neural plasticity, learning, and memory. TRPM4 has also been found to be expressed in the mammalian hippocampus and is important for plasticity and spatial working and reference memory (Bovet-Carmona et al., 2018). Several recent studies have implicated mammalian TRPV1 in memory formation, including fear memory consolidation behavior in mice (Genro et al., 2012; Marsch et al., 2007; Li et al., 2008). Acute stress was found to block spatial memory retrieval in young rats and also blocked LTP and drove LTD in

CA1 slices of the hippocampus, whereas TRPV1 agonists allowed spatial memory and LTP while blocking LTD, even in the presence of stress (Li et al., 2008). These TRPV1 memory studies were done with either pharmacological agent infusion to activate TRPV1 or by studying the behavior of TRPV1 knockout mice. Further dissection of the exact cellular or molecular interactions occurring in the behaviorally-defective mice would help gain a mechanistic understanding of how learning and memory are driven. An outstanding question to also answer is which stage of memory formation is mediated by TRP channels: acquisition, consolidation, or recall? In order to study the required genes in a live animal model as it is behaving, unbiased screens for genes required for learning and memory would need to be performed.

Using *C. elegans*, several unexpected genes have been identified more than 25 years ago in screens for short-term circuit plasticity, one being the transient receptor potential vanilloid 5 and 6 (TRPV5 and TRPV6) channel, OSM-9 (Colbert and Bargmann, 1995). The *C. elegans* nematode exhibits olfactory classical conditioning: prolonged exposure to innately attractive food-related odors in the absence of food elicits a downregulated response to the odor (Colbert and Bargmann, 1995). The *osm-9* gene is required for short-term olfactory memory in this paradigm. However, the mechanisms and dynamics of TRPV function in memory formation remain unknown. In addition, a role for *osm-9* in long-term memory has not been reported. Examination of the mechanisms and dynamics underlying TRPV-mediated memory in live *C. elegans* would help us understand how these channels act in an endogenous setting to integrate signaling over time to promote memory formation as the worms behave.

C. elegans provides a good model system to approach this problem. It is genetically-tractable and its nervous system is comprised of 302 neurons connected via 7,000 synapses. Also, it is the only organism where the entire connectome has been mapped (White et al., 1986; Cook et al., 2019, whereas the mammalian nervous system has 100 billion neurons connected by trillions of synapses and the entire neural connectivity map remains unknown (Kaiser, 2015). Additionally, it can form long-term associative memories of olfactory stimuli (Kaufmann et al., 2011). Of great help is that the neural circuit underlying olfaction is well established (White et al., 1986; Cho et al., 2016; Gordus et al., 2015). Importantly, it is transparent, making live cell imaging in the live animal a possibility. Thus, studying plasticity in the olfactory circuit in *C. elegans* has the potential to give us insight into the mechanisms by which experience changes complex neural circuits to promote memory formation.

The *osm-9* gene is an ortholog of human TRPV5 and TRPV6. TRPV5 and TRPV6 not like the rest of the TRPV family, as they are not ligand-gated, nor are they thermosensitive (Vennekens et al., 2000; Nilius et al., 2000). TRPV5 and TRPV6 are localized to epithelial cells in the kidney and intestine (van Goor et al., 2017) and are calcium-selective channels constitutively open at physiological membrane potentials and are modulated by calmodulin in a calcium-dependent manner (Dang et al., 2019). Initially, *osm-9*/TRPV5/TRPV6 was first discovered in a screen for *C. elegans* mutants defective for sensing high osmolarity. It was subsequently studied for its role in short-term associative olfactory memory where the nematodes learn to ignore food-related odors when in the absence of food (Colbert and Bargmann, 1995; Colbert et al., 1997). Later studies revealed that *osm-9* also has a role in sensing noxious stimuli, causing

SDS avoidance behavior through expression in the ASH sensory neurons (Tobin et al., 2002). This avoidance behavior can be phenocopied through heterologous expression of mammalian TRPV1 in ASH and application of the capsaicin agonist (Tobin et al., 2002), where calcium is likely driven into the cell through the pore loop region to elicit depolarization (Lindy et al., 2014). Polyunsaturated fatty acids, including the TRPV1 endogenous activator arachidonic acid, function upstream of *osm-9* to mediate sensory transduction (Kahn-Kirby et al., 2004). The endogenous agonist nicotinamide was discovered to activate an OSM-9 and OCR-4 heteromer expressed heterologously in *Xenopus* oocytes, and nicotinamide was sufficient to phenocopy *osm-9* mutant nose-touch defect behavior (Upadhyay et al., 2016). The *osm-9* gene has also been shown to play a role in developmental programming and is downregulated transcriptionally post environmental stress exposure, causing avoidance of specific olfactory cues (Hall et al., 2010; Sims et al., 2016). These changes in *osm-9* expression were shown to be mediated by chromatin remodeling and endogenous siRNA pathways (Sims et al., 2016). Thus, *osm-9* has roles in sensory transduction in response to noxious stimuli, can be activated by polyunsaturated fatty acids, and plays a role in learning and memory, just like TRPV1. OSM-9 shares about ~25-26% protein sequence similarity to human TRPV1, TRPV5, and TRPV6, and also has intracellular N and C termini, six N-terminal ankyrin domains, and six transmembrane domains, with a calcium-permeable pore loop between the fifth and sixth. Thus, studies on *osm-9* may help to uncover conserved mechanisms of learning and memory.

In our classical conditioning paradigm, we focus on the *C. elegans* response to the food-related odorant butanone, which is specifically sensed by the AWC olfactory

sensory neurons (OSNs; Bargmann and Horvitz, 1991; Bargmann et al., 1993). The *C. elegans* nematode exhibits olfactory classical conditioning: one 80-minute exposure cycle to butanone in the absence of food causes the nematode to downregulate its chemotactic response to that odor. The second messenger for odor sensation within the AWCs is cGMP (L'Etoile and Bargmann, 2000; Birby et al., 2000). Prolonged odor stimulation leads to AIA interneuron circuit activity and PI3K signaling to the AWC neurons to drive accumulation of the cGMP-dependent protein kinase EGL-4 (L'Etoile et al., 2002) within the AWC nucleus. These events promote memory of the odor being profitless after 80 minutes of conditioning (O'Halloran et al., 2009; Lee et al., 2010; Cho et al., 2016). Loss-of-function mutations in *osm-9* cause defective learning that AWC-sensed odors can be profitless, and defective chemo-, osmo-, and thermosensation promoted by other sensory neurons (Colbert et al., 1997). Importantly, loss of *osm-9* restores function to mutants that ignore AWC-sensed odors as a consequence of expressing nuclear EGL-4. After EGL-4 nuclear translocation, nuclear endogenous RNAi promotes a dampened response to butanone by transcriptionally-downregulating the *odr-1* gene through heterochromatin remodeling via *hpl-2/HP1*, and the *osm-9* gene is epistatic to gain-of-function *hpl-2* or *egl-4* (O'Halloran et al., 2009; Juang et al., 2013). Thus, the TRPV channel *osm-9* is required downstream of both of these nuclear events and is the most downstream component of this paradigm currently known. However, the role of *osm-9* in this plasticity paradigm is still poorly understood. We were also curious if *osm-9* plays a role in long-term olfactory memory since its role in short-term olfactory memory is established. We wanted to understand the *osm-9* dynamics in plasticity

necessary for olfactory memory formation, and what the structural components of the gene are that allow it to drive this plasticity.

We previously found that the 80-minute butanone conditioned response is temporary and is lost after only 30 minutes recovery on food (Muñoz-Lobato et al., 2019). However, after odor spaced-training, *C. elegans* can exhibit long-term aversive memory phenotypes (Lakhina et al., 2015; Muñoz-Lobato et al., 2019). Worms subjected to three cycles of 80-minute exposure to the unprofitable odor in the absence of food with recovery periods on food in between each cycle will keep the memory and continue to ignore the odor for much longer periods of time (at least 16 hours after training; Muñoz-Lobato et al., 2019). Here, we find that the *osm-9* null mutants can actually be conditioned to ignore butanone after undergoing a spaced-training protocol, just like wild-type animals. Interestingly, we show that long-term memory consolidation, and not acquisition, requires *osm-9,* independent of sleep. Specifically, we find that *osm-9* mutants lose this odor memory after only 30 minutes, where it remains lost. The wild-type animals also lose the memory after 30 minutes, but regain it and keep it for at least 16 hours (Muñoz-Lobato et al., 2019). The wild-type trained animals undergo a period where the odor memory is fragile and is lost after only 30 minutes of recovery on food, only to be regained at 120 minutes of recovery and to last for at least 16 hours. The *osm-9* gene is not required for this 30-minute memory fragility period, but is required during the post 30-minute to 120-minute period where the memory is consolidated. Memory fragility in the period after conditioning is a hallmark of a consolidation (Dudai, 1996; Dudai, 2004). Thus, *osm-9* likely plays a role in olfactory long-term memory consolidation in addition to its previously defined role in short-term

memory. We previously found that wild-type animals, like mammals, require sleep during this fragile memory period to consolidate odor memory, but *osm-9* animals sleep just as much as wild-type, but are still unable to consolidate and mediate long-term memory. We also find that both the N- and C-terminus are required for long-term memory consolidation or maintenance. Finally, we show that the short-term memory defect is rescued only partially by *osm-9* cDNA expressed under its own promoters, but the defect may be more completely rescued when expressing its gDNA, suggesting a role for its introns in driving expression for memory.

Though TRP channels have been extensively studied as sensory receptors, they have not been well studied as integrators of prolonged stimulation. The goal of this work was to understand how the *osm-9* TRPV channel mediates long-term memory after prolonged exposure to odor, thereby elucidating TRP function in signal integration triggered by extended exposure to stimuli. We show that *osm-9* is important for the long-term memory consolidation step of memory formation. These data suggest the exciting possibility that a TRPV channel promotes long-term memory consolidation, and does this independent of sleep.

RESULTS

Although it has been previously shown that *osm-9* is required for olfactory short-term memory of food-related odorants (**Fig 3.1**, **Fig 3.S1**), its role in long-term memory formation hasn't been reported. We utilized a long-term memory spaced-training paradigm where we performed odor conditioning in three spaced intervals with recovery periods on food in between (**Fig 3.S1**). We tested *osm-9(ky10)* null mutants versus wild-type animals and found that although *osm-9(ky10) IV* animals are unable to form short-term odor memory after one cycle of conditioning (**Fig 3.1**), they can acquire memory immediately after spaced-training, like wild-type animals (**Fig 3.1**), shown by a chemotaxis index (**Fig 3.1A**) and learning index (**Fig 3.1B**). Wild-type animals lose the memory after 30 minutes of recovery on food, but regain it back after two hours of recovery (**Fig 3.2**, Muñoz-Lobato et al., 2019), and keep it for at least 16 hours post training (**Fig 3.3**). By contrast, *osm-9* animals lose the memory completely after only 30 minutes (**Fig 3.2**) of recovery on food and never gain it back, shown at two hours and 16 hours of recovery after training (**Figs 3.2** and **3.3**, respectively). This could indicate that *osm-9* is responsible for memory consolidation, but not acquisition, immediately post odor spaced-training. What is also interesting to note is that although *osm-9(ky10) IV* animals are able to acquire memory after three cycles of odor training, their chemotaxis behavior looks distinct from wild-type animals – *osm-9(ky10)* animals have an average chemotaxis index closer to zero (0.1, **Fig 3.1A**), which looks like wild-type animals after one-cycle of odor training (**Fig 3.1A**), whereas wild-type animals after three cycles of odor training look averse to butanone, with an average chemotaxis index of -0.3 (**Fig 3.1A**). Although odor spaced training can induce memory acquisition in

osm-9(ky10) animals as opposed to training them with one odor cycle, their behavioral state may be different from that observed in wild-type animals.

Since sleep has been suggested to promote memory consolidation and is required for long-term memory in our paradigm (Muñoz-Lobato et al., 2019), we tested if the *osm-9(ky10)* mutants sleep after spaced training by quantifying their quiescence behavior in one hour post spaced training. To analyze movement, we utilized the WorMotel (Churgin et al., 2017), where we could take videos of individual worms as they recover for one-hour post training, and subsequently analyze their behavior with Matlab analysis. We measured sleep by testing if the worms exhibited any quiescence behavior for more than 30 seconds and generated raster maps from these data for visualization of the movement (**Fig 3.4A**). We then recorded the mean total quiescence (in minutes per hour) of each dataset. The *osm-9(ky10) IV* movements showed the same amount of quiescence as wild type, signifying that the *osm-9(ky10) IV* animals sleep as much as wild type animals, but are still unable to consolidate olfactory memory (**Fig 3.4B**).

We next tested extra *osm-9* alleles to uncover if this olfactory long-term memory consolidation defect is unique to the *osm-9(ky10)* mutants, and as a way to perform structure-function analysis. The *osm-9* gene has fourteen exons. The *ky10* allele is an early stop codon at the beginning of the fourth exon from the 5' end, occurring in the middle of the third ankyrin repeat (**Fig 3.5A**). We tested the *yz6* allele, also an early stop codon, at the end of the fifth exon, 3' of the six ankyrin repeats, thus leaving them intact, assuming the mRNA is translated (**Fig 3.5A**). We also examined the *ok1677* allele, a deletion of the twelfth, thirteenth, and part of the fourteenth exons, removing most of the

C-terminal intracellular tail, and the sequence that produces a non-coding RNA and tRNA (**Fig 3.5A**). The *ok1677* and *yz6* animals showed similar behavior to *ky10* since memory acquisition is still intact, but memory maintenance is defective, although the defect in these two alleles is not as severe as in *ky10* animals (**Figs 3.3** and **3.5B**). These data support that *osm-9* is not required for memory acquisition, but is important for memory consolidation or maintenance in long-term olfactory memory.

To study the expression requirements for *osm-9*/*TRPV5/TRPV6* in olfactory classical conditioning, we took a molecular genetic approach by performing rescue experiments with different *osm-9* transgenes under various promoters in the *osm-9(ky10)* mutant background versus their non-transgenic siblings and wild type as controls. We performed a short-term memory paradigm involving training with and without a food-related odorant for 80 minutes in the absence of food, as previously published (Colbert and Bargmann, 1995; Juang et al., 2013; **Fig 3.S1**). We were unable to rescue the *osm-9(ky10) IV* odor-learning defect (Colbert and Bargmann, 1995) when using a partial *osm-9* cDNA driven under its endogenous upstream and downstream promoters (**Fig 3.S4D**), which was previously shown to drive *osm-9* expression and localization (Colbert et al., 1997; Tobin et al., 2002). We also could not achieve rescue with the cDNA driven by an AWC promoter (*ceh-36*, **Fig 3.S4A**), the olfactory sensory neuron promoter (*odr-3*, **Fig 3.S4B** and **3.S4C**), under both of its own upstream and downstream promoters (**Fig 3.S4E**), or a ciliated neuron promoter (*nphp-4,* Jauregui and Barr, 2005; **Fig 3.S4G**). We also could not achieve rescue using a fosmid containing the whole *osm-9* gene (**Fig 3.S4F**). Partial rescue was achieved using the full-length *osm-9* cDNA under both the olfactory sensory neuron promoter *odr-3* and its

own downstream promoter (**Fig 3.6**). However, full rescue was obtained when expressing the *osm-9* genomic DNA under both its upstream and downstream promoters, although the extrachromosomal array silenced in all of the transgenic lines, precluding further rescue analysis (**Fig 3.S3**). The gDNA rescuing the short-term memory defects of *osm-9* mutants may signify that the introns contain something required for expression of the *osm-9* gene in order to mediate butanone short-term memory. The fosmid should have also rescued if the introns are indeed required, but it could have been an expression issue that prevented rescue with the fosmid.

In sum, we report here that the *osm-9/TRPV5/TRPV6* gene is required for long-term olfactory memory consolidation independent of sleep, and may require its introns for proper function in memory.

DISCUSSION

Transient receptor potential (TRP) channels are proteins best understood in their role as sensors of harmful environmental stimuli, yet they have a less understood role in regulating neural plasticity—a fundamental process in the brain that governs information storage and adaptation to environmental cues. We found that the *osm-9* TRPV channel, which has a known role in short-term olfactory learning (Colbert and Bargmann, 1995), requires its intronic regions for proper function in this paradigm. The requirement for genomic DNA to rescue the defective short-term memory in *osm-9(ky10) IV* mutants could signify a type of gene regulation required for proper odor learning. It has been reported that *osm-9* has endogenous small RNAs (endo-siRNAs) that are required for sensing aversive pheromones post-stress exposure (Sims et al., 2016). Endo-siRNAs or other RNAs produced from the *osm-9* locus could potentially also be required for this short-term associative odor memory. We were interested if *osm-9* also plays a role in long-term olfactory memory, and thus tested the mutants in a spaced-training paradigm that induces long-lasting memory in wild-type animals. The *osm-9(ky10)* mutants were able to acquire the odor memory after training, but lost it within 30 minutes of recovery on food, and it remained lost, whereas wild-type animals lose the memory at 30 minutes of recovery, regain it two hours later, and keep it at least 16 hours later. Thus, the *osm-9* TRPV channel is required for memory consolidation, a key component of long-term memory. Proper functioning TRPV channels may be necessary to drive the synaptic plasticity required for memory formation. Studies have shown that TRPV1 contributes to synaptic plasticity, specifically LTD induction across the hippocampus, mPFC, and NAc (Ruggiero et al. 2017; Gibson et al. 2008, Grueter et al. 2010, Lovelace et al. 2014).

Because these are regions required for long-term memory formation, it could be this alteration in synaptic plasticity that is required for proper memory consolidation. We tested different alleles of *osm-9* to perform structure function analysis for the long-term memory paradigm. The *ky10* allele is an early stop codon that removes the fourth to sixth and part of the third ankyrin repeats on the N-terminal tail, as well as the transmembrane domain, pore loop, and C-terminus. The *yz6* allele is also an early stop, but is directly after the ankyrin repeats, and removes the rest of the transcript like *ky10* does. To additionally test if the C-terminal tail is important for long-term memory, we tested the *ok1677* allele, which removes most of the C-terminus as well as a region that produces a non-coding RNA and tRNA. Both the *yz6* and *ok1677* animals behaved just like *ky10* mutants, which potentially shows a requirement for both the N- and C-terminus, including ankyrin repeats, the transmembrane domains, or the pore loop, in memory consolidation or maintenance.

Animals must respond and learn from their ever-changing surroundings to ensure survival. TRP channels emerged early in eukaryotic evolution to allow sensation of the environment. Over the course of evolution, they became coincidence detectors, sensing a range of mechanical to chemical cues, which are vital for learning and memory. Originally thought of as only having peripheral nerve expression, TRPV channel proteins are also found in the central nervous system throughout the brain. Could pleiotropy be occurring, where TRPV channels in the sensory neurons can respond to cues such as heat and protons, and then subsequently drive learning and long-term memory of those cues in the brain? The evolution of TRP channels could have

potentially driven survival through ambient sensation and simultaneous or subsequent triggering of memory formation.

TRP channels are found throughout the domain Eukaryota, in the animal, fungi, and protist kingdoms, meaning they evolved before multicellularity. TRPY1 is found in the single-celled fungus, *S. cerevisiae* and TRPA, C, M, L, and V channels, are found in the single-celled protist choanoflagellates (Peng et al., 2015), as well as in multicellular, bilaterally-symmetric animals, including protostome ecdysozoan invertebrates such as *Drosophila* and *C. elegans*, and deuterostome chordate vertebrates, including zebrafish, whale and Australian ghost sharks, rodents, and humans. TRPNs are found in *Hydra magnipapillata,* which is the last common ancestor of Cnidaria and Bilateria. Fourteen TRPA and TRPML channels were found in the sponge *A. queenslandica*, showing a diverse conservation of TRP channels since sponges are the oldest living metazoan phyletic lineage, diverging from other metazoans ~600 million years ago (Peng et al., 2015). TRPA1 was found to have evolved from a chemical sensor in a common bilaterian ancestor to invertebrates and vertebrates, conserved across ~500 million years of evolution (Kang et al., 2010). TRP channels themselves are likely even older than the nociceptive family of sensors, since fungi branched off from other life during the Proterozoic Era, about 1.5 billion years ago (Wang et al., 1999). These early TRP channels evolved the ability to sense multiple stimuli and drive distinct responses to ensure organismal survival. For example, the TRPA1 channel likely evolved through adaptive evolution via amino acid changes in response to the environment, explaining the temperature and compound sensitivities observed in different mammalian species (Chen et al., 2008; Xiao et al., 2008; Nagatomo et al., 2010; Peng et al., 2015). The

TRP channel predecessors were non-neuronally expressed, but as animals became more evolved, such as through development of a neural net or cephalization, TRP channels evolved neuronal roles such as sensory perception and polymodality. However, the distinct functions of TRP channels in higher level processes such as plasticity, learning, and memory are still being uncovered.

Since TRPV channels are required for acute sensation and in plasticity, considered short and long-term processes, respectively, then how does its function and regulation differ between them? Distinct from the TRPV1-4 channels, TRPV5 and TRPV6 are highly-selective for calcium and mediate calcium signaling through their constitutive opening at physiologic membrane potentials, without the need for ligand activation. Potentially, the TRPV5 and 6 ortholog OSM-9 may also be constitutively open and mediating the calcium homeostasis necessary to drive long-term memory formation. Calcium is a known requirement for synaptic transmission. We previously showed that synaptic plasticity occurs in animals that maintain the memory and that slept post spaced-training (Muñoz-Lobato et al., 2019). Thus, OSM-9 may be involved in regulating the calcium levels required for this synaptic plasticity in spaced-trained animals. Another confound is understanding how TRPV1 mediates long-term memory. TRPV1-4 channel agonists cause a downstream signaling cascade to mediate sensation. Prolonged exposure causes desensitization of the channel. If the channel is similarly desensitized in plasticity, then how does its function continue to occur for long-term biological processes, including long-term memory? Understanding the agonists driving TRPV1-mediated plasticity that do not cause desensitization of the channel may help to answer this confounding question. The polymodality of TRP channels is alluring,

yet mystifying since it can be a number of individual or combinations of agonists or antagonists driving varied downstream responses. Yet, since Ca^{2+} signaling is important for synaptic plasticity, it could be that TRPV proteins are specifically required for regulating intracellular calcium to promote plasticity and thus learning and memory.

Besides being a current focus for chronic pain treatment (e.g. through topical capsaicin), the TRPVs are also emerging as a new drug target for diseases affecting neural plasticity. Indeed, a vast array of neurological diseases, including Alzheimer's disease (Di Marzo et al. 2008), Parkinson's disease, schizophrenia (Tzavara et al. 2006, Almeida et al. 2014, Madasu et al, 2015), epilepsy, and Charcot-Marie-Tooth disease (Morelli et al., 2013), as well as sense disorders (e.g. anosmia; Nilius, 2007) result from or are linked to defects in TRP function, with affected individuals exhibiting decreased neural plasticity. It has also been shown that TRPV1 could be a target for cognitive decline in Alzheimer's patients since applying its agonist capsaicin to neurons from AD rodents shows restoration of Aβ-induced degradation of hippocampal gamma oscillations (Balleza-Tapia et al., 2018). Rat models of biliary cirrhosis, which induces memory impairment, have decreased memory impairment when treated with capsaicin, which also increased TRPV1 and CREB mRNA in the CA1 area of the hippocampus (Bashiri et al., 2018). Recent research even suggests the use of TRPV1 agonists as therapeutics to aid in ameliorating the effects of schizophrenia since TRPV1 is linked to pain and cognitive defects in schizophrenic patients (Madasu et al. 2015). This could indicate that TRPV1-mediated plasticity defects may underlie some of these neurological disorders. Performing *in vivo* studies to understand how TRPV proteins regulate proper neurological function may uncover a role in learning and memory and

could potentially help to understand what happens in the TRPV1-mediated disease states. We aimed to elucidate how TRP protein functions at the molecular level to promote plasticity and memory formation. Understanding the molecular mechanisms and dynamics by which animals learn to ignore non-beneficial stimuli through TRP-mediated neural plasticity may be of importance to understanding not only how animals learn and form memories, but may also give insights into the etiology of TRP-mediated neurological diseases.

ACKNOWLEDGEMENTS

We would like to thank all past and present members of the L'Etoile lab. We thank Piali Sengupta for her gift of the *nphp-4* promoter and Cori Bargmann for her gift of the *osm-9::GFP5* construct. We would also like to thank Chris Fang-Yen and Matt Churgin for their help with the WorMotel and the Matlab analysis, and Joe Hill for the artwork used in Figs 3.S1 and 3.S2. We are grateful to the team behind wormbase.org (NIH grant #U24 HG002223), SMART (Schultz et al., 1998, EMBL), and Nikhil Bhatla for the wormweb.org exon-intron graphic maker used for Fig 3.7A. This work was funded by the NIH, specifically R01DC005991 (NDL), R01NS087544 (NDL), R25GM56847 (KB), R01 supplement NS87544 (KB), and F31DC014921 (KB).

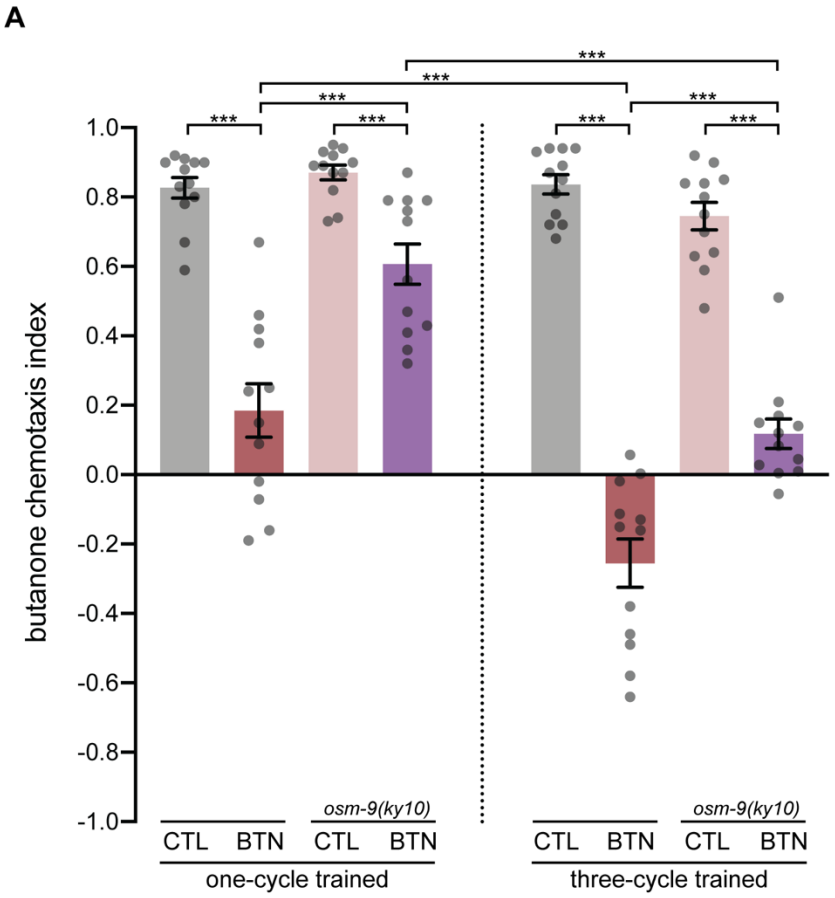
A
butanone chemotaxis index
1.0
0.8
0.6
0.4
0.2
0.0
-0.2
-0.4
-0.6
-0.8
-1.0
***
***
***
***
***
***
***
***
CTL
BTN
osm-9(ky10)
CTL
BTN
one-cycle trained
CTL
BTN
osm-9(ky10)
CTL
BTN
three-cycle trained

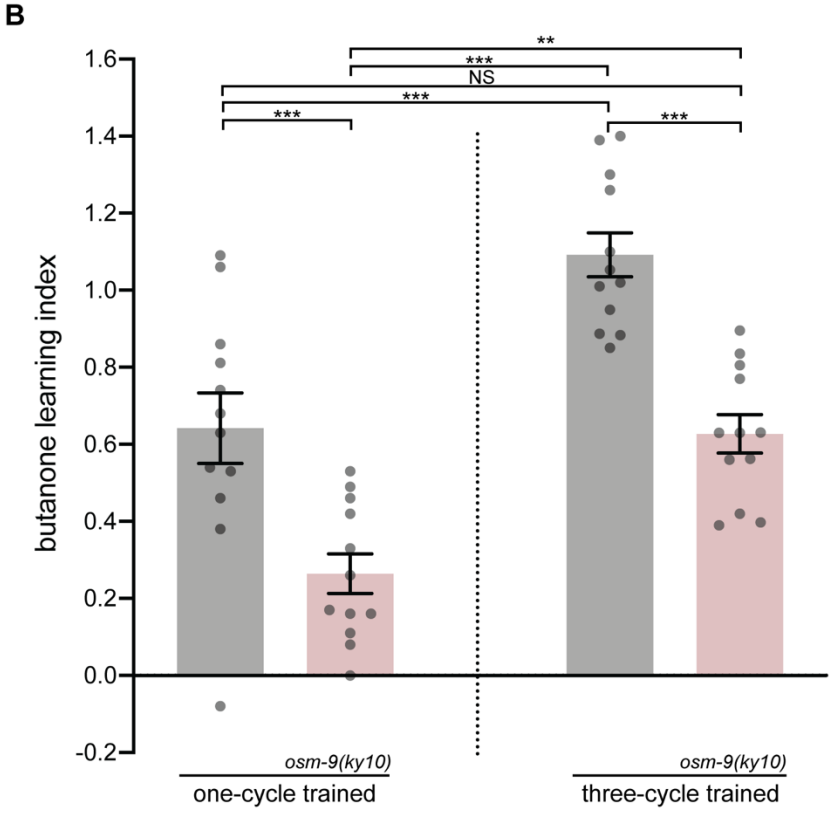
B
butanone learning index
1.6
1.4
1.2
1.0
0.8
0.6
0.4
0.2
0.0
-0.2
**
***
NS
***
***
***
osm-9(ky10)
one-cycle trained
osm-9(ky10)
three-cycle trained

Fig 3.1. The TRPV channel *osm-9* is required for short-term memory, but is not required for memory acquisition post spaced training. (A) Chemotaxis indices for one-cycle odor conditioned and three-cycle odor wild-type vs *osm-9(ky10)* spaced-trained animals. The chemotaxis index (CI) is calculated as the number of worms at the diluent (200-proof ethanol) subtracted from the number at the butanone point source, divided by the total number or worms (excluding any at the origin). Wild-type one- or three-cycle buffer trained (CTL, grey bar), wild-type one- or three-cycle butanone-trained (BTN, red bar), *osm-9(ky10)* one- or three-cycle buffer-trained (CTL, pink bar) and *osm-9(ky10)* one- or three-cycle butanone-trained (BTN, purple bar) are shown, and are denoted this way throughout the rest of the manuscript. “Three-cycle trained” label means 0’ recovery (fifth to eighth bars) and will be annotated this way throughout the paper. N = number of trials where all trials are done on independent days and each grey dot represents an individual assay day, with 50-200 animals/day. The Shapiro-Wilk`` normality test was performed to determine data distribution, and if data were non-normally distributed, the analysis was done with the Kruskal-Wallis test, an analysis of variance of multiple comparisons for non-parametric data. If pairwise comparisons were normally distributed, then p-values were generated with a Student’s unpaired t-test. If any of the datasets were non-parametric, then p-values were generated with the Mann-Whitney u-test. Hochberg adjustment for multiple comparisons was performed on all p-values generated from data included in the same graph to control Type I statistical error. If the data were normally distributed, then one-way ANOVA was performed, followed by Bonferroni correction of pairwise comparisons. Error bars represent S.E.M. Statistical significance was reported as ***p<0.001, ** p< 0.01, *p<0.05, and NS is p>0.05. Behavioral data throughout the paper are represented in this same way with the same numbers of animals on independent days. Additionally, throughout the paper, the same statistical analysis was performed on the data. Note that for every figure in this manuscript, that the Kruskal-Wallis or one-way ANOVA test was performed and yielded ***p<0.001, unless otherwise noted. The Kruskal-Wallis test was performed. The u-test was performed for one-cycle CTL vs BTN, one-cycle *osm-9(ky10)* CTL vs *osm-9(ky10)* BTN, three-cycle trained *osm-9(ky10)* CTL vs *osm-9(ky10)* BTN, one-cycle *osm-9(ky10)* BTN vs three-cycle *osm-9(ky10)* BTN, and three-cycle BTN vs *osm-9(ky10)* BTN. The t-test was performed for one-cycle BTN vs *osm-9(ky10)* BTN, three-cycle CTL vs BTN, and one-cycle BTN vs three-cycle BTN.
(B) Learning indices for one-cycle conditioned and three-cycle spaced-trained wild-type vs *osm-9(ky10)* animals. The learning index (LI) is calculated as the chemotaxis index of the BTN animals subtracted from the chemotaxis index of the CTL animals. The higher the learning index, the more the animals have learned and thus kept the BTN memory. Wild type is shown with grey bars and *osm-9(ky10)* with pink bars, and will be denoted this way throughout the manuscript. One-way ANOVA followed by Bonferroni correction was performed for one-cycle wild type vs *osm-9(ky10)*, one-cycle vs three-cycle wild type, one-cycle wild type vs three-cycle *osm-9(ky10),* one-cycle *osm-9(ky10)* vs three-cycle wild type, one-cycle vs three-cycle *osm-9(ky10)*, and three-cycle wild type vs *osm-9(ky10).*

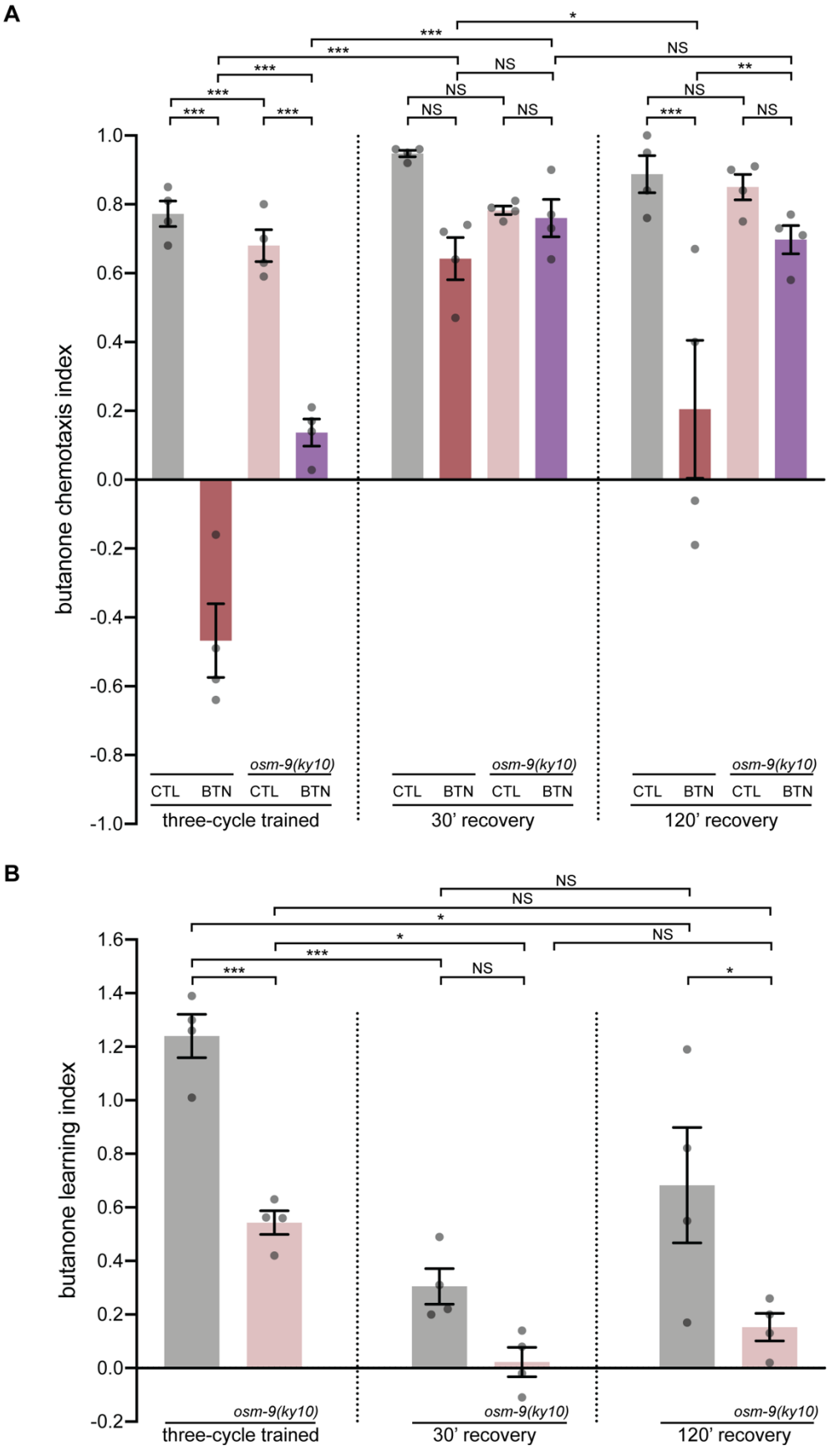
A
butanone chemotaxis index
1.0
0.8
0.6
0.4
0.2
0.0
-0.2
-0.4
-0.6
-0.8
-1.0
***
***
***
***
***
NS
NS
NS
NS
NS
NS
**
*
osm-9(ky10)
CTL
BTN
CTL
BTN
three-cycle trained
30' recovery
120' recovery
B
butanone learning index
1.6
1.4
1.2
1.0
0.8
0.6
0.4
0.2
0.0
-0.2
***
*
***
NS
NS
NS
*
*
osm-9(ky10)
three-cycle trained
30' recovery
120' recovery

Fig 3.2. The TRPV channel *osm-9* is required for long-term olfactory memory consolidation post spaced training. (A) Chemotaxis indices for three-cycle spaced-trained animals after 0', 30' or 120' post recovery on plates seeded with OP50 as a food source. One-way ANOVA followed by Bonferroni correction was performed for CTL vs BTN, *osm-9(ky10)* CTL vs *osm-9(ky10)* BTN, CTL 30' vs BTN 30', *osm-9(ky10)* CTL 30' vs *osm-9(ky10)* BTN 30', CTL 120' vs BTN 120', *osm-9(ky10)* CTL 120' vs *osm-9(ky10)* BTN 120', CTL vs *osm-9(ky10)* CTL, BTN vs *osm-9(ky10)* BTN, CTL 30' vs *osm-9(ky10)* CTL 30', BTN 30' vs *osm-9(ky10)* BTN 30', CTL 120' vs *osm-9(ky10)* CTL 120', BTN 120' vs *osm-9(ky10)* BTN 120', BTN vs BTN 30', *osm-9(ky10)* BTN vs *osm-9(ky10)* BTN 30', BTN 30' vs BTN 120', and *osm-9(ky10)* BTN 30' vs *osm-9(ky10)* BTN 120'. (B) Learning indices for three-cycle spaced-trained animals after 0', 30', or 120' recovery on food. One-way ANOVA followed by Bonferroni correction was performed for wild-type vs *osm-9(ky10)* after 0' recovery (compare first two bars), 30' recovery (compare third and fourth bars), 120' recovery (compare fifth and sixth bars), wild-type 0' vs 30' *osm-9(ky10)* 0' vs 30', *osm-9(ky10)* 30' vs 120', wild-type 0' vs 120', *osm-9(ky10)* 0' vs 120', and wild-type 30' vs 120', all after three-cycle spaced-training.

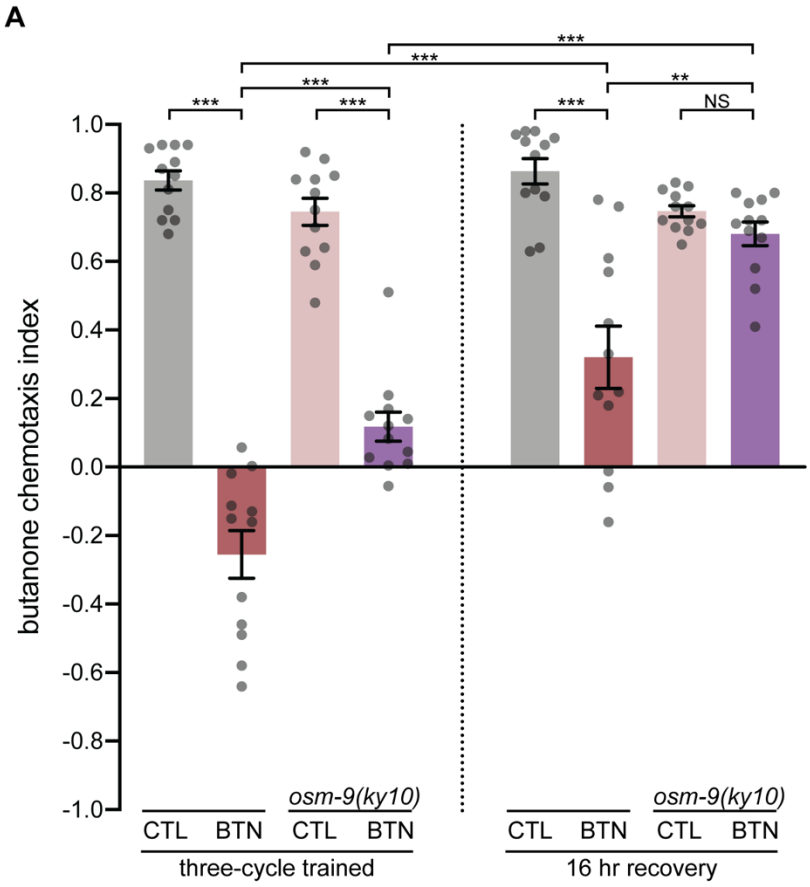
A
butanone chemotaxis index
1.0
0.8
0.6
0.4
0.2
0.0
-0.2
-0.4
-0.6
-0.8
-1.0
***
***
***
***
***
**
NS
CTL
BTN
osm-9(ky10)
CTL
BTN
three-cycle trained
CTL
BTN
osm-9(ky10)
CTL
BTN
16 hr recovery

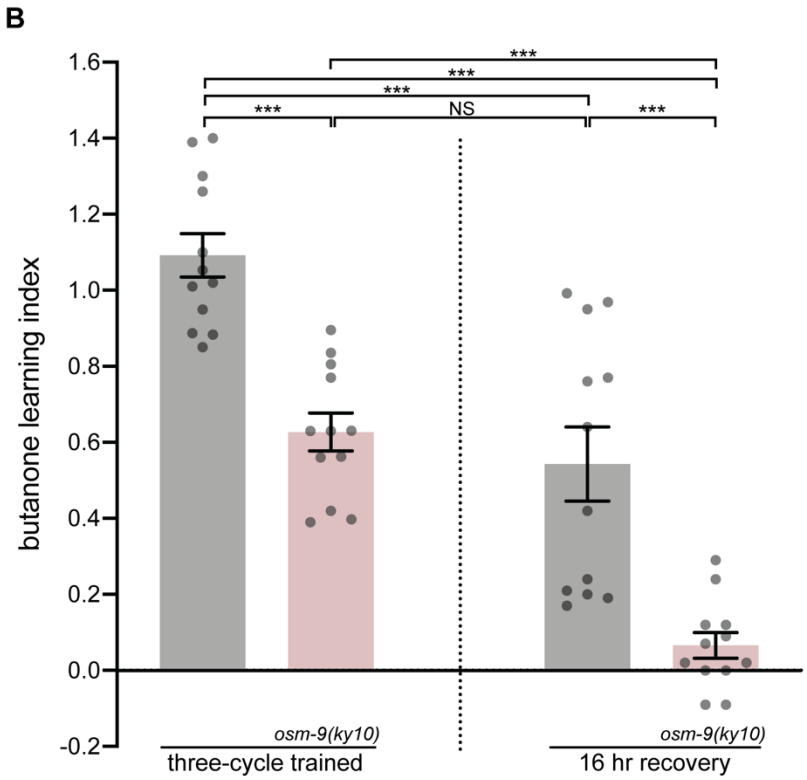
B
butanone learning index
1.6
1.4
1.2
1.0
0.8
0.6
0.4
0.2
0.0
-0.2
***
***
***
***
NS
***
osm-9(ky10)
three-cycle trained
osm-9(ky10)
16 hr recovery

Fig 3.3. *osm-9* animals do not maintain the memory 16 hours after training. (A) Chemotaxis indices for three-cycle trained animals after 0' vs 16 hours of recovery on food. The Kruskal-Wallis test was performed. The u-test was performed for *osm-9(ky10)* CTL vs *osm-9(ky10)* BTN, CTL 16 hr vs BTN 16 hr, *osm-9(ky10)* BTN vs *osm-9(ky10)* BTN 16hr, and BTN vs *osm-9(ky10)* BTN. The t-test was performed for CTL vs BTN, BTN 16 hr vs *osm-9(ky10)* BTN 16 hr, *osm-9(ky10)* CTL 16 hr vs *osm-9(ky10)* BTN 16 hr, and BTN vs BTN 16 hr.
(B) Learning indices for three-cycle trained animals after 0' vs 16 hours of recovery on food. The Kruskal-Wallis test was performed. The u-test was performed for wild type 16 hr vs *osm-9(ky10)* 16 hr, wild type 0' vs wild type 16 hr, and *osm-9(ky10)* 0' vs wild type 16 hr. The t-test was performed for wild type 0' vs *osm-9(ky10)* 0', *osm-9(ky10)* 0' vs *osm-9(ky10)* 16 hr, and wild type 0' vs *osm-9(ky10)* 16 hr.

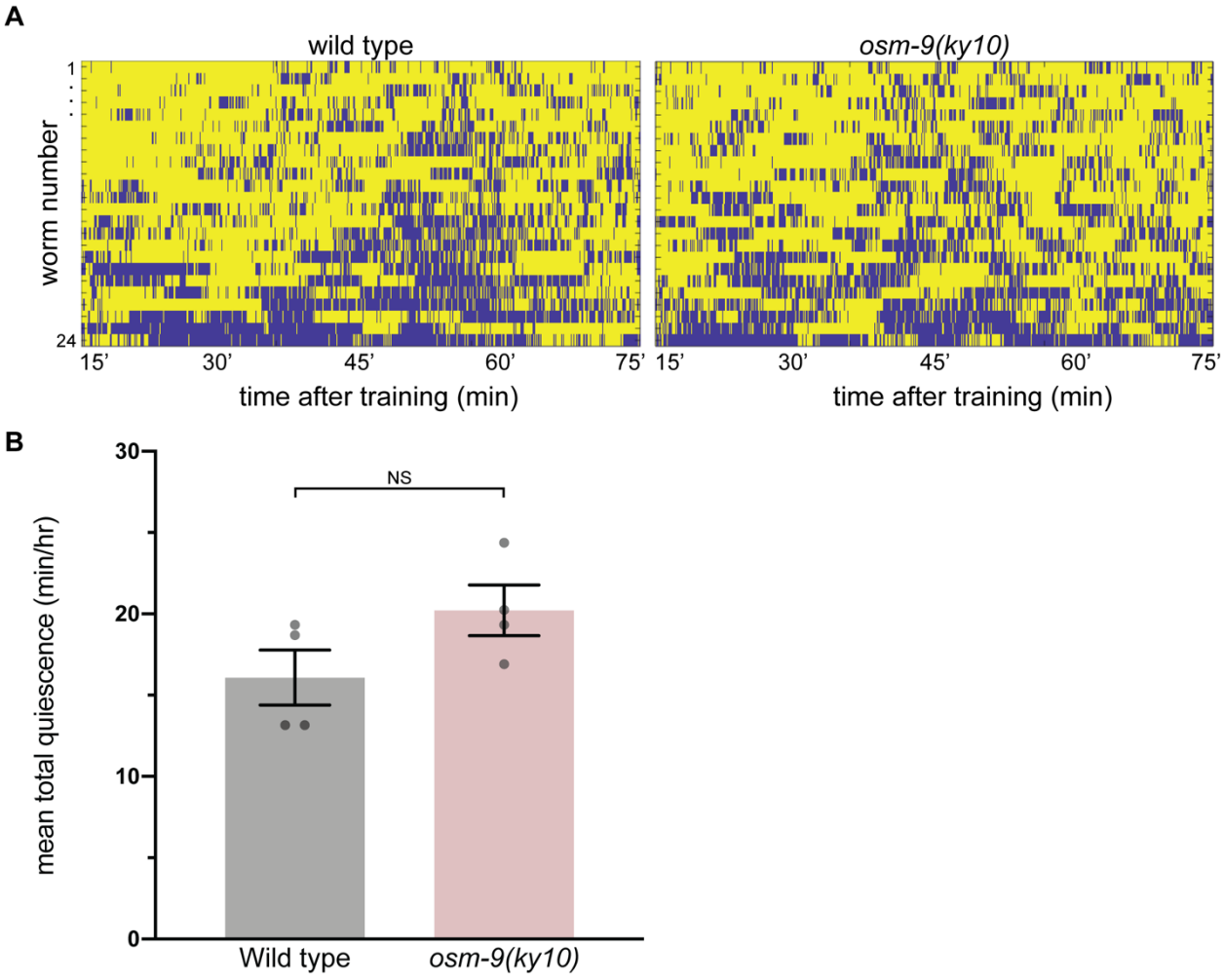

Fig 3.4. Spaced-training does not induce a difference in quiescence between wild type versus *osm-9(ky10)* in the hour post training. (A) Raster plot of activity of wild-type and *osm-9(ky10)* animals 15-75 minutes after three-cycle spaced training. Animals were placed in a WorMotel (Churgin et al., 2017) and videos were taken of their movement. Worm number is shown on the y-axis where each row represents one worm, with 24 worms total shown per plot. Yellow indicates activity and blue indicates quiescence, which was defined as no movement for more than 30 seconds.
(B) The mean total quiescence after spaced training is not significantly different between wild-type and *osm-9(ky10)* animals. Mean total quiescence in minutes per hour of animals in a WorMotel. Each grey dot represents 24 animals tested per condition on an independent day. The t-test was performed.

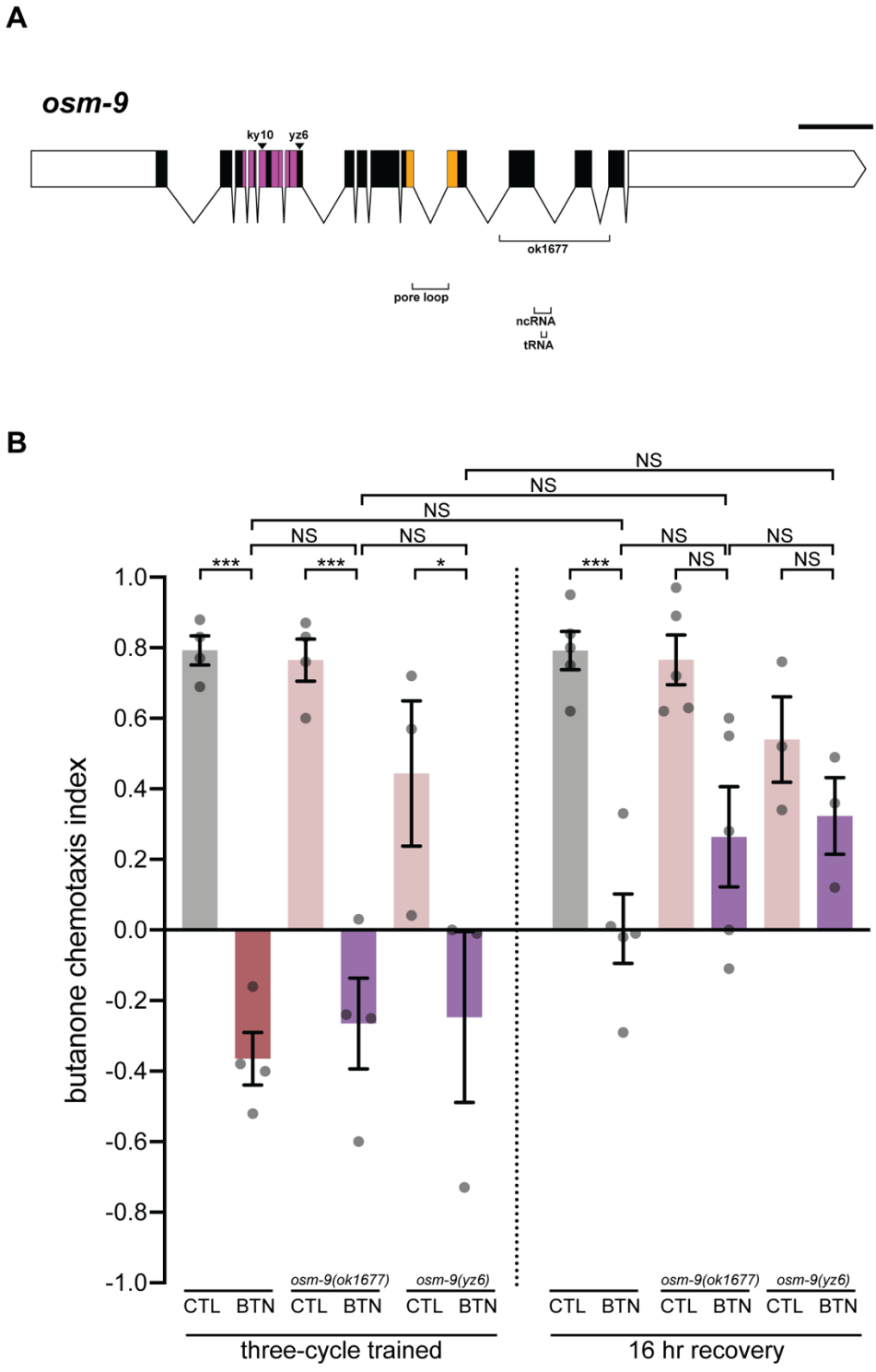

Fig 3.5. The *osm-9(ok1677)* and *osm-9(yz6)* animals can acquire, but cannot maintain long-term memory. (A) Gene map of *osm-9.* Exons are denoted by black boxes and introns are black lines connecting the exons. Red-violet indicates ankyrin repeats (six total). Orange indicates a PKD channel domain. The 5' end white box represents an ~1.6 kb promoter region (Colbert et al., 1997). The 3' end white box

represents an ~3.2 kb promoter region (Colbert et al., 1997). Scale bar indicates 1000 bases. Black arrowheads indicate alleles with point mutations producing early stop codons (*ky10* and *yz6*). The bracket labeled *ok1677* denotes a deletion allele. The brackets labeled ncRNA and tRNA are predicted RNAs produced from these regions. The bracket labeled pore loop denotes the region permeable to calcium, located between the fifth and sixth transmembrane domains.
(B) Chemotaxis indices for three-cycle trained animals with no recovery or 16 hours recovery on food for wild-type, *osm-9(ok1677)* and *osm-9(yz6)* animals. Grey and red bars are wild-type buffer- and butanone-trained animals and pink and purple are *osm-9* buffer- and butanone-trained animals. One-way ANOVA, followed by Bonferroni correction was performed for three-cycle CTL vs BTN, three-cycle *osm-9(ok1677)* CTL vs *osm-9(ok1677)* BTN, three-cycle *osm-9(yz6)* CTL vs *osm-9(yz6)* BTN, 16 hr CTL vs BTN, 16 hr *osm-9(ok1677)* CTL vs *osm-9(ok1677)* BTN, 16 hr *osm-9(yz6)* CTL vs *osm-9(yz6)* BTN, three-cycle BTN vs three-cycle *osm-9(ok1677)* BTN, three-cycle *osm-9(ok1677)* BTN vs three-cycle *osm-9(yz6)* BTN, 16 hr BTN vs 16 hr *osm-9(ok1677)* BTN, 16 hr *osm-9(ok1677)* BTN vs 16 hr *osm-9(yz6)* BTN, three-cycle BTN vs 16 hr BTN, three-cycle *osm-9(ok1677)* BTN vs 16 hr *osm-9(ok1677)* BTN, and three-cycle *osm-9(yz6)* BTN vs 16 hr *osm-9(yz6)* BTN.

A

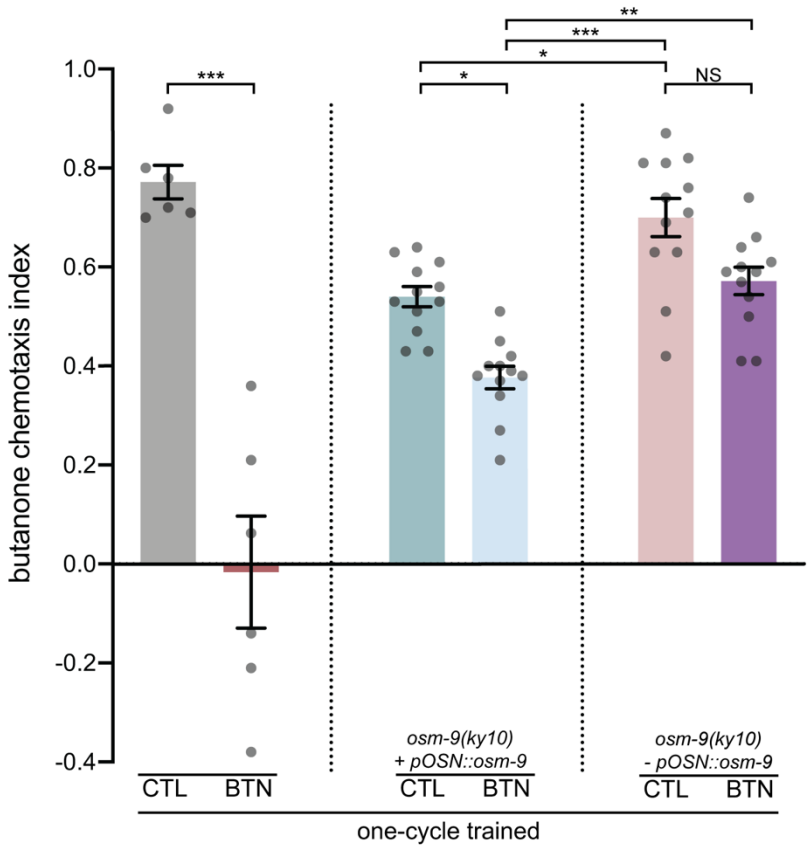
butanone chemotaxis index
1.0
0.8
0.6
0.4
0.2
0.0
-0.2
-0.4
***
*
*
***
**
NS
CTL
BTN
osm-9(ky10)
+ pOSN::osm-9
CTL
BTN
osm-9(ky10)
- pOSN::osm-9
CTL
BTN
one-cycle trained

B

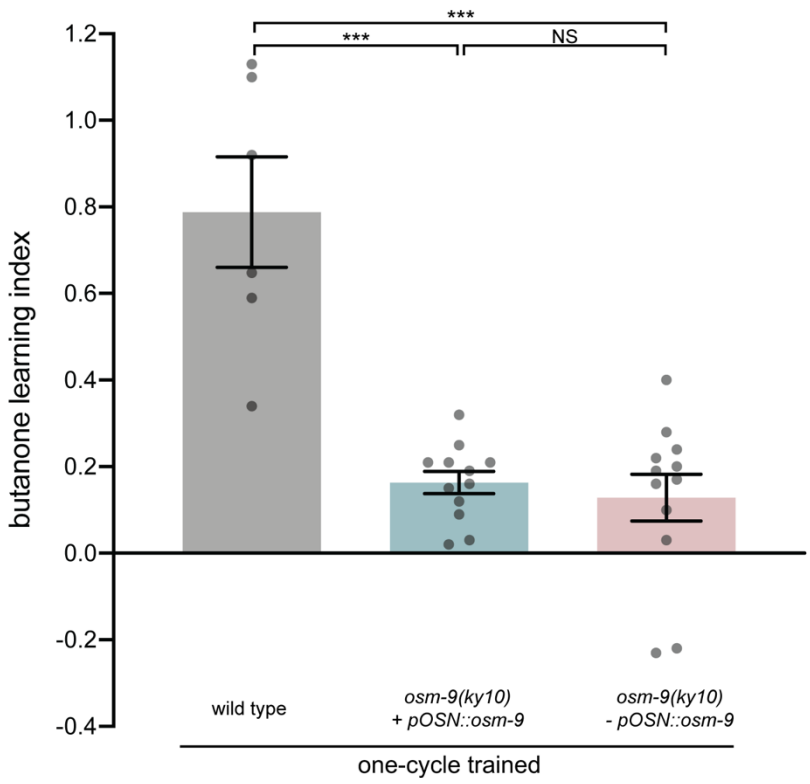
butanone learning index
1.2
1.0
0.8
0.6
0.4
0.2
0.0
-0.2
-0.4
***
***
NS
wild type
osm-9(ky10)
+ pOSN::osm-9
osm-9(ky10)
- pOSN::osm-9
one-cycle trained

Fig 3.6. Expressing *osm-9* cDNA under the endogenous and OSN promoters in the *ky10* background only partially rescues short-term memory defects. (A) Chemotaxis indices of one-cycle trained animals. Chemotaxis indices of one 80-minute cycle buffer (CTL, first bar, grey) vs butanone-trained (BTN, second bar, red) wild-type animals, buffer-trained (CTL, third bar, teal) vs butanone-trained (BTN, fourth bar, light blue) *osm-9(ky10) IV;* $_p$*OSN::osm-9* animals, and buffer-trained (CTL, fifth bar, pink) vs butanone-trained (BTN, sixth bar, purple) non-transgenic siblings. The transgene is *KBC41/*$_p$*OSN::osm-9::UTR.* The $_p$*OSN* is the $_p$*odr-3* olfactory sensory neuron promoter, driving expression in the AWA, AWB, and AWC neurons, *osm-9* is the full length cDNA (~2.8 kb), and is also driven by the 3' UTR downstream endogenous promoter (~3.2 kb) shown to drive expression in various sensory neurons (Colbert et al., 1997). Transgenic data is from two combined lines. For Fig 1A, one-way ANOVA was performed, followed by the Bonferroni correction for multiple comparisons for CTL vs BTN, CTL vs BTN *osm-9(ky10); +*$_p$*OSN::osm-9*, CTL vs BTN *osm-9(ky10); -* $_p$*OSN::osm-9* (non-transgenic siblings), CTL *osm-9(ky10); +*$_p$*OSN::osm-9* vs CTL *osm-9(ky10); -*$_p$*OSN::osm-9*, BTN *osm-9(ky10); +*$_p$*OSN::osm-9* vs CTL *osm-9(ky10); -*$_p$*OSN::osm-9*, and BTN *osm-9(ky10); +*$_p$*OSN::osm-9* vs BTN *osm-9(ky10); -*$_p$*OSN::osm-9.*
(B) Learning indices for the odor-conditioned animals. One-way ANOVA followed by Bonferroni correction for wild type (first bar, grey) vs *osm-9(ky10); +*$_p$*OSN::osm-9* (second bar, teal), *osm-9(ky10); +*$_p$*OSN::osm-9* vs *osm-9(ky10); -*$_p$*OSN::osm-9* (third bar, pink), and wild type vs *osm-9(ky10); -*$_p$*OSN::osm-9*.

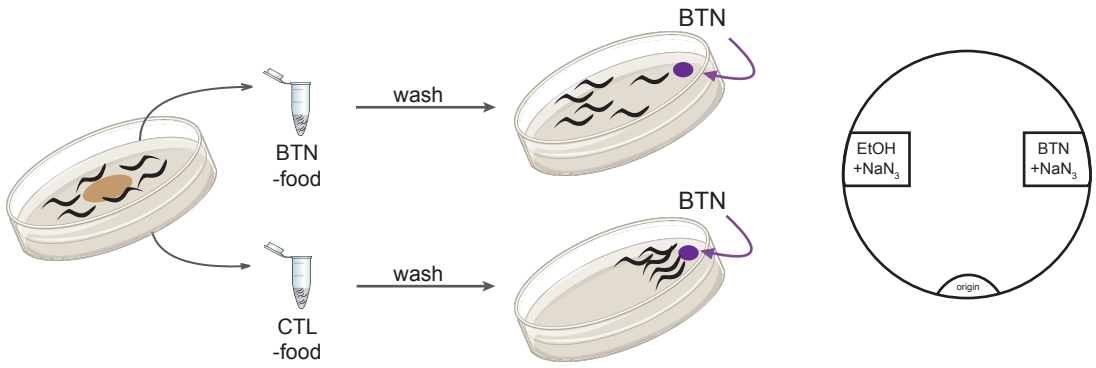

Fig 3.S1. Schematic of one-cycle odor-conditioning. Animals are conditioned to butanone as previously published (Juang et al., 2013). In brief, age-synchronized, one-day old adult animals are washed with buffer from NGM plates containing OP50 food to tubes with either buffer or butanone, both containing no food, for 80 minutes. After the 80-minute incubation, animals are washed and then plated onto chemotaxis assay plates. The chemotaxis index (See Fig 1 legend) is then calculated after at least two hours of the animals roaming.

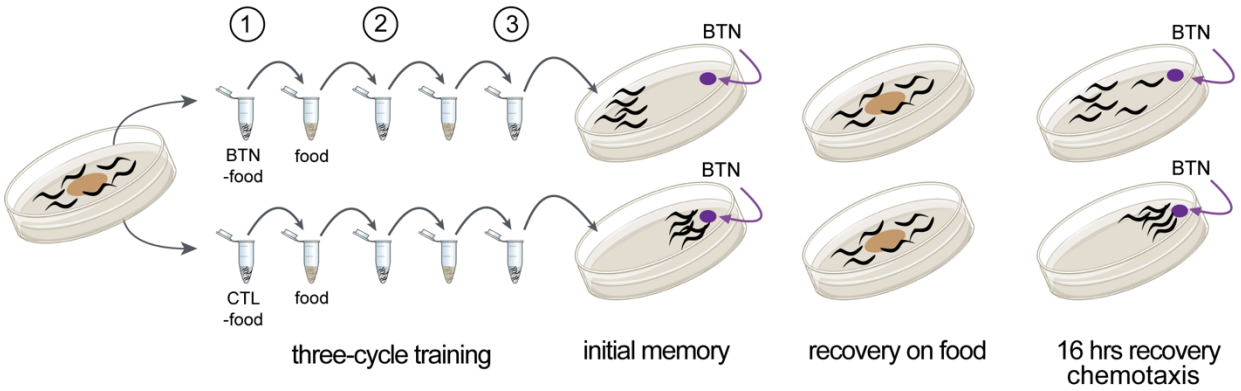

Fig 3.S2 Spaced-training paradigm. Schematic of associative olfactory memory assay to induce long-term odor memory. Age-synchronized, one-day old adult animals are washed from plates with food into tubes and are conditioned to either buffer (CTL) or butanone (BTN) for 80 minutes per cycle in the absence of food for three cycles total, with a 30-minute recovery on food (OP50, OD = 10) in between cycles. After spaced-training, animals are either tested in a butanone chemotaxis assay or are recovered on OP50-seeded NGM plates and then tested.

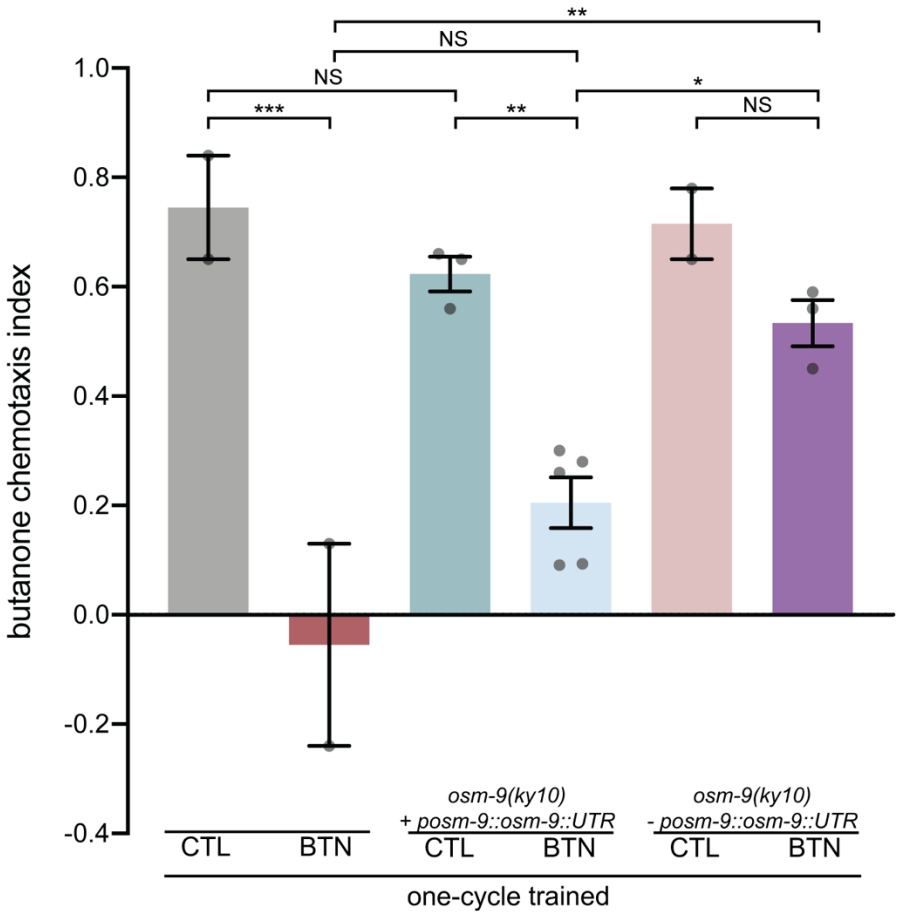

Fig 3.S3. Expressing *osm-9* gDNA under its upstream and downstream endogenous promoters in the *ky10* background rescues short-term memory defects. Chemotaxis indices of one-cycle trained animals. *KBC56/*$_p$*osm-9::osm-9::UTR* is the rescue transgene, where $_p$*osm-9* is the 1.6 kb upstream promoter (Fig 7A), *osm-9* is the full-length gDNA (6342 bp), and UTR is the 3.2 kb downstream promoter (Fig 7A). Teal and blue bars are *osm-9(ky10)* animals expressing $_p$*osm-9::osm-9::UTR* and pink and purple bars are the *osm-9(ky10)* non-transgenic siblings. Uneven number of grey dots because only datasets with N>50 were counted in the graph and analysis. One-way ANOVA was performed, followed by Bonferroni correction for CTL vs BTN, *osm-9(ky10)* + $_p$*osm-9::osm-9::UTR* CTL vs *osm-9(ky10)* + $_p$*osm-9::osm-9::UTR* BTN, *osm-9(ky10)* - $_p$*osm-9::osm-9::UTR* CTL vs *osm-9(ky10)* - $_p$*osm-9::osm-9::UTR* BTN, BTN vs *osm-9(ky10)* + $_p$*osm-9::osm-9::UTR* BTN, *osm-9(ky10)* + $_p$*osm-9::osm-9::UTR* BTN vs *osm-9(ky10)* - $_p$*osm-9::osm-9::UTR* BTN, CTL vs *osm-9(ky10)* + $_p$*osm-9::osm-9::UTR* CTL, and BTN vs *osm-9(ky10)* - $_p$*osm-9::osm-9::UTR* BTN.

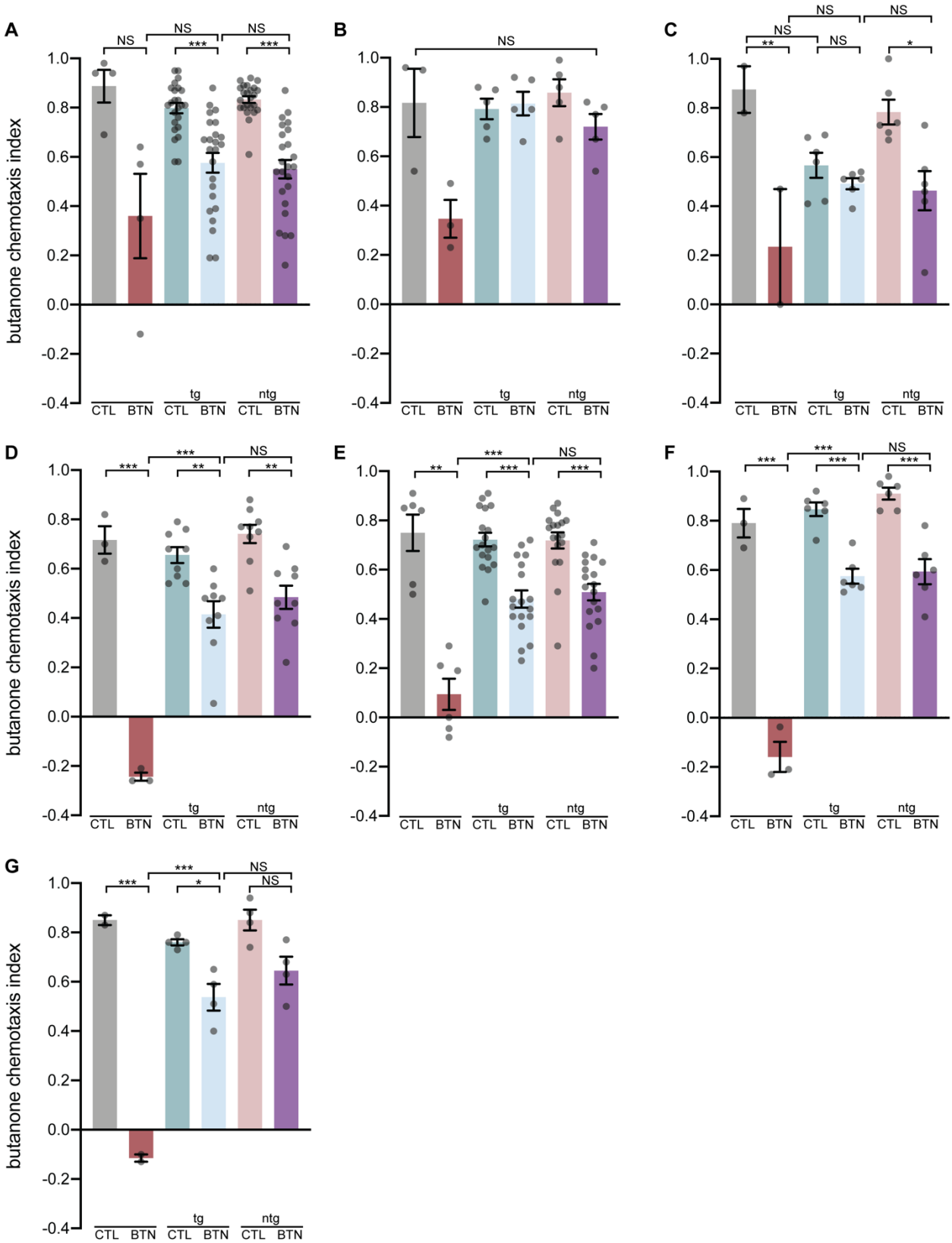

Fig 3.S4. Various *osm-9* expression transgenes are not sufficient to achieve rescue of *osm-9(ky10)* one-cycle butanone conditioning defects. (A) Chemotaxis

indices of wild type versus *osm-9(ky10),* with or without the transgene *KBC8/$_p$ceh-36::osm-9SS::GFP::osm-9.* The *pceh-36* is a promoter driving expression in both of the AWC olfactory sensory neurons. The *osm-9SS* (signal sequence) cDNA was 5' of the GFP and the rest of the cDNA was 3' of the GFP. Data shown from six combined transgenic lines. The Kruskal-Wallis test was performed. Transgenic is tg and non-transgenic is ntg. The u-test was used for CTL vs BTN and ntg CTL vs ntg BTN. The t-test was performed for tg CTL vs tg BTN, BTN vs tg BTN, and tg BTN vs ntg BTN.
(B) Chemotaxis indices of wild type versus *osm-9(ky10),* with or without the transgene *pJK21/$_p$odr-3::GFP::osm-9.* The *$_p$odr-3* promoter drives expression in all three of the pairs of olfactory sensory neurons, including AWA, AWB, and AWC. The *$_p$odr-3* used was the short promoter, 2653 bp in length. The *osm-9* used in the same partial cDNA as in panel A. Data shown from two combined transgenic lines. The Kruskal-Wallis test was used and p>0.05.
(C) Chemotaxis indices of wild type versus *osm-9(ky10),* with or without the transgene *KBC24/$_p$odr-3::GFP::osm-9.* The *$_p$odr-3* promoter drives expression in all three of the pairs of olfactory sensory neurons, including AWA, AWB, and AWC. The *$_p$odr-3* used was the long promoter, 2686 bp in length. The *osm-9* used in the same partial cDNA as in panel A. Data shown from three combined transgenic lines. One-way ANOVA was performed, followed by Bonferroni correction for CTL vs BTN, tg CTL vs tg BTN, ntg CTL vs ntg BTN, BTN vs tg BTN, tg BTN vs ntg BTN, CTL vs tg CTL, and tg CTL vs ntg CTL.
(D) Chemotaxis indices of wild type versus *osm-9(ky10),* with or without the transgene *osm-9::GFP5* (Colbert et al., 1997), which includes the *osm-9* partial cDNA (2497 bp, missing the last 317 bp) driven by the upstream ~1.6 kb promoter and downstream ~3.2 kb promoter, and GFP, cloned into the pBS parent vector. Data shown from three combined transgenic lines. One-way ANOVA was performed, followed by Bonferroni correction for CTL vs BTN, tg CTL vs tg BTN, ntg CTL vs ntg BTN, BTN vs tg BTN, and tg BTN vs ntg BTN.
(E) Chemotaxis indices of wild type versus *osm-9(ky10),* with or without the transgene *KBC42/$_p$osm-9::osm-9::UTR*, where *posm-9* is the upstream ~1.6 kb promoter, *osm-9* is the full-length cDNA (2814 bp), and *UTR* is the ~3.2 kb downstream promoter. Data shown from three combined transgenic lines. The Kruskal-Wallis test was performed. The u-test was used for CTL vs BTN and ntg CTL vs ntg BTN. The t-test was performed for tg CTL vs tg BTN, BTN vs tg BTN, and BTN tg vs ntg BTN.
(F) Chemotaxis indices of wild type versus *osm-9(ky10),* with or without the transgene WRM065bE12, a ~32 kb fosmid containing the entire *osm-9* gene its upstream and downstream UTR regions. Data shown from two combined transgenic lines. One-way ANOVA was performed, followed by Bonferroni correction for CTL vs BTN, tg CTL vs tg BTN, ntg CTL vs ntg BTN, BTN vs tg BTN, and tg BTN vs ntg BTN.
(G) Chemotaxis indices of wild type versus *osm-9(ky10),* with or without the transgene *KBC38/$_p$nphp-4::osm-9::GFP.* The *$_p$nphp-4* promoter drives expression in all of the ciliated neurons (~60) in the adult worm. The *osm-9* transgene was the full-length cDNA. Data shown from two combined transgenic lines. One-way ANOVA was performed, followed by Bonferroni correction for CTL vs BTN, tg CTL vs tg BTN, ntg CTL vs ntg BTN, BTN vs tg BTN, and tg BTN vs ntg BTN.

MATERIALS AND METHODS

Strains and genetics

Strains were maintained by standard methods (Brenner, 1974) and were grown on either 5.5 cm or 10 cm Petri dishes with NGM media seeded with OP50 *E. coli*. All strains were grown at and assayed at 20°C. The wild-type strain is the *C. elegans* N2 Bristol variant. Mutants used in the study include *osm-9(ky10) IV* (Colbert and Bargmann, 1995)*, osm-9(ok1677) IV,* and *osm-9(yz6) IV.* All rescue experiments (**Fig 3.1, Fig 3.S2, Fig 3.S4**) were performed in the *osm-9(ky10) IV* background. The transgenic lines used for the rescue experiments are JZ1967 and JZ1968 [*KBC41/$_p$odr-3::osm-9::UTR* (50 ng/µl), *$_p$unc-122::mCherry* (20 ng/µl)], (**Fig 3.1**); JZ2034, JZ2035, and JZ2036 [*KBC56/$_p$osm-9::osm-9::UTR* (50 ng/µl), *pCFJ90/pmyo-2::mCherry* (2.5 ng/µl), *pSMdelta* (100 ng/µl)], (**Fig 3.S2**); JZ1655 and JZ1656 [*KBC8/$_p$ceh-36::GFP::osm-9* (100 ng/µl), *$_p$unc-122::GFP* (20 ng/µl)], (**Fig 3.S4A**); JZ1621 and JZ1622 [*pJK21/$_p$odr-3::GFP::osm-9* (50 ng/µl), *$_p$unc-122::mCherry* (20ng/µl), ScaI-digested N2 DNA (30 ng/µl)], (**Fig 3.S4B**); JZ1819 and JZ1874 [*KBC24/$_p$odr-3::osm-9* (50 ng/µl), *pCFJ104/$_p$myo-3::mCherry* (5 ng/µl)], (**Fig 3.S4C**); JZ1940 and JZ1941 [fosmid WRM065bE12 (from Source BioScience, 5 ng/µl), *$_p$unc-122::GFP* (20 ng/µl), *$_p$str-2::GCaMP3::mCherry* (25 ng/µl)], (**Fig 3.S4D**); lines containing *osm-9::GFP5* (25 ng/µl), *$_p$unc-122::mCherry* (20 ng/µl), (**Fig 3.S4E**); lines containing *KBC42/$_p$osm-9::osm-9::UTR* (50 ng/µl), *$_p$unc-122::mCherry* (20 ng/µl) or *KBC42/$_p$osm-9::osm-9::UTR* (10 ng/µl), *pCFJ90/$_p$myo-2::mcherry* (2.5 ng/µl), *pSMdelta* (140 ng/µl), (**Fig 3.S4F**); JZ1905 and JZ1906 [*KBC38/$_p$nphp-4::osm-9::GFP* (5 ng/µl), *$_p$unc-122::mCherry* (20 ng/µl); *osm-*

9(ky10) IV gDNA (8 ng/µl); *$_p$ceh-36::mCherry* (5 ng/µl)], (**Fig 3.S4G**). ScaI-digested N2 DNA, *osm-9(ky10) IV* gDNA, or *pSMdelta* (empty vector) were used to bring up the total injection concentration to ensure transgenesis (Evans, 2006). JZ designations are L'Etoile lab strain names.

Molecular Biology

Constructs were made using standard molecular techniques. The construct *pJK21/$_p$odr-3::osm-9SS::GFP::osm-9cDNA* was made by replacing the *$_p$str-2* promoter in *pJK17/$_p$str-2::osm-9SS::GFP::osm-9cDNA*, digested with NotI and AscI restriction enzymes, with the subcloned *$_p$odr-3* fragment from *pJK15/$_p$odr-3::osm-9SS::GFP::osm-9cDNA*, using NotI and AscI. *KBC8/$_p$ceh-36::osm-9SS::GFP::osm-9cDNA* was made by amplifying *$_p$ceh-36* with primers KLB30 (TAACGGCCGGCCTCATCAGCCTACACGTCATC) and KLB31 (ACATAGGCGCGCCCGCAAATGGGCGGAGGGT) to add FseI and AscI sites on and digesting *pAW1/$_p$odr-3::osm-9SS::GFP::osm-9cDNA* with FseI and AscI to remove *$_p$odr-3* and subclone the *$_p$ceh-36* fragment in. *KBC41/$_p$odr-3::osm-9cDNA::UTR* was made by digesting *KBC24/$_p$odr-3::osm-9cDNA* with NheI and NcoI and subcloning in the *osm-9* downstream promoter (~3.2kb), amplified off of phenol-extracted followed by ethanol precipitated whole-worm gDNA (Phenol pH 8 from Sigma Aldrich), using the KLB161 (AGACGCTAGCGAACTTTTTTCTTCTAATTTTTTGA) and KLB162 (AACTCCATGGTTAGGTACATTTAAGGTCGATC) primers, adding on the NheI and NcoI sites. *KBC24/$_p$odr-3::osm-9cDNA* was made by digesting *KBC23/$_p$odr-3* with KpnI and NheI and subcloning in *osm-9* cDNA, amplified from whole-worm cDNA (a kind gift

from Maria Gallegos) using primers KLB25 (AACTGGTACCTCATTCGCTTTTGTCATTTGTC) and KLB90 (AGACGCTAGCATGGGCGGTGGAAGTTCG), which add on the KpnI and NheI sites. *KBC42/$_p$osm-9::osm-9cDNA::UTR* was made by digesting *KBC41/$_p$odr-3::osm-9cDNA::UTR* with NotI and XmaI and subcloning in the upstream *osm-9* promoter (~1.6 kb), amplified off of phenol-extracted followed by ethanol precipitated whole-worm gDNA (Phenol pH 8 from Sigma Aldrich), using the primers KLB163 (AGACGCGGCCGCCGCGGGAGTACTTTACGGG) and KLB164 (AACTCCCGGGGTTTGGTTTCTGAAAAAATTGG), adding on NotI and XmaI sites. *KBC38/$_p$nphp-4::GFP::osm-9* was made by digesting *KBC26/$_p$odr-3::osm-9cDNA::GFP* with NotI and NruI and subcloning in the *nphp-4* promoter amplified from *pAK59/$_p$nphp-4::GFP::npp-19* (a kind gift from Piali Sengupta) with primer KLB127 (AGACGCGGCCGCCAACATTATTAATCACTGCAAC) and KLB128 (AACTTCGCGAACTTCCACCGCCCATCTCATTTTTCGAGACTTTGTTA), adding on NotI and NruI sites. KBC56 was made by the following instructions: osm-9 gDNA was amplified with the primers KLB289 (GTTGTTTACCTTTTATGTTCATCCG) and KLB290 (AAATTTTCTACTGCCTGGTATCAAA) off of phenol-extracted followed by ethanol precipitated whole-worm gDNA (Phenol pH 8 from Sigma Aldrich). The *osm-9* gDNA fragment plus extra upstream and downstream homologous sequence was amplified off of the gDNA amplified with KLB289 and KLB290, using the primers KLB298 (GTTGTTTACCTTTTATGTTCAT) and KLB299 (AAAATGATCCACATAAAATTTTCTACTGCCTGGTAT). The *osm-9* upstream partial fragment (~1.2 kb) was amplified using the primers KLB296

(TGATTACGCCAAGCTTCGCGGGAGTACTTTACGG) and KLB297 (TAAAAGGTAAACAACTAGTTTTTAGTACATGAAATAATT) off of the template KBC42/ *$_p$osm-9::osm-9cDNA::UTR*, and the downstream promoter partial fragment was amplified with KLB300 (TATGTGGATCATTTTTGTCTC) and KLB301 (CCGCGCATGCAAGCTTTTAGGTACATTTAAGGTCGAT) off of KBC42/ *$_p$osm-9::osm-9cDNA::UTR*. The three fragments were then recombined in the *pSM* plasmid (linearized with HindIII) using the Takara Infusion HD Cloning kit. The *pSM* plasmid was from Steve McCarroll.

Chemotaxis assay

We utilized the chemotaxis assay from Bargmann et al., 1993. About 4-5 Larval stage 4 (L4) animals were put onto NGM plates seeded with OP50 *E. coli* for 5 days at 20°C, or until populations are one-day old adults. Any plates with fungal or bacterial contamination were not included in the assays. Animals were then washed off the plates using S. basal buffer and into microfuge tubes (sterile, but not autoclaved), where they were conditioned to either S. basal buffer (0.1M NaCl, 0.05M K_3PO_4, pH 6.0), or 2-butanone (Sigma) diluted in S. basal buffer, 1:10,000 (1.23 mM) concentration. Animals were incubated for 80 minutes on a rotating microfuge tube stand. Next, animals were washed two times with S. basal, where the worms were allowed to pellet (about two to three minutes) without spinning them down. Next, the worms were washed with ddH_2O to ensure all salts were removed, and then placed onto a 10 cm Petri dish chemotaxis plate. The chemotaxis plate media was made by adding 100 mL ddH_2O to 1.6 g of Difco bacto agar, then boiled, and then 500 µl of 1M K_3PO_4, 100 µl 1M $CaCl_2$ and 100 µl 1M

$MgSO_4$ were added, and then the media was pipetted at 10 ml per 10 cm plastic petri dish and let cool to solidify, and then square odor arenas and an origin were drawn (S1 Fig). The chemotaxis plate was made with two point sources – one arena with 1 ul of 200-proof ethanol, and the other arena with 1 µl of 1:1000 butanone in ethanol. Each point source also contained 1 µl of 1M sodium azide (Fisher Scientific) to paralyze worms once they reached the arenas (S1 Fig). Animals were placed at the origin, the liquid was removed with a Kim Wipe, and then animals were allowed to roam for at least two hours. Then, the chemotaxis index or learning index was calculated (Fig 1 legend). For reference, most untrained or buffer-trained wild-type animals have a butanone chemotaxis index from 0.6 to 0.9. If pairwise comparisons between the chemotaxis indices of the buffer-trained and butanone-trained populations of the same genotype were not significantly different from each other, then we deemed them memory defective.

LTM chemotaxis assay

The assay is performed as written above in the “Chemotaxis assay” section, but for three cycles instead of just one, with recovery periods on food in between. Animals are incubated for 80 minutes in either buffer or butanone diluted in buffer. Animals are washed, and then incubated for 30 minutes in OP50 diluted in S. basal buffer (OD = 10). Animals are washed as before, but then conditioned for another 80 minutes in either buffer or diluted butanone, making this the second odor-treatment cycle. Animals are then washed and incubated with OP50 for another 30 minutes, washed, and then subjected to a third buffer or odor conditioning cycle. Animals are then washed as

before, and plated onto chemotaxis plates (this is the 0' recovery, three-cycle trained worms), or recovered on 5.5 cm NGM plates seeded with OP50 for either 30', 120', or 16 hours, where they are then subjected to the chemotaxis assay.

WorMotel assay

The WorMotel (Churgin et al., 2017) was used according to previously published methods, as well as this link with more detailed methods (http://fangyenlab.seas.upenn.edu/links.html). In brief, a 48-well PDMS chip called the WorMotel was filled with media and seeded with OP50 (OD = 10), and one worm was placed into each individual well. Behavior was recorded by video using the Multiple Worm Tracker software (https://sourceforge.net/projects/mwt/) and movement was analyzed with Matlab software (KS_analysis_CFY_Jan2019.m and MC_QuiescenceActivity_v1202.fig, both at https://github.com/cfangyen/LEtoile_WorMotel). Excel sheets with total quiescence for each worm is generated from the Matlab code. The mean total quiescence was then taken for statistical analysis.

Statistical Analysis

All data included in the same graph were subjected to the Shapiro-Wilk normality test. If all of the datasets were normally distributed, then one-way ANOVA was performed, followed by Bonferroni correction for pairwise comparisons. If any datasets were non-normally distributed, then the Kruskal-Wallis test was performed. If $p>0.05$, then no further analysis was performed. If $p<0.05$, then the test was followed up by either the

Mann-Whitney u-test for non-parametric data pairwise comparisons or the Student's unpaired t-test for parametric data pairwise comparisons. All p-values included in the same graph were then adjusted using the Hochberg test to remove any type I statistical error, which prevents incorrect rejection of the null hypothesis. ***$p<0.001$, **$p<0.01$, *$p<0.05$, NS indicates $p>0.05$. All graphs show S.E.M. Graphpad Prism and R studio were used for all of the statistical tests. Each data point (represented by grey dots) on the graphs indicates one population of $400>N>50$, run on independent days.

REFERENCES

Almeida, V., Peres, F.F., Levin, R., Suiama, M.A., Calzavara, M.B., Zuardi, A.W., Hallak, J.E., Crippa, J.A., and Abílio, V.C. (2014). Effects of cannabinoid and vanilloid drugs on positive and negative-like symptoms on an animal model of schizophrenia: The SHR strain. Schizophrenia Research *153*, 150–159.

Bailey, C.H., Kandel, E.R., and Harris, K.M. (2015). Structural Components of Synaptic Plasticity and Memory Consolidation. Cold Spring Harb Perspect Biol *7*, a021758.

Balleza-Tapia, H., Crux, S., Andrade-Talavera, Y., Dolz-Gaiton, P., Papadia, D., Chen, G., Johansson, J., and Fisahn, A. TrpV1 receptor activation rescues neuronal function and network gamma oscillations from Ab-induced impairment in mouse hippocampus in vitro. 24.

Bargmann, C.I., and Horvitz, H.R. (1991). Chemosensory neurons with overlapping functions direct chemotaxis to multiple chemicals in C. elegans. Neuron *7*, 729–742.

Bargmann, C.I., Hartweig, E., and Horvitz, H.R. (1993). Odorant-selective genes and neurons mediate olfaction in C. elegans. Cell *74*, 515–527.

Bashiri, H., Hosseini-Chegeni, H., Alsadat Sharifi, K., Sahebgharani, M., and Salari, A.-A. (2018). Activation of TRPV1 receptors affects memory function and

hippocampal TRPV1 and CREB mRNA expression in a rat model of biliary cirrhosis. Neurological Research *40*, 938–947.

Birnby, D.A., Link, E.M., Vowels, J.J., Tian, H., Colacurcio, P.L., and Thomas, J.H. (2000). A Transmembrane Guanylyl Cyclase (DAF-11) and Hsp90 (DAF-21) Regulate a Common Set of Chemosensory Behaviors in Caenorhabditis elegans. Genetics *155*, 85–104.

Bovet-Carmona, M., Menigoz, A., Pinto, S., Tambuyzer, T., Krautwald, K., Voets, T., Aerts, J.-M., Angenstein, F., Vennekens, R., and Balschun, D. (2018). Disentangling the role of TRPM4 in hippocampus-dependent plasticity and learning: an electrophysiological, behavioral and FMRI approach. Brain Struct Funct *223*, 3557–3576.

Brenner, S. (1974). The genetics of Caenorhabditis elegans. Genetics *77*, 71–94.

Chen, J., Zhang, X.-F., Kort, M.E., Huth, J.R., Sun, C., Miesbauer, L.J., Cassar, S.C., Neelands, T., Scott, V.E., Moreland, R.B., et al. (2008). Molecular Determinants of Species-Specific Activation or Blockade of TRPA1 Channels. Journal of Neuroscience *28*, 5063–5071.

Cho, C.E., Brueggemann, C., L'Etoile, N.D., and Bargmann, C.I. (2016). Parallel encoding of sensory history and behavioral preference during Caenorhabditis elegans olfactory learning. ELife *5*, e14000.

Churgin, M.A., Jung, S.-K., Yu, C.-C., Chen, X., Raizen, D.M., and Fang-Yen, C. (2017). Longitudinal imaging of Caenorhabditis elegans in a microfabricated device reveals variation in behavioral decline during aging. ELife *6*, e26652.

Colbert, H., and Bargmann, C.I. (1995). Odorant-specific adaptation pathways generate olfactory plasticity in C. elegans. Neuron *14*, 803–812.

Colbert, H.A., Smith, T.L., and Bargmann, C.I. (1997). OSM-9, A Novel Protein with Structural Similarity to Channels, Is Required for Olfaction, Mechanosensation, and Olfactory Adaptation in *Caenorhabditis elegans*. J. Neurosci. *17*, 8259–8269.

Cook, S.J., Jarrell, T.A., Brittin, C.A., Wang, Y., Bloniarz, A.E., Yakovlev, M.A., Nguyen, K.C.Q., Tang, L.T.-H., Bayer, E.A., Duerr, J.S., et al. (2019). Whole-animal connectomes of both Caenorhabditis elegans sexes. Nature *571*, 63–71.

Coswna, D.J., and Manning, A. (1969). Abnormal Electroretinogram from a Drosophila Mutant. Nature *224*, 285–287.

Dang, S., van Goor, M.K., Asarnow, D., Wang, Y., Julius, D., Cheng, Y., and van der Wijst, J. (2019). Structural insight into TRPV5 channel function and modulation. Proc Natl Acad Sci USA *116*, 8869–8878.

De Petrocellis, L., Ligresti, A., Moriello, A.S., Allarà, M., Bisogno, T., Petrosino, S., Stott, C.G., and Di Marzo, V. (2011). Effects of cannabinoids and cannabinoid-enriched Cannabis extracts on TRP channels and endocannabinoid metabolic enzymes:

Novel pharmacology of minor plant cannabinoids. British Journal of Pharmacology *163*, 1479–1494.

De Petrocellis, L., Nabissi, M., Santoni, G., and Ligresti, A. (2017). Actions and Regulation of Ionotropic Cannabinoid Receptors. In Advances in Pharmacology, (Elsevier), pp. 249–289.

Di Marzo, V., Gobbi, G., and Szallasi, A. (2008). Brain TRPV1: a depressing TR(i)P down memory lane? Trends in Pharmacological Sciences *29*, 594–600.

Dudai, Y. (1996). Consolidation: Fragility on the Road to the Engram. Neuron *17*, 367–370.

Dudai, Y. (2004). The Neurobiology of Consolidations, Or, How Stable is the Engram? Annu. Rev. Psychol. *55*, 51–86.

Eguchi, N., Hishimoto, A., Sora, I., and Mori, M. (2016). Slow synaptic transmission mediated by TRPV1 channels in CA3 interneurons of the hippocampus. Neuroscience Letters *616*, 170–176.

Evans, T. (2006). Transformation and microinjection. WormBook.

Fox, K., and Stryker, M. (2017). Integrating Hebbian and homeostatic plasticity: introduction. Philosophical Transactions of the Royal Society B *372*.

Genro, B.P., de Oliveira Alvares, L., and Quillfeldt, J.A. (2012). Role of TRPV1 in consolidation of fear memories depends on the averseness of the conditioning procedure. Neurobiology of Learning and Memory *97*, 355–360.

Gibson, H.E., Edwards, J.G., Page, R.S., Van Hook, M.J., and Kauer, J.A. (2008). TRPV1 Channels Mediate Long-Term Depression at Synapses on Hippocampal Interneurons. Neuron *57*, 746–759.

van Goor, M.K.C., Hoenderop, J.G.J., and van der Wijst, J. (2017). TRP channels in calcium homeostasis: from hormonal control to structure-function relationship of TRPV5 and TRPV6. Biochimica et Biophysica Acta (BBA) - Molecular Cell Research *1864*, 883–893.

Gordus, A., Pokala, N., Levy, S., Flavell, S.W., and Bargmann, C.I. (2015). Feedback from network states generates variability in a probabilistic olfactory circuit. Cell *161*, 215–227.

Grueter, B.A., Brasnjo, G., and Malenka, R.C. (2010). Postsynaptic TRPV1 triggers cell type–specific long-term depression in the nucleus accumbens. Nat Neurosci *13*, 1519–1525.

Hall, S.E., Beverly, M., Russ, C., Nusbaum, C., and Sengupta, P. (2010). A Cellular Memory of Developmental History Generates Phenotypic Diversity in C. elegans. Current Biology *20*, 149–155.

Hellmich, U.A., and Gaudet, R. (2014). Structural Biology of TRP Channels. In Mammalian Transient Receptor Potential (TRP) Cation Channels, B. Nilius, and V. Flockerzi, eds. (Cham: Springer International Publishing), pp. 963–990.

Jauregui, A.R., and Barr, M.M. (2005). Functional characterization of the C. elegans nephrocystins NPHP-1 and NPHP-4 and their role in cilia and male sensory behaviors. Experimental Cell Research *305*, 333–342.

Juang, B.-T., Gu, C., Starnes, L., Palladino, F., Goga, A., Kennedy, S., and L'Etoile, N.D. (2013). Endogenous Nuclear RNAi Mediates Behavioral Adaptation to Odor. Cell *154*, 1010–1022.

Julius, D. (2013). TRP channels and pain. Annual Review of Cell and Developmental Biology *29*, 355—384.

Kahn-Kirby, A.H., Dantzker, J.L.M., Apicella, A.J., Schafer, W.R., Browse, J., Bargmann, C.I., and Watts, J.L. (2004). Specific Polyunsaturated Fatty Acids Drive TRPV-Dependent Sensory Signaling In Vivo. Cell *119*, 889–900.

Kaiser, M. (2015). Neuroanatomy: Connectome Connects Fly and Mammalian Brain Networks. Current Biology *25*, R416–R418.

Kang, K., Pulver, S.R., Panzano, V.C., Chang, E.C., Griffith, L.C., Theobald, D.L., and Garrity, P.A. (2010). Analysis of Drosophila TRPA1 reveals an ancient origin for human chemical nociception. Nature *464*, 597–600.

Kaufmann, A.L., Ashraf, J.M., Corces-Zimmerman, R., Landis, J.N., and Murphy, C.T. (2010). Insulin Signaling and Dietary Restriction Differentially Influence the Decline of Learning and Memory with Age. PLOS Biology *8*, e1000372.

Lee, J.I., O'Halloran, D.M., Eastham-Anderson, J., Juang, B.-T., Kaye, J.A., Scott Hamilton, O., Lesch, B., Goga, A., and L'Etoile, N.D. (2010). Nuclear entry of a cGMP-dependent kinase converts transient into long-lasting olfactory adaptation. Proceedings of the National Academy of Sciences *107*, 6016–6021.

Lent, C.M. (1977). Cellular Basis of Behavior. An Introduction to Behavioral Neurobiology. Eric R. Kandel. The Quarterly Review of Biology *52*, 326–327.

L'Etoile, N.D., and Bargmann, C.I. (2000). Olfaction and Odor Discrimination Are Mediated by the C. elegans Guanylyl Cyclase ODR-1. Neuron *25*, 575–586.

L'Etoile, N.D., Coburn, C.M., Eastham, J., Kistler, A., Gallegos, G., and Bargmann, C.I. (2002). The Cyclic GMP-Dependent Protein Kinase EGL-4 Regulates Olfactory Adaptation in C. elegans. Neuron *36*, 1079–1089.

Li, H.-B., Mao, R.-R., Zhang, J.-C., Yang, Y., Cao, J., and Xu, L. (2008). Antistress Effect of TRPV1 Channel on Synaptic Plasticity and Spatial Memory. Biological Psychiatry *64*, 286–292.

Lindy, A.S., Parekh, P.K., Zhu, R., Kanju, P., Chintapalli, S.V., Tsvilovskyy, V., Patterson, R.L., Anishkin, A., van Rossum, D.B., and Liedtke, W.B. (2014). TRPV

channel-mediated calcium transients in nociceptor neurons are dispensable for avoidance behaviour. Nat Commun *5*, 4734.

Lovelace, J.W., Vieira, P.A., Corches, A., Mackie, K., and Korzus, E. (2014). Impaired Fear Memory Specificity Associated with Deficient Endocannabinoid-Dependent Long-Term Plasticity. Neuropsychopharmacol *39*, 1685–1693.

Madasu, M.K., Roche, M., and Finn, D.P. (2015). Supraspinal Transient Receptor Potential Subfamily V Member 1 (TRPV1) in Pain and Psychiatric Disorders. In Modern Trends in Pharmacopsychiatry, D.P. Finn, and B.E. Leonard, eds. (S. Karger AG), pp. 80–93.

Marsch, R., Foeller, E., Rammes, G., Bunck, M., Kossl, M., Holsboer, F., Zieglgansberger, W., Landgraf, R., Lutz, B., and Wotjak, C.T. (2007). Reduced Anxiety, Conditioned Fear, and Hippocampal Long-Term Potentiation in Transient Receptor Potential Vanilloid Type 1 Receptor-Deficient Mice. Journal of Neuroscience *27*, 832–839.

Minke, B. (2010). The History of the *Drosophila* TRP Channel: The Birth of a New Channel Superfamily. Journal of Neurogenetics *24*, 216–233.

Montell, C., and Rubin, G.M. (1989). Molecular characterization of the drosophila trp locus: A putative integral membrane protein required for phototransduction. Neuron *2*, 1313–1323.

Morelli, M.B., Amantini, C., Liberati, S., Santoni, M., and Nabissi, M. (2013). TRP Channels: New Potential Therapeutic Approaches in CNS Neuropathies. CNS & Neurological Disorders - Drug Targets *12*, 274–293.

Muller, C., Morales, P., and Reggio, P.H. (2019). Cannabinoid Ligands Targeting TRP Channels. Front. Mol. Neurosci. *11*, 487.

Muñoz-Lobato, F., Benedetti, K.L., Farah, F., Nordquist, S.K., Bokka, A., Brueggemann, C., Li, J., Chang, E., Varshney, A., Andersen, K., Dunn, R.L., Tsujimoto, B., Tran, A., Duong, A., Churgin, M.A., Fang-Yen, C., Kato, S., VanHoven, M.K., and L'Etoile, N.D. (2019). Sleep is required to remodel specific synapses for memory consolidation. Manuscript submitted for publication.

Nagatomo, K., Ishii, H., Yamamoto, T., Nakajo, K., and Kubo, Y. (2010). The Met268Pro Mutation of Mouse TRPA1 Changes the Effect of Caffeine from Activation to Suppression. Biophysical Journal *99*, 3609–3618.

Nilius, B. (2007). TRP channels in disease. Biochimica et Biophysica Acta (BBA) - Molecular Basis of Disease *1772*, 805–812.

Nilius, B., Vennekens, R., Prenen, J., Hoenderop, J.G., Bindels, R.J., and Droogmans, G. (2000). Whole-cell and single channel monovalent cation currents through the novel rabbit epithelial Ca2+ channel ECaC. J Physiol *527 Pt 2*, 239–248.

O'Halloran, D.M., Altshuler-Keylin, S., Lee, J.I., and L'Etoile, N.D. (2009). Regulators of AWC-Mediated Olfactory Plasticity in Caenorhabditis elegans. PLoS Genet *5*, e1000761.

Peng, G., Shi, X., and Kadowaki, T. (2015). Evolution of TRP channels inferred by their classification in diverse animal species. Molecular Phylogenetics and Evolution *84*, 145–157.

Ruggiero, R.N., Rossignoli, M.T., De Ross, J.B., Hallak, J.E.C., Leite, J.P., and Bueno-Junior, L.S. (2017). Cannabinoids and Vanilloids in Schizophrenia: Neurophysiological Evidence and Directions for Basic Research. Front. Pharmacol. *8*, 399.

Sakai, T., Sato, S., Ishimoto, H., and Kitamoto, T. (2012). Significance of the centrally expressed TRP channel painless in Drosophila courtship memory. Learning & Memory *20*, 34–40.

Sawamura, S., Shirakawa, H., Nakagawa, T., Mori, Y., and Kaneko, S. (2017). TRP Channels in the Brain. pp. 295–322.

Sims, J.R., Ow, M.C., Nishiguchi, M.A., Kim, K., Sengupta, P., and Hall, S.E. (2016). Developmental programming modulates olfactory behavior in C. elegans via endogenous RNAi pathways. ELife *5*, e11642.

Tai, Y., Feng, S., Ge, R., Du, W., Zhang, X., He, Z., and Wang, Y. (2008). TRPC6 channels promote dendritic growth via the CaMKIV-CREB pathway. Journal of Cell Science *121*, 2301—2307.

Tobin, D.M., Madsen, D.M., Kahn-Kirby, A., Peckol, E.L., Moulder, G., Barstead, R., Maricq, A.V., and Bargmann, C.I. (2002). Combinatorial Expression of TRPV Channel Proteins Defines Their Sensory Functions and Subcellular Localization in C. elegans Neurons. Neuron *35*, 307–318.

Turrigiano, G., Leslie, K.R., Desai, N.S., Rutherford, L.C., and Nelson, S.B. (1998). Activity-dependent scaling of quantal amplitude in neocortical neurons. Nature *391*, 892–896.

Tzavara, E.T., Li, D.L., Moutsimilli, L., Bisogno, T., Di Marzo, V., Phebus, L.A., Nomikos, G.G., and Giros, B. (2006). Endocannabinoids Activate Transient Receptor Potential Vanilloid 1 Receptors to Reduce Hyperdopaminergia-Related Hyperactivity: Therapeutic Implications. Biological Psychiatry *59*, 508–515.

Upadhyay, A., Pisupati, A., Jegla, T., Crook, M., Mickolajczyk, K.J., Shorey, M., Rohan, L.E., Billings, K.A., Rolls, M.M., Hancock, W.O., et al. (2016). Nicotinamide is an endogenous agonist for a C. elegans TRPV OSM-9 and OCR-4 channel. Nat Commun *7*, 13135.

Vennekens, R., Hoenderop, J.G.J., Prenen, J., Stuiver, M., Willems, P.H.G.M., Droogmans, G., Nilius, B., and Bindels, R.J.M. (2000). Permeation and Gating Properties of the Novel Epithelial Ca $^{2+}$ Channel. J. Biol. Chem. *275*, 3963–3969.

Wang, D.Y.-C., Kumar, S., and Hedges, S.B. (1999). Divergence time estimates for the early history of animal phyla and the origin of plants, animals and fungi. Proc. R. Soc. Lond. B *266*, 163–171.

White, J.G., Southgate, E., Thomson, J.N., and Brenner, S. (1986). The structure of the nervous system of the nematode C. elegans. Philosophical Transactions of the Royal Society B *314*, 1–340.

Xiao, B., Dubin, A.E., Bursulaya, B., Viswanath, V., Jegla, T.J., and Patapoutian, A. (2008). Identification of Transmembrane Domain 5 as a Critical Molecular Determinant of Menthol Sensitivity in Mammalian TRPA1 Channels. Journal of Neuroscience *28*, 9640–9651.

Zhou, J., Du, W., Zhou, K., Tai, Y., Yao, H., Jia, Y., Ding, Y., and Wang, Y. (2008). Critical role of TRPC6 channels in the formation of excitatory synapses. Nature Neuroscience *11*, 741—743.

CHAPTER FOUR: EXPRESSION OF AN EXPANDED CGG-REPEAT RNA IN A SINGLE PAIR OF PRIMARY SENSORY NEURONS IMPAIRS OLFACTORY ADAPTATION IN *C. ELEGANS*

SUMMARY

Fragile X-associated tremor/ataxia syndrome (FXTAS) is a severe neurodegenerative disorder that affects carriers of premutation CGG-repeat expansion alleles of the fragile X (FMR1) gene; current evidence supports a causal role of the expanded CGG-repeat within the FMR1 mRNA in the pathogenesis of FXTAS. Though the mRNA has been observed to induce cellular toxicity in FXTAS, the mechanisms are unclear. One common neurophysiological characteristic of FXTAS patients is their inability to properly attenuate their response to an auditory stimulus upon receipt of a small pre-stimulus. Therefore, to gain genetic and cell biological insight into FXTAS, we examined the effect of expanded CGG repeats on the plasticity of the olfactory response of the genetically tractable nematode, *Caenorhabditis elegans* (*C. elegans*). While *C. elegans* is innately attracted to odors, this response can be downregulated if the odor is paired with starvation. We found that expressing expanded CGG repeats in olfactory neurons interfered with this plasticity without affecting either the innate odor-seeking response or the olfactory neuronal morphology. Interrogation of three RNA regulatory pathways indicated that the expanded CGG repeats act via the *C. elegans* microRNA (miRNA)-specific Argonaute ALG-2 to diminish olfactory plasticity. This observation suggests that the miRNA-Argonaute pathway may play a pathogenic role in subverting neuronal function in FXTAS.

INTRODUCTION

The molecular pathogenesis of the fragile X family of disorders involves expansions of a non- coding CGG-repeat microsatellite in the 5′untranslated region (5′UTR) of the *FMR1* gene (Fu et al., 1991; Hagerman, 2013; Verkerk et al., 1991; Willemsen et al., 2011). Fragile X syndrome (FXS), the most common heritable form of intellectual disability and most common single- gene form of autism, is associated with CGG-repeat expansions that exceed 200 repeats (full mutation), almost always accompanied by epigenetic silencing (McLennan et al., 2011). Repeat expansions in the 55-200 range (premutation) give rise to the neurodegenerative disorder, fragile X-associated tremor/ataxia syndrome (FXTAS) (Capelli et al., 2010; Hagerman and Hagerman, 2013; Leehey and Hagerman, 2012), and to the reproductive disorder, fragile X-associated primary ovarian insufficiency (FXPOI) (Sullivan et al., 2011; Wittenberger et al., 2007). The repeat is also associated with early onset attention and intellectual deficit disorders (Hagerman, 2013; Ludwig et al., 2014).

FXTAS is a progressive movement disorder seen in older males in or beyond the sixth decade in life (Hagerman, 2013; Jacquemont et al., 2003; Leehey, 2009), with the preponderance of evidence to date indicating a pathogenic mechanism involving “toxicity” (functional cellular impairment) of the expanded CGG-repeat element within the *FMR1* mRNA (Hagerman, 2013; Li and Jin, 2012). Several observations have led to the hypothesis that the premutation-allele message is likely to be the key pathogenic agent causing cellular toxicity in FXTAS. First, intranuclear inclusions containing the expanded CGG-repeat *FMR1* mRNA in post-mortem brain tissue have been observed in FXTAS patients (Tassone et al., 2004). Similar intranuclear inclusions and neuronal

cell death were observed in Purkinje neurons in a mouse model that expressed premutation CGG repeats upstream of an EGFP reporter in the absence of the *FMR1* gene (Hashem et al., 2009). Second, intranuclear inclusions were observed in neural cell culture following overexpression of a premutation-length CGG element upstream of a GFP reporter (Arocena et al. 2005; Iwahashi et al., 2006). However, inclusions were not found in the same model in the absence of transcription, implicating the message and not CGG-repeat DNA in inclusion formation. Third, recent evidence suggests that (*i*) sequestration of one or more proteins by the CGG repeat (as RNA) leads to a functional deficiency of those proteins (Sofola et al., 2007; Sellier et al., 2013), and that (*ii*) expression of additional proteins may be dysregulated by miRNAs that target the *FMR1* mRNA (Zongaro et al., 2013). These results have established a linkage between the expansion of the premutation CGG- repeat of *FMR1* mRNA and FXTAS (Arocena et al., 2005). Finally, premutation alleles are associated with a substantial increase (2-8 fold) of *FMR1* mRNA (Kenneson et al., 2001; Tassone et al., 2000); thus, RNA toxicity may arise through increased CGG- repeat length or increased mRNA expression, or both (Hoem et al., 2011). *FMR1* transcript levels were also increased in mouse models of FXTAS, up to 6-fold in brain, when the mouse endogenous CGG repeat was replaced by premutation-length CGG repeats (Brouwer et al., 2007; Entezam et al., 2007; Qin et al., 2011).

While CGG-repeat expressing mammalian cell and animal models are able to reproduce the formation of intranuclear inclusions, as well as the increased levels of expanded CGG-repeat mRNA, cell culture systems cannot capture the intricacy of complex neural circuits in an intact organism, nor can they probe non-cell-autonomous

effects only produced within an organism, such as aging and metabolism, on neural function. Moreover, an additional CGG-repeat toxicity model, *Drosophila melanogaster*, is limited because the affected neurons in the eye-expression model die in substantial numbers, an outcome not seen in other FXTAS models. Further, working with mouse models requires significant time and expense to create and study the appropriate phenotypes, thus preventing the use of these animal models in high- throughput screens for genetic pathways that may either enhance or suppress the phenotype.

Here we have established a nematode (*Caenorhabditis elegans, C. elegans*) premutation model, which has a well-defined and genetically tractable neuronal circuit, and exhibits robust behavioral plasticity. The model offers an attractive alternative to the mouse or fly models with which to explore the cellular and molecular mechanisms underlying the neuronal pathologies induced by expression of expanded (99 CGG) *FMR1* repeats. Additionally, though *C. elegans* is an invertebrate, we share ~83% of the same proteins (Lai et al., 2000), and its simple nervous system, comprised of 302 neurons, is capable of producing complex, malleable behaviors. In particular, the odor-seeking behavior of the nematode is simple in that it is generated by just four olfactory sensory neurons (two pairs of AWA and AWC neurons for attractive olfactory behaviors; (Bargmann and Mori, 1997)), and yet it is complex in that the attractiveness of an odor is modified by experience (Colbert and Bargmann, 1995; L'Etoile and Bargmann, 2000). Indeed, a single AWC neuron senses butanone and causes naïve nematodes to move toward this odor source (Wes and Bargmann, 2001), and prolonged odor exposure in the absence of food reduces the animal's attraction to butanone (Colbert and Bargmann, 1995; L'Etoile and Bargmann, 2000). We have shown that this behavioral

plasticity results from processes that occur within the primary odor-sensory (AWC) neuron (Juang et al., 2013; Kaye et al., 2009; Lee et al., 2010; L'Etoile et al., 2002; O'Halloran et al., 2009).

To model FXTAS in *C. elegans*, we developed transgenic animals that expressed a GFP reporter containing the human *FMR1* 5′UTR either without any CGG repeats (0CGG), with an intermediate number of repeats (16CGG or 30CGG), or with 99 CGG repeats (99CGG), driven by an AWC-specific promoter. Here we find that the plasticity of the response to butanone is impaired in animals that express 99 CGG repeats. However, olfactory plasticity is not affected by expression of the control *FMR1* 5′UTR lacking CGG repeats or expressing the intermediate number of repeats. The reduced neuronal plasticity seen in the 99 CGG-repeat lines is reminiscent of the reduced pre-pulse inhibition seen in FXTAS patients (Schneider et al., 2012). Finally, we show that the microRNA-specific Argonaute ALG-2 is required for the decreased plasticity of animals expressing expanded repeats in the AWC neurons.

RESULTS

Expression of a premutation CGG-repeat expansion in the 5′UTR of a GFP reporter results in loss of olfactory adaptation in *C. elegans*

The *C. elegans* AWC sensory neurons allow worms to track and pursue (chemotax towards) attractive volatile chemical stimulants and provide an exquisitely sensitive and specific neuronal model for assessing the effects of CGG-repeat-induced RNA toxicity; the neurons govern both the primary olfactory response and a secondary adaptive response, which requires neuronal plasticity (L'Etoile et al., 2002; Bargmann et al., 1993). Moreover, *C. elegans* provides a powerful system for genetic screens aimed at exploring the mechanism of CGG-repeat-induced RNA toxicity. To assess the sensitivity of AWC neurons to expanded CGG- repeat RNA, we first determined whether expression of a premutation CGG-repeat expansion affected either the primary (chemotaxis) or secondary (adaptive or reduced chemotaxis) olfactory responses.

Human genomic sequences encoding the *FMR1* 5′UTR, with either 0 or 99 CGG repeats, were sub-cloned into a low-copy plasmid (pBR322) upstream of a GFP reporter sequence (Fire lab vector, pPD95.75). These sequences were placed transcriptionally downstream of the AWC-specific promoter p*ceh36*^{prom3} (referred to herein as p*AWC*; (Etchberger et al., 2007)). A 3′UTR from *unc-54*, a standard *C. elegans* 3′UTR used in transgene expression in somatic cells (Hunt-Newbury et al., 2007), was inserted downstream of the GFP coding sequence. The resulting reporter is designated p*AWC*::FMR(CGG)$_{99}$::GFP (referred to as 99CGG in all figures; **Fig 4.1A**). As a control for transgene expression, the CGG-repeat element was removed from the 5′UTR; the

control plasmid was designated p*AWC*::FMR(CGG)$_0$::GFP (referred to as 0CGG **in all figures**; **Fig 4.1A**). These GFP reporters were injected into wildtype animals with the AWC^{ON} marker, p*str-2*::DsRed, and the co- injection marker, p*unc-122*::GFP, which is expressed in coelomocytes. GFP expression in the AWC neuron could be visualized in these transparent transgenic animals (**Fig 4.1B**), and transgenic worms carrying either the 0CGG or 99CGG element were observed to express GFP throughout each AWC neuron. Importantly, the morphology of the neurons was not altered when the p*AWC*::FMR(CGG)$_{99}$::GFP was expressed (compare 0CGG to 99CGG in **Fig 4.1B**).

An initial screen for chemotaxis was conducted to determine whether expression of the 0CGG or 99CGG transgene affects olfactory behavior. The olfactory assay was performed as shown in **Fig 4.2.** Approximately 200 adult worms from an individual transgenic line were split into two populations; one group was exposed to S-basal buffer alone (to test for chemotaxis), while the other was pre-exposed to the AWC-sensed odor, butanone, in S-basal buffer for 80 min under otherwise identical conditions (to test for adaptation). After removing the odorant by washing the worms with S-basal buffer, animals were placed on an assay plate, with an ethanol-diluted butanone point source opposite from an ethanol point source, and were allowed to roam for 2 h at 20°C. Olfactory behavior was quantified in terms of the chemotaxis index (CI): the number of animals in a defined area near the attractive odor (point source) minus the number of animals in an equivalent area near the ethanol point source; the difference is divided by the total worms on the assay plate, excluding the origin area (Bargmann et al., 1993). A CI of 1 indicates strong attraction to the odor (primary response; chemotaxis), while a CI of 0 indicates the absence of any attraction to the odorant (secondary response;

adaptation). For wildtype animals, prolonged odor pre-exposure led to olfactory adaptation and reduced CI to less than one half of the value of the naïve animals exposed to S-basal buffer alone. Using these assays, transgenic animals could be analyzed for both primary and adaptive responses to odorant.

Ten transgenic strains expressing p*AWC*::FMR(CGG)$_0$::GFP from independent injections all behaved like their sibling wildtype animals for both chemotaxis (exposure to S-basal buffer alone; **Fig 4.3A**, gray bars) and adaptation to butanone (butanone-diluted S-basal buffer exposure; hatched bars). Siblings without transgenes also had normal behaviors for both chemotaxis (**Fig 4.3A**, white bars) and adaptation responses (black bars). The wildtype behavior of p*AWC*::FMR(CGG)$_0$::GFP-expressing lines demonstrated that the *FMR1* 5′UTR element without CGG repeats, though highly-GC-rich (~74% GC) relative to the *C. elegans* genome (~36% GC; (The *C. elegans* Sequencing Consortium, 1998)), did not appreciably affect either primary or adaptive responses to an AWC-sensed odor.

Eight transgenic strains expressing p*AWC*::FMR(CGG)$_{99}$::GFP were produced by separate injections. The transgenic animals and their non-transgenic siblings displayed similar attraction to butanone (**Fig 4.3B**, white and gray bars). However, when we analyzed adaptation, we found that seven out of eight transgenic strains were impaired in their ability to adapt to butanone and remained attracted to the odor point source (**Fig 4.3B**, hatched bars); a Student's two-tailed t-test was performed to examine the difference between the adapted responses of the transgenic and non-transgenic siblings. This finding was in contrast to their sibling strains, which had lost the transgene and exhibited normal plasticity in response to prolonged butanone pre-exposure (**Fig**

4.3B, black bars). To determine whether the absence of a behavioral difference in the one adaptive line (line 8) was due to loss of p*AWC*::FMR(CGG)99::GFP sequences, we performed PCR analysis. Genomic DNA from individual strains was isolated, and the crude extracts were genotyped by PCR amplification through the CGG-repeat element (Saluto et al., 2005). **Figure 4.3C** shows that the p*AWC*::FMR(CGG)99::GFP transgene was lost in line 8. Thus, expression of the expanded repeat reduced neuronal plasticity in *C. elegans*. These lines were also tested for their ability to chemotax towards and adapt to the two other AWC-sensed odors, benzaldehyde and isoamyl alchohol. We found that naïve chemotaxis was unaffected, but adaptation to benzaldehyde, as with butanone, was impaired in animals that expressed 99CGG (Supplementary Materials, **Fig 4.S1**).

The penetrance of the adaptation defects were 100% since all lines that expressed p*AWC*::FMR(CGG)99::GFP were impaired for adaptation. To determine whether behavioral plasticity was affected by the GC "load" on the animals, we examined the copy number of each transgene by PCR of the *FMR1* 5´UTR-GFP junction. When *C. elegans* gonads are injected with plasmid DNA, they package the concatenated DNA into an extrachromosomal array that is maintained like an extra X chromosome. Each line will have a unique number of transgenes within the array. This number is stable over the generations, though the array itself can be lost. When genomic DNA (gDNA) levels from each line were normalized to the endogenous housekeeping gene *act-3*, we found that the relative gDNA levels mostly ranged from 2 to 4 (**Fig 4.3A** and **4.3B**), and yet the adaptation defects of the 99CGG line 5, which carries 10-fold more transgenes, was no more adaptation-defective than line 6 (**Fig**

4.3B). We chose to integrate the extrachromosomal DNA of line 6 p*AWC*::FMR(CGG)$_0$ and line 6 p*AWC*::FMR(CGG)$_{99}$ into the genome, as this facilitates strain maintenance and allowed us to have a stable baseline for the 0CGG and 99CGG analysis that would follow. Importantly, each line had comparable numbers of transgenes prior to and after integration (0CGG: 3.2/2.5 transgenes /10^2 *act-3,* before/after integration*;* 99CGG: 2.4/1.9 transgenes /10^2 *act-3,* before/after integration*).*

CGG-repeat length has a greater effect on plasticity than copy number

To understand which affected plasticity more, the copy number or repeat length, we constructed 5 lines expressing extrachromosomal arrays with 30 CGG repeats and examined their behavior (**Fig 4.4A**). We also tried to obtain lines with 16 CGG repeats but we could only generate two lines, too small a number to use for assessment of penetrance. The behavior of the 16 CGG-repeat-expressing lines is shown in Supplementary Materials, **Fig 4.S2A**. When we examined the 30 CGG-repeat-expressing lines, we found that none (0/5) showed significantly higher adaptation values than those seen in the integrated line with 0CGG repeats. By contrast to the 0 CCG-expressing lines, 2/5 30 CGG-repeat-expressing lines (lines 30-2 and 30-3) had adapted CIs that were significantly higher than their non-transgenic siblings. The adapted CIs of these strains lay midway between the CI values of the 0 and 99CGG integrated strains and were not statistically different from either. Thus, the penetrance and severity of the adaptation defects correlates with the number of repeats such that 99 CGGs produce a very penetrant (100%) and moderate to severe adaptation defect, and the normal mode for human repeats (30) produces a mild defect that is only 40%

penetrant in *C. elegans*. When we examined the copy number and asked whether the repeat length or the copy number of the transgenes has a greater effect on adaptation, we found that repeat length affects the penetrance of the adaptation defect more than copy number. That is, 100% of the 99 CGG- expressing lines were impaired for adaptation, though their relative copy numbers varied from 1 (line 7) to 10 (line 5) transgenes/10^2 act-3 genes (**Fig 4.3B**). The penetrance of the adaptation defects was 40% in the lines with 30 CGGs, and the value of the adapted CIs did not correlate with the copy number of the transgenes (**Fig 4.4A**). That is, two lines with 30 CGGs (lines 3 and 5) had nearly identical copy numbers (3.45 *vs.* 3.29 genes/10^2 *act-3* respectively), but line 3 had mild adaptation defects, while line 5 behaved like wild type. Importantly, all lines retained the same number of repeats (see genotyping gel in **Fig 4.4B**). Thus, repeat size is more important than copy number, which rules out an ectopic CGG RNA-specific response.

FMR1 mRNA levels for 99CGG lines are increased over 0CGG in *C. elegans*

We previously showed that *FMR1* mRNA levels in premutation individuals are elevated 2-8 fold over normal (Kenneson et al., 2001; Tassone et al., 2000). Likewise, *FMR1* mRNA levels in cell and animal models expressing the premutation CGG-repeat element in the 5´UTR increased 2-6 fold compared with a lower number of repeats (Arocena et al., 2005; Brouwer et al., 2007; Entezam et al., 2007; Qin et al., 2011; Brouwer et al., 2008). To determine whether the level of mRNA in *C. elegans* is similarly increased in animals that contain 99 CGG repeats, we performed qRT-PCR analyses of total mRNA from each line. First, we integrated the transgene into the genome of each strain. We chose to integrate lines of 99CGG and 0CGG with similar transgene copy

numbers. The primers used in our analyses amplified a region from the very 3′ end of the *FMR1* 5′UTR to the 5′ portion of the GFP-coding region. Expression was normalized to the housekeeping gene, *act-3*. We found that the level of mRNA containing 99 CGG repeats was elevated by ~5-fold over that of the control reporter gene (**Fig 4.5**). Thus, by this second metric (mRNA level), expression of the 99 CGG-repeat allele in the *C. elegans* olfactory neuron mirrors what is observed in human patients with FXTAS.

Expression of the 99CGG transgene does not affect the morphology or the cell fate of the AWC neuron

Murine hippocampal neurons cultured from mice with premutation CGG repeats showed elevated *FMR1* mRNA and neurotoxicity phenotypes, such as decreased viability and dendritic complexity, as well as changed synaptic morphology (Chen et al., 2010). To determine whether expression of expanded CGG repeats might affect the structural integrity of the AWC neurons, we expressed the AWC^{ON} p*str-2*::DsRed reporter in double-transgenic lines, which showed diffuse red florescence throughout the neuron. No obvious change in morphology was observed in naïve animals expressing either p*AWC*::FMR(CGG)$_0$::GFP (**Fig 4.6**, middle) or p*AWC*::FMR(CGG)$_{99}$::GFP (bottom) compared with the wildtype animal alone (top). Note that the morphology of the 99 CGG-expressing AWC may be rounder in this image than the 0 CGG- expressing neuron, but this cell shape is polymorphic and does not represent a true deviation from the normal shape. Indeed, in **Figure 4.1B**, the cell shapes are very similar.

Although both AWC olfactory neurons have similar structures and functions, chemosensory receptor STR-2 is randomly expressed in either the left or right AWC

neuron in wildtype animals, termed the AWC^{ON} neuron (Troemel et al., 1999). AWC^{ON} senses the odor butanone and can promote either attractive or repulsive behaviors (Wes and Bargmann, 2001). In some cases, mutations that cause STR-2 to be expressed in both AWC neurons also cause the animal to fail to adapt to butanone (Wes and Bargmann, 2001; Torayama et al., 2007). To understand whether expressing 99CGG alters AWC cell fate, we examined STR-2-driven DsRed fluorescence in wild-type, 0CGG, and 99CGG on three separate days. Asymmetric expression of STR-2 was observed in all strains and on each day, with 93% of transgenic animals with the 99 CGG-repeat element in the 5′UTR of the GFP reporter displaying asymmetric STR-2 expression (**Table 4.1**). Therefore we conclude from these initial studies that the reduced olfactory plasticity seen in animals that express 99CGG is not due to changes either in cellular morphology or cell fate.

Identifying genes that interact genetically with 99CGG to interfere with neuronal plasticity

Although RNA toxicity imparted by premutation CGG-repeat elements is believed to be the pathogenic basis of FXTAS, downstream pathways by which this RNA effect is mediated remain obscure. To begin to address this issue, we examined three RNA-processing pathways required in AWC neurons to promote adaptation, and asked whether their adaptation defects could be modified by expression of 99 CGG repeats. Strains integrated with p*AWC*::FMR(CGG)::GFP were used for this investigation of candidate genetic modifiers.

The cGMP-dependent protein kinase EGL-4 is necessary for olfactory adaptation of the AWC neuronal response (L'Etoile et al., 2002), and butanone adaptation requires increased translation of *egl-4* mRNA, which is facilitated by the RNA-binding protein, FBF-1 (Kaye et al., 2009). Strains that lack *fbf-1* are adaptation defective because they fail to up-regulate the kinase EGL-4. FBF-1 is a member of the Pumilio/Fem-3 binding factor (PUF) family that binds to the *egl-4* 3´UTR and enhances its translation (Kaye et al., 2009). We asked whether expression of the p*AWC*::FMR(CGG)$_{99}$::GFP alters the adaptation defects resulting from loss of FBF-1. To this end, the integrated p*AWC*::FMR(CGG)$_{99}$::GFP strain was crossed with an *fbf-1* null mutant. We found that the adaptation defects of the *fbf-1(ok91*) strain were slightly, though significantly, increased when they expressed p*AWC*::FMR(CGG)$_{99}$::GFP [CI (adapted) of *fbf-1*=0.51, 99CGG=0.61, *fbf-1* and 99CGG=0.67; 2-tailed Student's t-test between *fbf-1* and *fbf-1/*99CGG; double mutant P = 0.04] (Fig. 7A), although the *fbf-1(ok91)* mutant that expressed 99 CGG repeats in the 5´UTR did not exhibit altered STR- 2 cell fate (**Table 4.2**). These olfactory behavioral results raise the possibility that the premutation expansion of the *FMR1* gene may partially reduce the translational enhancement of EGL-4 through interference with FBF-1 function.

The endogenous RNAi pathway is partially affected by expression of the premutation repeats

Recently, we reported that the endogenous nuclear RNAi pathway (Castel and Martienssen, 2013) is required in AWC for olfactory adaptation (Juang et al., 2013). The endogenously-produced small RNAs that we found to be required for odor adaptation

are amplified from mRNA by an RNA-dependent RNA polymerase; therefore, these 22-nt RNAs are antisense to the original template. The RNAs are bound by the Argonaute NRDE-3, which shuttles them into the nucleus where they base pair with the nascent strand of mRNA, stall Polymerase II, and guide repressive chromatin complexes to the gene by which they are encoded. In this way, endogenous siRNAs allow a gene to silence itself. We found that the nuclear RNAi and the FBF-1- mediated adaptation pathways function in parallel, such that double mutants are completely adaptation defective. To understand whether 99CGG expression interferes with RNAi-mediated adaptation, we turned to the RNAi defective strain, *mut-7(pk204)*. MUT-7 is a putative 3′-5′exonuclease required for transposon (Ketting et al., 1999) and transgene (Dernburg et al., 2000) silencing, as well as for nuclear RNAi maturation (Guang et al., 2008); this strain is adaptation defective (Juang et al., 2013). When we introduced the expanded-CGG-repeat strain into a *mut-7* null mutant strain (Ketting et al., 1999), we found that expression of the fragile X premutation in *mut-7(pk204)* animals led to significantly worse adaptation defects than seen either in wildtype animals expressing a CGG-repeat element, or in the *mut-7(null)* alone [CI (adapted) of *mut-7(pk204)* and 99CGG=0.75; *mut-7(pk204)*=0.59, P = 0.02; 99CGG=0.61, P = 0.02] (**Fig 4.7A**). However, the *mut-7(pk204)* mutant with the integrated 99 CGG repeat exhibited normal STR-2 cell fate (**Table 4.2**). These behavioral results suggest that the expanded repeats partially interfere with a MUT-7-driven adaptation process. Nevertheless, pathways in addition to RNAi are likely to be affected by the expanded repeat. HPL-2 is a counterpart of the human heterochromatin binding protein 1 (HP1) and acts in the same genetic pathway with MUT-7 (Juang et al., 2013). However, when we expressed the expanded repeat in

an *hpl-2* null mutant, *hpl-2(tm1489)*, the animals were sterile (data not shown). Importantly, in each genetic background mentioned above, the integrated repeats were the same length and copy number (**Fig 4.7B**).

Toxicity of the expanded repeat requires an intact miRNA pathway

Several studies have indicated that miRNAs are involved in neuronal development and in learning and memory formation (Olde Loohuis et al., 2012). In *C. elegans*, canonical miRNA biogenesis requires DRSH-1, the Drosha RNase III-type ribonuclease, and its binding partner, PASH-1 (Denli et al., 2004). PASH-1 is a counterpart of DGCR8 in human and Pasha in fly, and acts with DRSH-1 to process primary (pri)-miRNAs in the nucleus. The pri-miRNA is then exported to the cytoplasm where RNAse III DCR-1 recruits miRNA- specific Argonaute (AGO) proteins, such as ALG-1 and ALG-2 (Tops et al., 2006), to further process pri-miRNA into mature miRNA. These miRNAs repress translation of target mRNAs, and they may also have nuclear functions (Huang and Li, 2012). In addition to DROSHA/PASHA-dependent miRNAs, several other small non-coding RNAs, including small nucleolar RNA (snoRNA) and spliced intronic RNAs, can be exported from the nucleus and processed into miRNAs; these latter RNA species are termed mitrons and siRNAs (Babiarz et al., 2008).

To determine whether the neurotoxicity of the expanded repeats acts via an miRNA-dependent process, we introduced the integrated p*AWC*::FMR(CGG)$_{99}$::GFP into an *alg-2*(*ok304*) null mutant strain (Grishok et al., 2001). ALG-2 is one of two *C. elegans* miRNA Argonautes, and the primary species expressed in neurons (Vasquez-Rifo et al., 2012). We observed that loss of this Argonaute restored adaptation to strains that expressed the fragile X premutation CGG repeat (CI=0.23), compared to the

adaptation defects seen in wildtype animals that express the same transgene (CI=0.61, $P < 0.005$) (**Fig 4.7A**). Once again, STR-2 cell fate is unaltered in these strains (**Table 4.2**).

In *C. elegans*, ALG-2 associates with another miRNA specific Argonaute, ALG-1, in a DCR-1 complex in the cytoplasm to produce mature miRNA (Duchaine et al., 2006). Unfortunately, due to the small brood size of the *alg-1* null mutant strain, we were unable to perform behavioral assays.

Genotyping analysis showed that the transgenic array was invariant between all the strains we assessed (**Fig 4.7B**). The rescued behavior was not due to a reduction of repeat-containing RNA in *alg-2* null animals, as the levels of mRNA produced from the expanded repeat were the same in each strain (**Fig 4.7C**). Thus, ALG-2 is likely to be required to cause the adaptation defects resulting from expression of the fragile X premutation CGG repeat in AWC.

DISCUSSION

FXTAS is a human, progressive neurodegenerative disorder in which the abnormal CGG expansion within the 5′UTR of the *FMR1* gene is thought to be the source of abnormal cell function. Although expression of premutation-CGG-repeat alleles in cell and animal models has recapitulated several features of the cellular and behavioral phenotypes of FXTAS, including intranuclear inclusions and mRNA accumulation, the molecular basis of the relationship between the CGG-triplet expansion and progressive cognitive and behavioral difficulties remains unclear. Here we report a *C. elegans* model for premutation-driven dysfunction, and demonstrate that 99 CGG repeats (near the modal value for the repeat length among FXTAS patients) in the 5′UTR of a GFP reporter lead to defects in neuronal plasticity when expressed solely in an olfactory neuron. The defect is independent of neuronal development, as cell fate and morphology were not affected.

This impairment of behavioral plasticity in adult animals carrying 99 CGG repeats provides a model with which to examine how the 5′UTR premutation CGG expansion causes changes in behavior. In addition, our analysis of pathways that require RNA processing for adaptation shows that the CGG- repeat element is likely to interfere with plasticity via an miRNA pathway, since loss of miRNA-specific Argonaute ALG-2 restores behavioral plasticity. MicroRNAs, small non-coding RNAs that are not translated into proteins, have been implicated in the regulation of many cellular and organismal processes, including learning and memory (McNeill and Van Vactor, 2012). One speculative model for how loss of the Argonaute ALG-2 might suppress adaptation is presented in **Figure 4.8**. In the absence of an expanded CGG repeat (wildtype),

DROSHA/DGCR8 makes the bulk of the pre-miRNAs, which are processed into the bulk of miRNAs in the cell. These miRNAs are not required for adaptation, since loss of DROSHA (DRSH-1) or the microRNA Argonaute, ALG-2, does not affect adaptation ((Juang et al., 2013); Supplementary Materials, **Fig 4.S1**). We suggest that among the small fraction of miRNAs that are DROSHA/DGCR8-independent, there may be individual miRNAs that negatively regulate adaptation, but which would normally not have much of an effect. However, once DGCR8 is bound by 99CGGs and canonical miRNA production is repressed (Sellier et al., 2013), the relative fraction of mirtrons and other DGCR8-independent, small non-coding RNAs (sncRNAs) would increase. Babiarz et al. (Babiarz et al., 2008) show that the levels of many DGCR8-independent miRNAs increase in dgcr8-/- mouse ES cells, and Sellier et al. (Sellier et al., 2013) showed that the mirtron levels are not diminished. We speculate that the ALG-2-bound mirtrons and other DGCR8-independent miRNAs that repress genes required for adaptation are more active as they have no competition for ALG-2 and thus much of the ALG-2 function is redirected to minor targets; targets might include genes that are required for adaptation, such as OSM-9 and EGL-4. Consequently, loss of ALG-2 would relieve inhibition that arises from the DGCR8-independent miRNAs repressing their targets. This would indicate that a set of DGCR8- independent miRNAs can alter neuronal function in the context of 99CGG expression.

Biochemical studies of mouse and fly models of FXTAS show that many RNA-binding proteins, including those required for miRNA biogenesis and function, interact with premutation CGG repeats. Two lines of evidence indicate that miRNAs, or their associated factors, may play important roles in the pathogenic action of the expanded

repeat. First, in the FXTAS fly model, miRNA-277 (miR-277) was found to affect CGG-mediated neuronal toxicity by regulating expression of the DNA fragmentation factor-related protein 2 (Drep-2) and the visceral mesodermal armadillo-repeats (Vimar) at the mRNA level (Tan et al., 2012). Second, in the brains of individuals who died with FXTAS, the miRNA-processing, double- stranded RNA-binding protein, DGCR8, and its partner, DROSHA, were shown to associate with premutation CGG repeats (Sellier et al., 2013). This association sequestered pri-miRNAs and decreased levels of many miRNAs. Sellier et al. (2013) proposed that the CGG-mediated decrease in free DGCR8 and DROSHA, and the attendant reduction in key miRNAs, caused loss of neuronal dendritic complexity and cell viability. It remains to be determined whether the DGCR8 homolog, Pasha, interacts with the CGG repeat – and is therefore functionally sequestered – in the same manner as in humans, or whether other proteins are functionally impaired by the CGG-repeat element.

Our candidate approach revealed that miRNA-binding Argonaute ALG-2 is likely to be required for CGG-repeat induced defects in olfactory adaptation. ALG-2 appears to be the primary neuronal Argonaute in *C. elegans* head neurons (Vasquez-Rifo et al., 2012). In other tissues, ALG-2 can be associated with miRNA Argonaute ALG-1. These Argonaute proteins and miRNA are found in a complex with DCR-1, a Dicer ribonuclease III. It will be interesting to investigate whether loss of other ALG-2-associated factors likewise protects neurons from the toxic effects of expanded CGG repeats. One particularly compelling interaction is between ALG-2 and AIN-1, since this interaction implicates a *C. elegans* Sam68 homolog; Sam68 sequestration has been suggested as a participant in the pathogenesis of FXTAS (Sellier et al., 2010).

During development of *C. elegans* somatic tissues, the Argonaute binding partner, GW182 AIN-1, interacts with the core miRNA RNA-induced silencing complex (miRISC) components ALG-1 and ALG- 2 (Ding et al., 2005). This core machinery also associates with a TRIM-NHL protein, NHL-2, and a DEAD-Box protein, CGH-1, to enhance translational repression (Hammell et al., 2009). In addition to translational repression, CGH-1 and GLD-1 (an RNA-binding protein), also mediate mRNA stabilization in nematode oocytes (Scheckel et al., 2012). GLD-1 has a KH1 RNA-binding domain, which shows high similarity with Sam68. In the cytoplasm, GLD-1 is able to associate with AIN-2, a homolog of AIN-1 and an miRISC (Zhang et al., 2007). Thus, loss of ALG-2 from this complex may reduce the sequestration of Sam68 or PASH-1 (the *C. elegans* DGCR8 homolog), thereby releasing these factors and allowing them to perform their important cellular functions.

Though sequestration is likely to play a dominant role in the neuropathology of CGG repeats in *C. elegans* neurons, as in both human and other animal models, it is possible that other modes of toxicity could be operating as well, as in the repeat-associated non-ATG (RAN) translation mechanism proposed by Todd et al. (2013). However, it remains to be determined whether RAN products contribute to the neurological phenotype in FXTAS. In this regard, it is noteworthy that the “NIH” FXTAS mouse line of Usdin and co-workers (Entezam et al., 2007; Hoffman et al., 2012; Qin et al., 2011), which does not produce RAN products, exhibits a neurodegenerative phenotype; whereas the “Dutch” FXTAS mouse line, which is capable of generating RAN products, does not have a significant neurodegenerative phenotype (Hagerman, 2013).

The processes of releasing neurotransmitters are sensitive to downstream cellular changes. Studies of FXTAS mice demonstrated increased mRNA levels in GABAergic neurons (D'Hulst et al., 2009). Cell culture from hippocampal neurons of male FXTAS mice displayed imbalanced excitotoxicity from activation of glutamate receptors and inhibition of GABA receptor (Cao et al., 2012). The AWC sensory neuron is glutamatergic (Chalasani et al., 2010), and this nematode system may be able to clarify the regulation of glutamate-mediated transmission and aspects of plasticity caused by the premutation CGG repeats.

Finally, the finding that loss of ALG-2 ameliorates all the effects of the premutation repeat means that therapies based on the ability to inactivate an Argonaute or an Argonaute-mediated event might be designed. It would be particularly interesting to identify a drug target such as a kinase that is involved in regulation of the function of this Argonaute.

ACKNOWLEDGEMENTS

The authors wish to thank Greg Mayeur for assistance in an earlier phase of project development, and the families who have helped support our fragile X research. We thank Andrei Goga for use of his qPCR system; and the Caenorhabditis Genetics Center for worm strains. This work was supported by the National Institutes of Health [R01 HD040661 to P.J.H.; R01 DC005991 to N.D.L.; and R25 GM56847 graduate fellowship to K.L.B.].

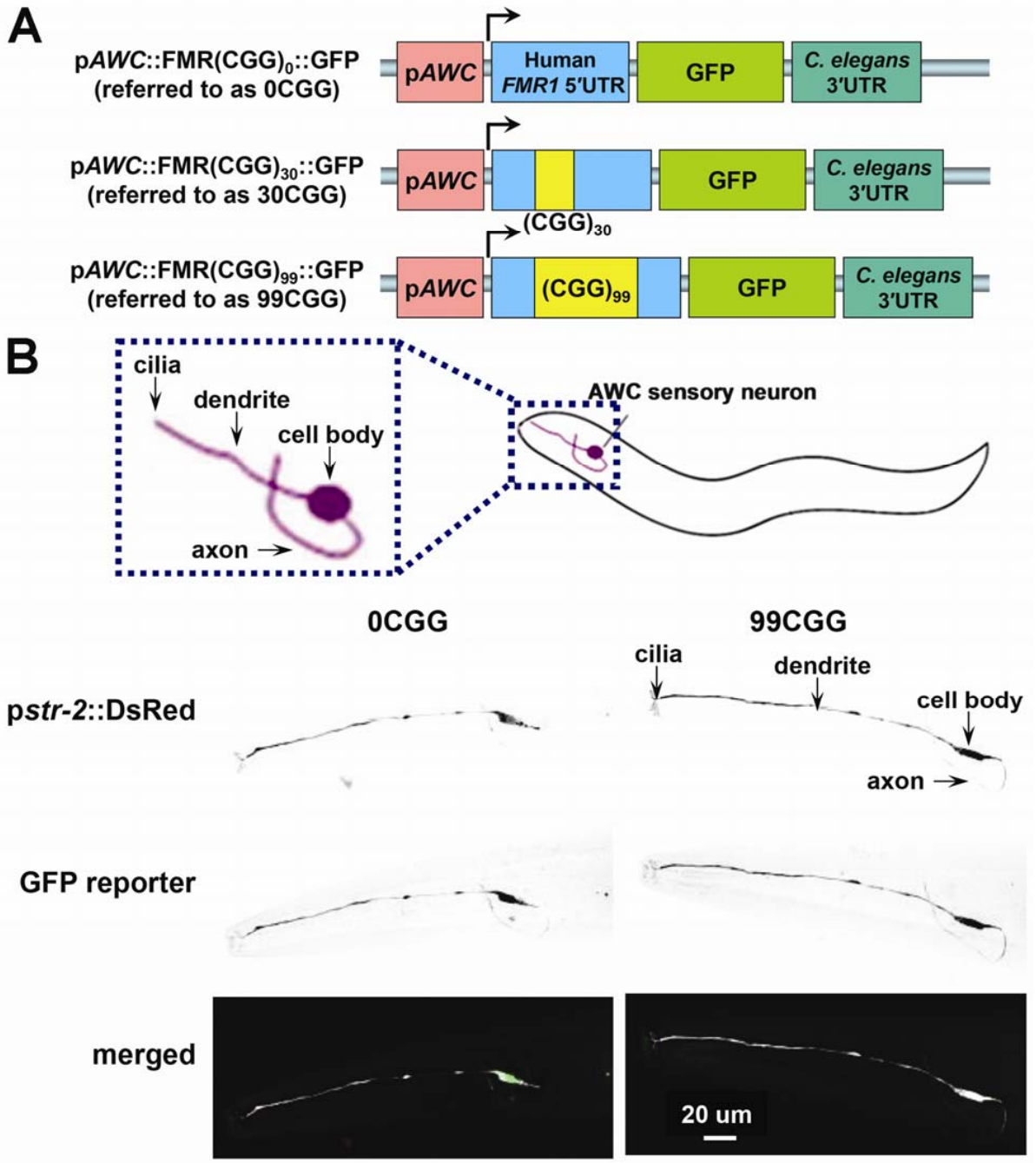

Figure 4.1. Expression of an expanded CGG-repeat reporter in AWC neurons. (**A**) Representation of the GFP reporter containing expanded CGG repeats. GFP reporters, carrying a human *FMR1* 5′UTR fragment with 0, 30, or 99 CGG repeats, were expressed under an AWC-specific promoter (p*AWC*); these reporters are referred to as 0CGG, 30CGG and 99CGG. The open reading frame for GFP was followed by a 3′UTR element from *unc-54*. Arrow denotes the start site of transcription. (**B**) Expression of the GFP reporter in the AWC neuron. (Top) Schematic diagram of the AWC neuron in the

head of *C. elegans*. Inset represents the area visualized in confocal florescence images below. The anatomy of the AWC neuron is diagramed in an enlarged cartoon in the left dotted box. (Bottom) Confocal florescence images of transgenic animals expressing GFP in the AWC neuron. GFP is expressed either from the *FMR1* 5′UTR without CGG repeats (left) or with 99 CGG repeats (right). The AWC neuron was identified by expression of DsRed from an AWC-specific promoter (p*str-2*) and the anatomy is labeled in the 99CGG animal. Anterior is left for both images.

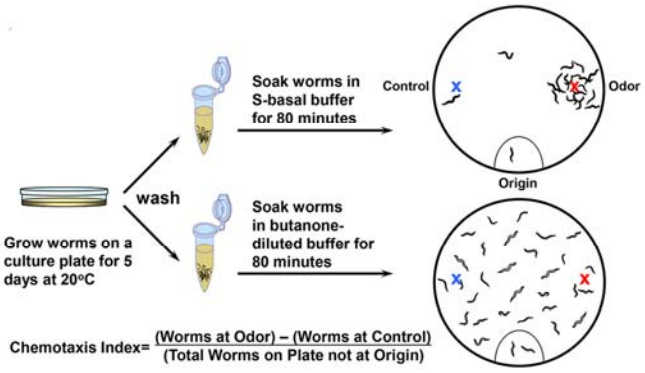

Figure 4.2. Scheme of olfactory adaptation. Adult animals were washed free from bacteria, then half of the population was exposed to buffer alone (naïve animals; top), and the other half exposed to buffer with diluted butanone (pre-exposed animals; bottom). After 80 min incubation, animals were placed at the “origin” of a 10 cm assay plate with a butanone spot (red “X”) and a control ethanol spot (blue “X”). Animals roamed for 2 h at 20°C, after which their olfactory behavior was quantified by the chemotaxis index (CI).

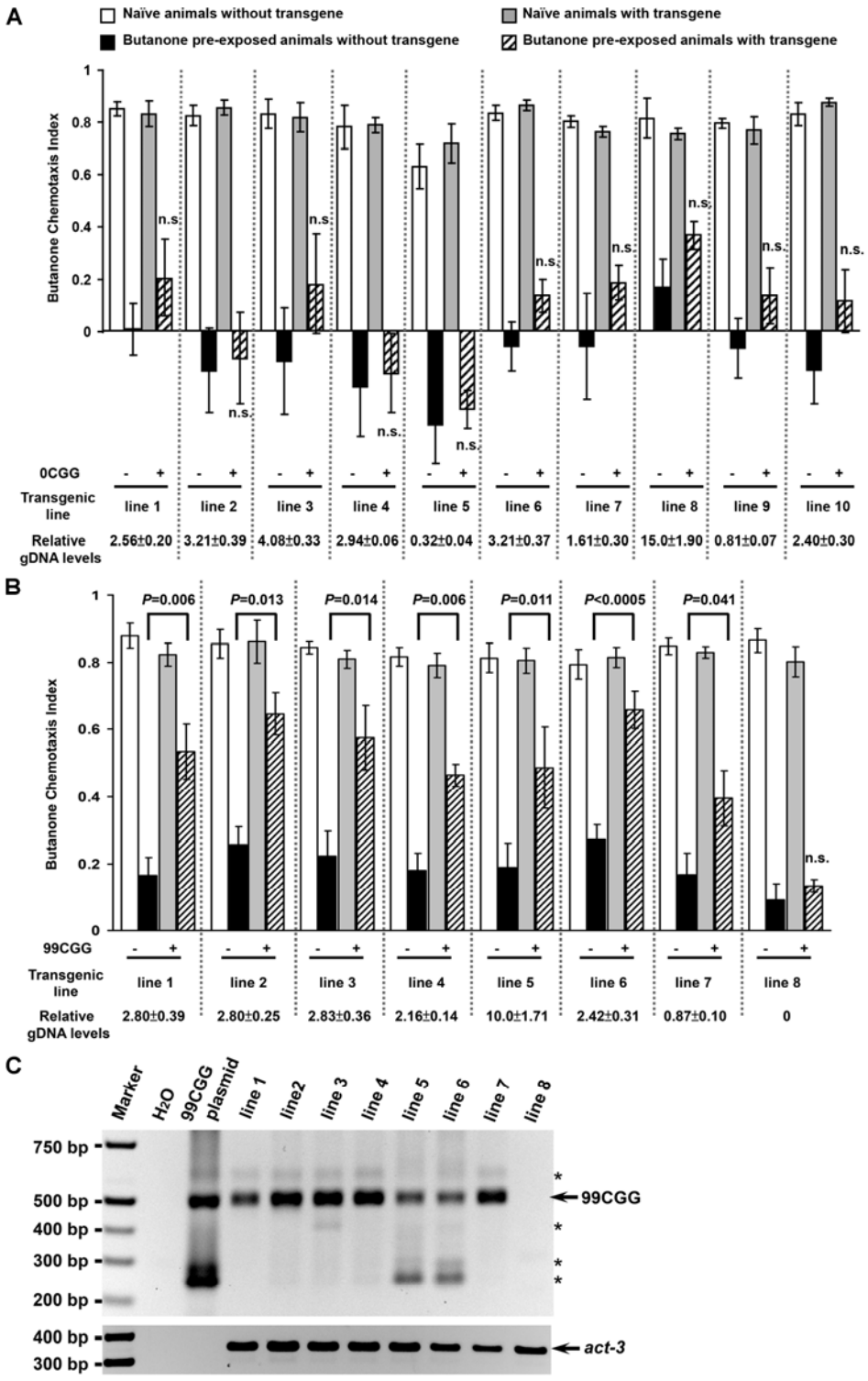

Figure 4.3. Expression of 99 CGG repeats in the 5′UTR results in olfactory adaptation defects. (**A**) Animals carrying the control GFP reporter with 0 CGGs in the 5′UTR behave like wildtype. Transgenic strains ("+"; express the *FMR1* reporter and

p*unc-122*::GFP in coelomocytes) and siblings that lost the transgene ("-") were grown on the same plates. Bars and error bars represent the mean CIs and standard errors of the mean (SEM) from at least 3 independent assay days from populations that were either naïve (white or gray bars) or pre-exposed to odor (black or hatched bars). To quantitate the relative gDNA levels, total genomic DNA from the larval stage 4 (L4) animals was extracted and subjected to real-time PCR. The relative levels of the 0CGG and 99CGG reporters were normalized to the housekeeping gene, *act-3*. The data were collected from three independent experiments. "±" indicates the values of SEM. (**B**) 100% of lines that express 99 CGG repeats are defective for olfactory adaptation. The chemotaxis and adaptation values for seven transgenic lines (lines 1-7) carrying the p*AWC*::FMR(CGG)99::GFP construct (labeled (+)) were compared with their siblings without transgenes (labeled (-)). Data are from at least five independent assays and are labeled as in Figure 3A. *P* values indicate results of two-tailed t-tests between the CIs of transgenic- (+) and non-trangenic (-) adapted animals in the same transgenic strain. "n.s." indicates no significant difference, as *P* value is greater than 0.05. The relative gDNA levels are presented at the bottom line. (**C**) PCR genotyping of transgenic animals carrying 99 CGG repeats. Genomic DNA from individual strains was extracted and genotyped with two primers flanking the CGG-repeat area. The PCR product is 505 bp, indicated by an arrow, and the p*AWC*::FMR(CGG)99::GFP plasmid, referred as CGG plasmid, was used as a positive control. Amplification of an endogenous control, *act-3*, is shown below. "*" indicates non-specific amplification. The absence of a band for line 8 indicates that this line had lost the *FMR1* reporter.

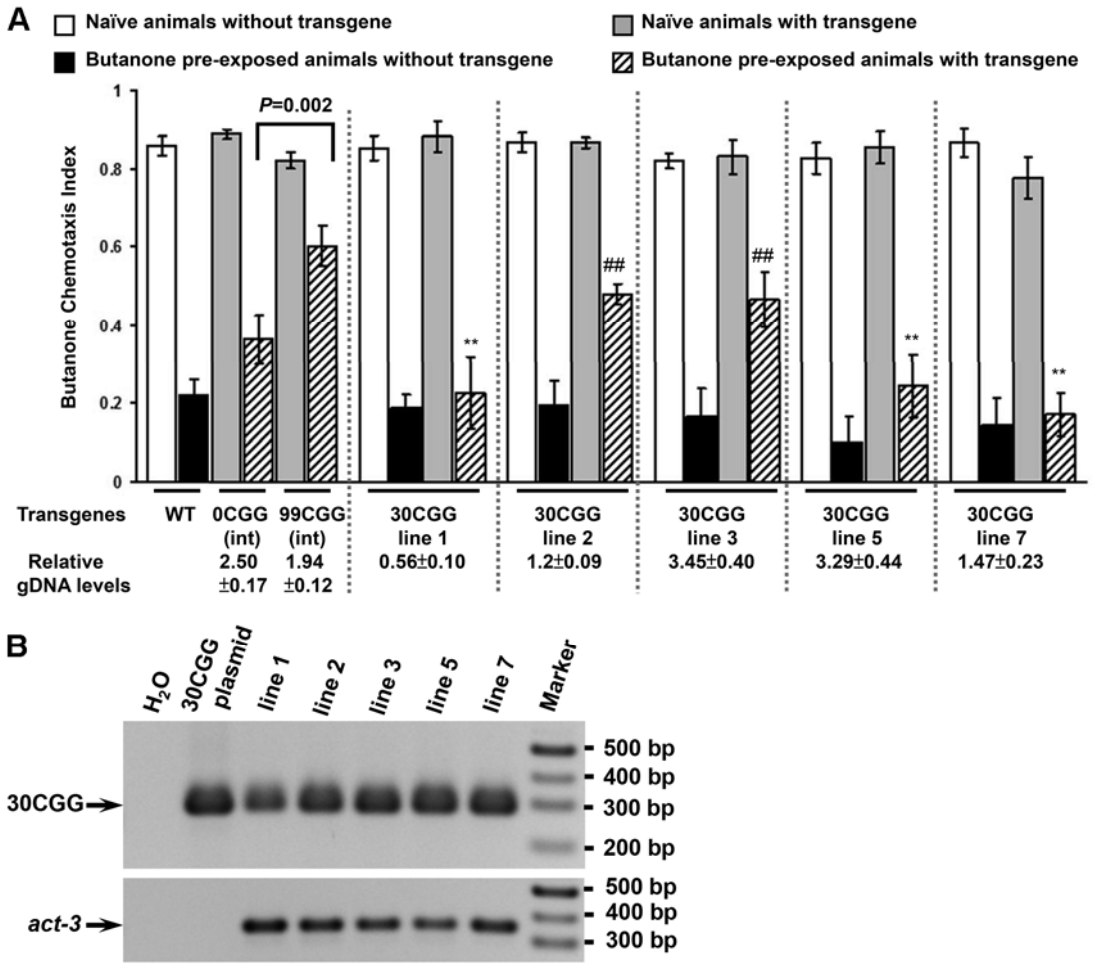

Figure 4.4. Animals that express 30 CGG repeats exhibit mild and variable adaptation defects. (**A**) Bars indicate the CI of lines that express 30 CGG repeats in the *FMR1* 5′UTR (last 5 sets of bars), as compared to wild type, and the integrated lines expressing 0 or 99 CGG repeats in the *FMR1* 5′UTR (first three sets of bars). The relative gDNA levels shown below each line were calculated by normalizing reporter levels to the housekeeping gene, *act-3.* gDNA was collected from three separated experiments. Student T-tests between the adapted values for animals that expressed the reporter (hatched bars) and animals that express 0CGG repeats showed no significant differences. Comparison between the adapted CIs of the transgenic animals (hatched bars) and those of their non-transgenic siblings (black bars) indicate that 2/5 lines (lines 2 and 3) showed significant differences, which are marked with #. Comparison between the adapted CIs of the transgenic animals (hatched bars) and the CIs from the 99CGG-expressing line (6th bar) showed that the adaptation behavior of lines 1, 5, and 7 were significantly different from the adaptation behavior of the 99CGG-expressing line. The *P* values <0.005. "##" indicates two tailed T-test showing *P*<0.005 between the adapted CI of animals with transgene and without transgene. Data were collected from at least 5 independent assay days. Error bars present SEM. (**B**) PCR genotyping of transgenic animals. 298 bp of PCR fragments were amplified in animals

carrying 30CGG repeats in the 5′UTR. The lower panel shows the amplified fragments from the endogenous gene, *act-3*.

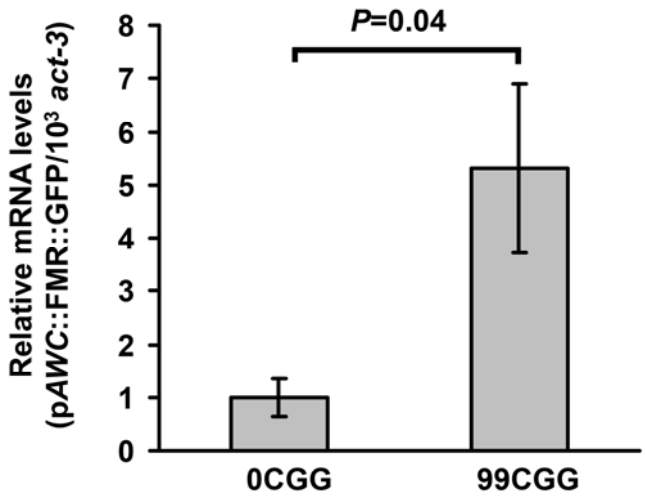

Figure 4.5. The 5′UTR CGG repeat causes a significant increase in mRNA level. Total RNA from adult transgenic animals was extracted, reverse-transcribed into cDNA, and quantified by real-time PCR. GFP mRNA expression was increased ~5-fold in animals expressing p*AWC*::FMR(CGG)$_{99}$::GFP compared with control (0CGG) animals, which was set to 1. (Error bars: SEM.) The data were collected from four independently isolated populations of animals.

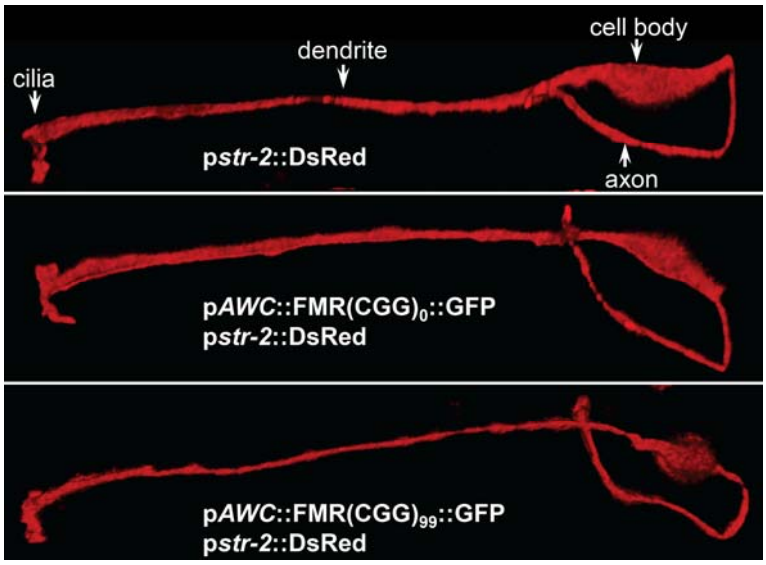

Figure 4.6. The expanded CGG repeats in the 5′UTR of the GFP reporter do not affect the morphology or the cell fate of the AWC neuron. The morphology of the AWC neuron was examined by observing expression of p*str-2*::DsRed. The shape of the neuron was identical in wildtype (top) and transgenic animals with 0CGG (middle) or 99CGG (bottom). Anatomy of the AWC neuron is indicated in the top panel.

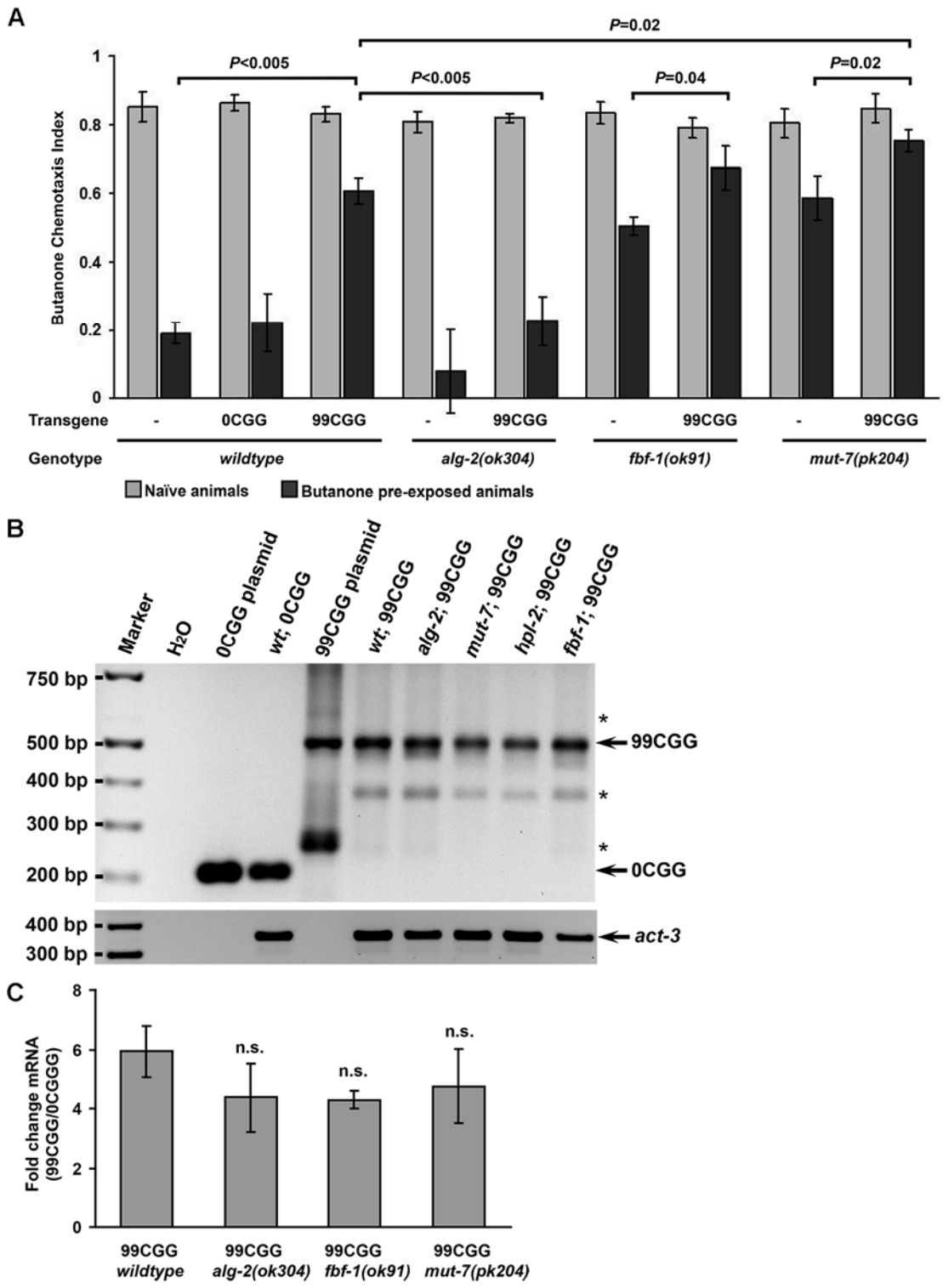

Figure 4.7. Interactions between the premutation CGG repeats and adaptation-promoting pathways. (**A**) Olfactory adaptation. 99CGG animals were crossed with mutants defining three pathways: ALG-2 is an miRNA-specific Argonaute, FBF-1 up-

regulates EGL-4 translation, and MUT-7 is required for siRNA processing. *alg-2* knockout decreased the effect of expanded CGG repeats, reducing adaptation defects in the double mutants. Conversely, the adaptation defects of 99CGG animals crossed with *fbf-1* and *mut-7* mutants were partially additive to defects in 99CGG animals alone. CI experiments were performed in at least triplicate, and error bars represent SEM. (**B**) Genotyping of animals with transgenes. 206- and 505- bp PCR fragments were amplified in animals carrying p*AWC*::FMR(CGG)$_0$::GFP and p*AWC*::FMR(CGG)$_{99}$::GFP plasmids. A few non-specific bands are indicated by "*". (**C**) Expanded- repeat mRNA levels had no significant change after crossing with *alg-2*, *fbf-1*, and *mut-7* knockout lines. Bars represent the fold change of FMR(CGG)$_{99}$ mRNA levels in p*AWC*::FMR(CGG)$_{99}$::GFP, or in either *alg-2*, *fbf-1* or *mut-7* double mutants, respectively, compared to the mRNA levels of a control p*AWC*::FMR(CGG)$_0$::GFP. The data were collected from four independent experiments.

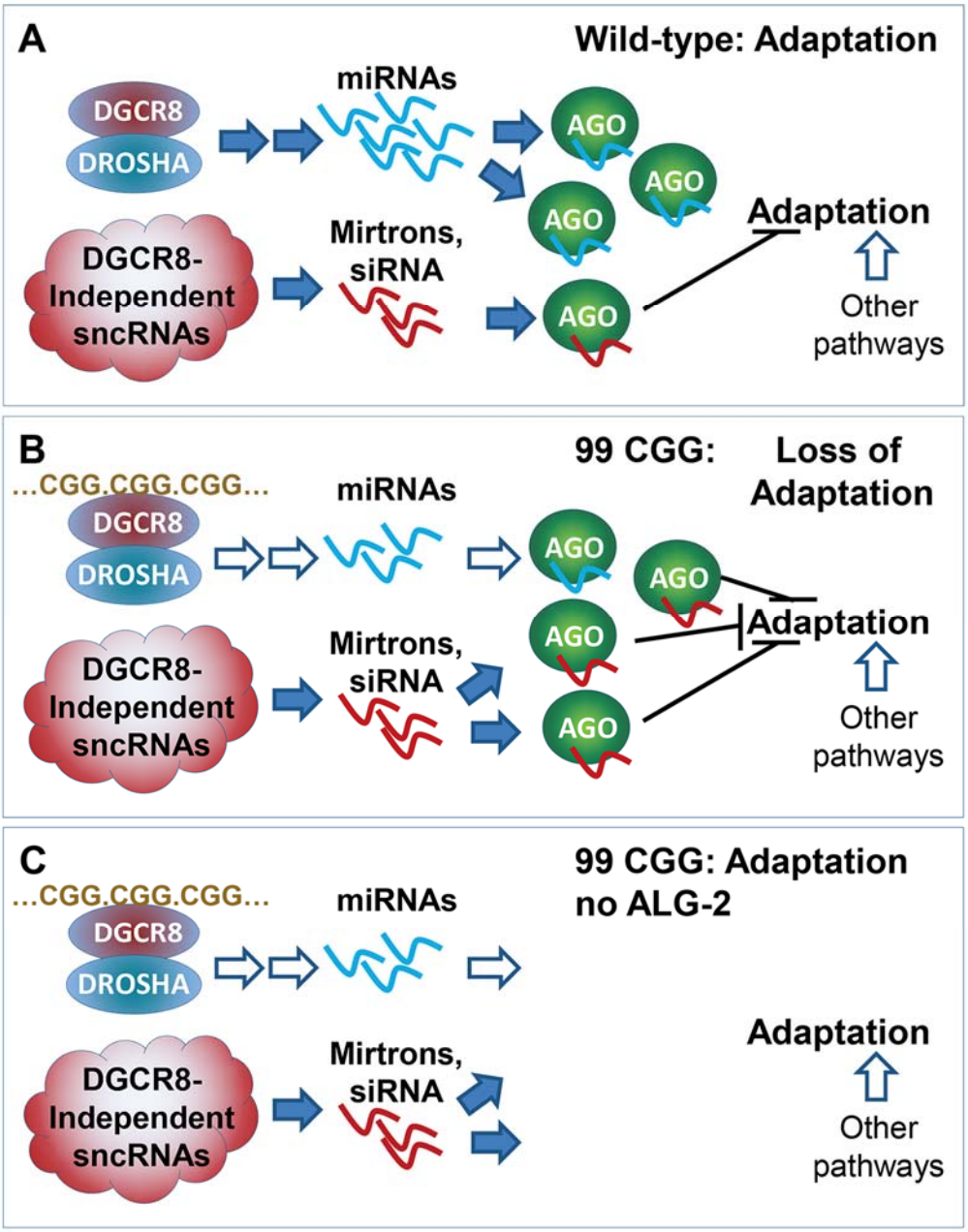

Figure 4.8. A speculative model for the rescue of adaptation by loss of the Argonaute, ALG-2. (**A**) In the wildtype animal, DROSHA/DGCR8 produces pre-miRNAs (labeled as blue squiggles), that do not interfere with adaptation. We postulate this because *drsh-1* and *alg-2* mutants are wildtype for adaptation ((Juang et al., 2013); Supplementary Materials, Fig. S1). One or more mirtrons/miRNAs produced from DROSHA/DGCR8-independent pathways (red squiggles) may negatively regulate adaptation, but normally play a minor role. (**B**) Once the 99CGG RNA sequesters DGCR8, blue miRNA expression is repressed and the balance between blue and red (adaptation neutral and adaptation repressive) microRNAs is tipped, with AGO-bound

repressive mirtron/miRNAs blocking adaptation. (**C**) In the absence of ALG-2, the inhibition of the adaptation response is relieved, since neither class of microRNA is active without an Argonaute.

Table 4.1. Asymmetric expression of *str-2* in AWC neurons[(1)]

Genotype	Percentage of animals with 0 AWCp*str-2* ON	1 AWCp*str-2* ON	2 AWCp*str-2* ON	n
wildtype	3	97	0	112
wildtype + FMR(CGG)$_0$	0	100	0	129
wildtype + FMR(CGG)$_{99}$	5	93	2	120

[(1)]Cell fate of the AWC neuron was examined by quantitating the asymmetric expression of p*str-2*::DsRed. Data were collected from three independent lines, and animals were scored by three categories according to p*str-2*::DsRed expression in neither AWC (0 AWC p*str-2* ON), in only one AWC (1 AWC p*str-2* ON), or in both AWC (2 AWC p*str-2* ON).

Table 4.2. *str-2* expression in AWC neurons (integrated)

Genotype	Percentage of animals with 0 AWCp*str-2* ON	1 AWCp*str-2* ON	2 AWC*pstr-2* ON	n
wildtype	1	99	0	90
wildtype + FMR(CGG)$_0$	0	100	0	90
wildtype + FMR(CGG)$_{99}$	0	100	0	90
alg-2(ok304) + FMR(CGG)$_{99}$	2	98	0	90
fbf-1(ok91) + FMR(CGG)$_{99}$	0	100	0	90
mut-7(pk204) + FMR(CGG)$_{99}$	0	100	0	90

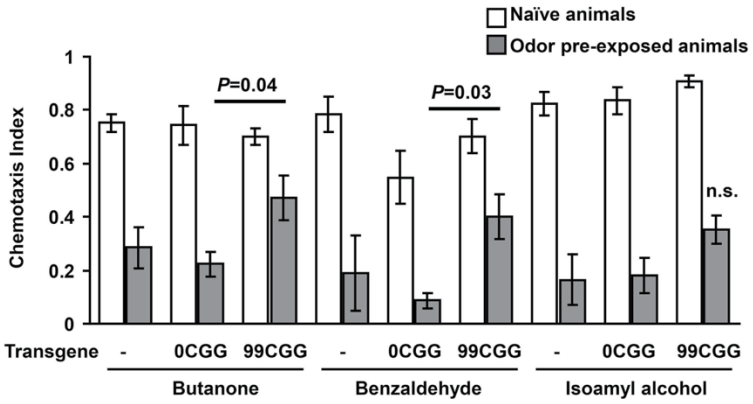

Figure 4.S1. Analysis of the adapted response to different odorants. Animals carrying 0CGG or 99CGG transgenic arrays were pre-exposed to different AWC-sensed odors including butanone, benzaldehyde, and isoamyl alcohol. Two-failed t-test was performed by comparing CIs of adapted animals carrying 0CGG and 99CGG from at least three independent assays in each odor exposure.

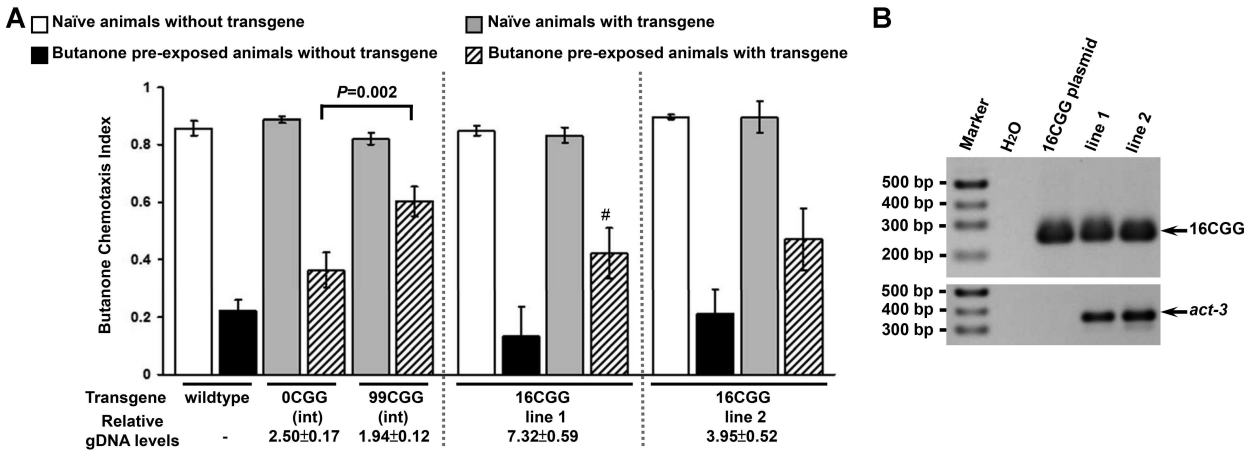

Figure 4.S2. The olfactory behavior of animals expressing 16 CGG repeats in the 5′UTR of the GFP reporter. (A) Transgenic animals carrying 16 CGG repeats in the 5′UTR behave similarly to the 0CGG integrated animals. "#" indicates that the CIs of adapted animals with transgene compared with nontransgene show significant difference ($P<0.05$). Each bar shows the mean from at least three independent experiments and error bar represents SEM. The average relative genomic DNA levels of transgenic animals from three independent experiments are quantified by real-time PCR and normalized to the housekeeping gene act-3. (B) PCR genotyping of transgenic animals. 256 bp of PCR fragments were amplified in animals carrying 16 CGG repeats in the 5′UTR. Each endogenous act-3 amplification is showed in the panel.

MATERIALS AND METHODS

Worm strains

The *C. elegans* Bristol N2 was used as a wildtype strain in this study; mutant alleles include *alg- 2*(*ok304*), *fbf-1*(*ok91*), *hpl-2*(*tm1489*), and *mut-7*(*pk204*). Strains were maintained at 20°C using standard protocols (Brenner, 1974). All transgenic lines were created by injecting 1 ng/µl of the constructs into wildtype N2 animals, along with co-injection markers, which included coelomocyte marker p*unc-122::GFP* (20 ng/µl) and AWC marker p*str-2::*DsRed (20 ng/µl). Transgenes were integrated into the nematode genome by trimethylpsoralen (TMP) (Yandell et al., 1994). Transgenic animals at L4 stage were exposed to TMP and UV, and ~100 F1 animals were clonally expanded. After hatching, ~500 F2s were randomly clonally expanded. The integrants were screened by 100% transmission of co-injection marker p*unc-122::*GFP. The integrated strains were outcrossed with wildtype animals at least three times to eliminate TMP-induced mutations in the genome. The integrated strain, carrying 99 CGG repeats in the 5′UTR of the GFP reporter, was crossed with mutant strains, including *alg-2*(*ok304*), *fbf-1*(*ok91*), *hpl-2(tm1489)*, and *mut-7*(*pk204*). The individual genotypes were confirmed by either sequencing for *mut-7*(*pk204*) with a point mutation near the 3′end, or by PCR for DNA deletions of *alg-2*(*ok304*), *fbf-1*(*ok91*), and *hpl-2(tm1489)*.

Plasmid construction

An AWC-specific promoter from a truncated form of the *ceh-36* promoter, termed p*ceh-36*^{prom3}, was inserted into pPD95.75 using PstI and BamHI upstream of GFP, referred to as p*AWC*::GFP (a kind gift from Oliver Hobert; (Etchberger et al., 2007)).

Before inserting the 5′UTR of the *FMR1* sequence, the plasmid was first changed to a low-copy plasmid with the origin of replication (Ori) in reverse orientation (opposite direction as the transcript) to ensure that CGG repeats do not delete during *E. coli* propagation (Chen et al., 2003). pBR322 (Balbas et al., 1986) was digested with PvuII and HindIII, and the larger fragment (2324 bp) containing the Ori and Amp-resistance gene was purified. p*AWC*::GFP was digested with HindIII and SspI, and the smaller fragment (1475 bp) containing the promoter and the GFP coding region was ligated to the Ori fragment (SspI and PvuII digest to blunt ends), making a p*AWC*::GFP-low-copy plasmid. Next, to facilitate insertion of *FMR1* 5′UTRs, a linker (5′ gatccccgggtcaggcgctcagcatccgttattggaagctagcagggctgaagagaacggtac), containing a BlpI site at the 5′ end and an NheI site at the 3′ end of the *FMR1* 5′UTR, was inserted between the *AWC* promoter and GFP with BamHI and KpnI digestion. The 5′UTR fragment of *FMR1* containing either 0 or 99 CGG repeats was obtained from *FMR1* 5′UTR(0 CGG)-FL and *FMR1* 5′UTR(99 CGG)-FL (Ludwig et al., 2011) by cutting with BlpI and NheI, and was inserted into the engineered p*AWC*::GFP, which was digested with the same restriction enzymes to create p*AWC*::FMR(CGG)$_0$::GFP and p*AWC*::FMR(CGG)$_{99}$::GFP plasmids. An *unc-54* 3′UTR element was required for stably expressing GFP in *C. elegans*; thus, this fragment was amplified from pPD95.75 using two primers (5′-TGGAAACATTCTTGGACACAA and 5′-tattctgtcatttaagtatacGGCAAAAACCCCATAGACAC containing an AccI recognition site, and a few extended bases (lower case) required for efficient enzyme cleavage). The PCR product was digested with MfeI and AccI, and was then inserted downstream of

GFP in the p*AWC*::FMR(CGG)$_0$::GFP and p*AWC*::FMR(CGG)$_{99}$::GFP constructs, which had been cut with the same restriction enzymes.

Isolation of genomic DNA from worms and CGG-repeat genotyping

Total genomic DNA from each transgenic strain was extracted in single worm lysis buffer (50 mM KCl, 10 mM Tris-Cl pH 8.0, 2.5 mM $MgCl_2$, 0.45% NP40, 0.45% Tween-20, and 60 µg/ml proteinase K). The mixture was frozen at -80°C for 10 min, followed by incubation at 60°C for 1 h, and proteinase K was inactivated at 95°C for 15 min. Using a modification of a PCR protocol (Saluto et al., 2005), animals were genotyped for the expanded CGG repeat by using the Expand Long Template PCR System (Roche Diagnostics Corporation, Indianapolis, IN). PCR of either 20 ng genomic or 2 ng plasmid DNA was performed in a 30-µl reaction with 2.25 M betaine (Affymetrix, Santa Clara, CA), 500 µM dNTP (GeneAmp, Life Technologies, Grand Island, NY), 0.33 µM of each primer (MWG-Biotech AG, Huntsville, Alabama), and 1 U DNA polymerase using 10X buffer 2 (both are included in PCR kit). The primer sequences are 5′-TCAGGCGCTCAGCTCCGTTTCGGT and 5′-TCTACCGGTACCGTTCTCTTCAGCCCTGCTAGC. The amplification cycling was as follows: initial denaturation at 98°C for 10 min, 10 cycles of 97°C for 35 s, 62°C for 35 s, and 68°C for 4 min; then 25 additional cycles in which the elongation step is increased by 20 s every cycle, and a final elongation at 68°C for 10 min. To prevent non-specific amplification, the reaction was allowed to denature for 8 min before the polymerase was pipetted into each reaction. Amplification of the endogenous actin gene was performed as follows: either 20 ng genomic or 2 ng plasmid DNA, and 0.42 mM dNTP (GeneAmp), 0.33 µM each primer, 1.25 U Amplitaq Gold (Life Technologies), 1.5 mM $MgCl_2$, and 3.0

µl 10X PCR Gold buffer were combined in a final volume of 30 µl. The primer sequences are *act-3* forward primer 5′- cggtatgggacagaaggac and a reverse primer 5′- ggaagcgtagagggagagga. Reactions were denatured at 95°C for 1 min, cycled 30 times at 95°C for 15 s, 60°C for 15 s, and 72°C for 1 min, followed by a final elongation at 72°C for 2 min. A portion of each reaction was then run next to the HiLo DNA Marker (Bionexus, Inc, Oakland, CA) on a 0.9% agarose gel, and was imaged according to standard procedures.

mRNA quantitation

Two 10 cm plates of adult animals were harvested by washing with S-Basal and split into two populations: ~50 animals were lysed in 40 µl of single worm lysis buffer for genomic DNA preparation, as described above; the remaining animals were frozen at -80°C for total RNA preparation. Total RNA was extracted by Trizol reagent (Life Technologies) and miRNeasy micro kit (Qiagen, Valencia, CA), and then treated with Turbo DNase I (Ambion, Life Technologies) at 37°C for 20 min for removing contaminated genomic DNA. One µg of total RNA was used in a cDNA synthesis reaction with iScript cDNA Synthesis Kit (Bio-Rad Laboratories, Hercules, CA). Two µl of cDNA was used in real-time PCR with Brilliant III Ultra-Fast SYBR Green qPCR Master Mix (Agilent Technologies, Santa Clara, CA) containing 200 nM of forward and reverse primers (5′-cagggctgaagagaacggta and 5′- cgagaagcattgaacaccataa) in a 20 µl reaction volume. This amplicon includes sequences downstream of the CGG-repeat element and extending to the first 267 bp of GFP genomic DNA. The qPCR reaction mixtures were prepared in triplicate for each sample and thermocycling conditions were

carried out on a Bio-Rad Chromo4 system, with denaturation at 95°C for 10 min, followed by 40 cycles of 20 s at 95°C, and 20 s at 60°C. All reactions showed a single dissociation curve, which indicated specific amplification.

The mRNA expression level of each CGG-GFP reporter was first normalized to the mRNA of the housekeeping gene, *act-3*; *act-3* mRNA was amplified by the primers: ggttgccgctcttgttgtag and accgaccatgactccttgat. The final CGG-mRNA expression per genomic DNA was calculated by taking the respective ratio of the mRNA to the value of genomic DNA normalized to the *act-3* DNA; qPCRs were performed by using 2 µl of genomic DNA extract under the same conditions.

Copy-number analysis

Genomic DNA (gDNA) from 20 animals at larval stage 4 (L4) was extracted in 40 µl of single worm lysis buffer, as described above. For 0CGG and 99CGG analysis, 2 µl of gDNA was used in real- time PCR with Brilliant III Ultra-Fast SYBR Green qPCR Master Mix (Agilent Technologies), and the samples were prepared as described above. Thermocycling was carried out on a Stratagene Mx3000P instrument with denaturation at 95°C for 10 minutes, followed by 40 cycles of 15 seconds at 95°C and 1 minute at 60°C. For 16CGG and 30CGG analysis, 2 µl of gDNA was mixed with SensiFAST SYBR Lo- ROX mix (Bioline), and thermocycling conditions were performed on a Viia7 qPCR machine (Life Technologies) with denaturation at 95°C for 3 minutes, followed by 40 cycles of 5 seconds at 95°C, and 30 seconds at 60°C. The relative gDNA levels were calculated by normalizing to the *act-3* gDNA.

Behavioral assays

Behavioral assays were performed as described in Colbert and Bargmann (1995). Briefly, L4 animals were grown on NGM agar plates (2.5 g peptone, 17 g agar, 3 g NaCl per 1 liter) seeded with bacterial strain HB101 as animals' food at 20°C for 5-6 days; adults were collected by washing with S- basal buffer (5 g NaCl and 50 ml of 1 M potassium phosphate (pH 6.0) per liter) and equally transferred into two unautoclaved 1.5 ml microcentrifuge tubes. After three washes and sedimenting the worms by gravity, half of the animals were pre-exposed to 1.5 ml diluted butanone (11 µl butanone in 100 ml S- basal), and the other half were incubated with S-basal buffer as a control population. Pre-exposure was carried out for 80 min at 20°C on a Labquake rotor (Thermo Fisher Scientific Inc., Waltham, MA). Animals were washed twice with S-basal and once with water, then the animals were placed on 10 cm chemotaxis assay plates (10 ml of 1.6% agar in 5 mM potassium phosphate (pH 6.0), 1 mM $CaCl_2$ and 1 mM $MgSO_4$). During the washes, 1 µl of 1 M sodium azide was applied to two odorant spots on the assay plates. After transferring ~100 worms to the assay plates, 1 µl diluted butanone (1:1000 dilution in ethanol) was applied to an odorant spot on an assay plate, while 1 µl 100% ethanol was applied opposite to the odorant spot. Animals on the assay plates were allowed to move for 2 h at 20°C and then their positions were scored. Transgenic animals were scored under the fluorescence-dissecting scope using co-injection marker p*unc-122*::GFP. Each experiment was conducted through at least three separate assays, with >100 animals per assay.

Olfactory behavior was quantified by calculating the chemotaxis index (CI), which is calculated by subtracting the number of animals at the ethanol spot from the number at the odor, and dividing this sum by the number of animals that left the origin.

REFERENCES

Arocena, D.G., Iwahashi, C.K., Won, N., Beilina, A., Ludwig, A.L., Tassone, F., Schwartz, P.H. and Hagerman, P.J. (2005) Induction of inclusion formation and disruption of lamin A/C structure by premutation CGG-repeat RNA in human cultured neural cells. *Hum. Mol. Genet.*, **14**, 3661-3671.

Babiarz, J.E., Ruby, J.G., Wang, Y., Bartel, D.P. and Blelloch, R. (2008) Mouse ES cells express endogenous shRNAs, siRNAs, and other Microprocessor-independent, Dicer-dependent small RNAs. *Genes Dev.*, **22**, 2773-2785.

Balbas, P., Soberon, X., Merino, E., Zurita, M., Lomeli, H., Valle, F., Flores, N. and Bolivar, F. (1986) Plasmid vector pBR322 and its special-purpose derivatives--a review. *Gene*, **50**, 3-40.

Bargmann, C.I. and Mori, I. (1997) Chemotaxis and Thermotaxis. Riddle, D.L., Blumenthal, T., Meyer, B.J. and Priess, J.R. (eds.), In *C. elegans II*. Cold Spring Harbor Laboratory Press, Cold Spring Harbor (NY).

Bargmann, C.I., Hartwieg, E. and Horvitz, H.R. (1993) Odorant-selective genes and neurons mediate olfaction in *C. elegans*. *Cell*, **74**, 515-527.

Brenner, S. (1974) The genetics of *Caenorhabditis elegans*. *Genetics*, **77**, 71-94.

Brouwer, J.R., Huizer, K., Severijnen, L.A., Hukema, R.K., Berman, R.F., Oostra, B.A. and Willemsen, R. (2008) CGG-repeat length and neuropathological and molecular correlates in a mouse model for fragile X-associated tremor/ataxia syndrome. *J. Neurochem.*, **107**, 1671-1682.

Brouwer, J.R., Mientjes, E.J., Bakker, C.E., Nieuwenhuizen, I.M., Severijnen, L.A., Van der Linde, H.C., Nelson, D.L., Oostra, B.A. and Willemsen, R. (2007) Elevated

Fmr1 mRNA levels and reduced protein expression in a mouse model with an unmethylated Fragile X full mutation. *Exp. Cell Res.*, **313**, 244-253.

Cao, Z., Hulsizer, S., Tassone, F., Tang, H.T., Hagerman, R.J., Rogawski, M.A., Hagerman, P.J. and Pessah, I.N. (2012) Clustered burst firing in *FMR1* premutation hippocampal neurons: amelioration with allopregnanolone. *Hum. Mol. Genet.*, **21**, 2923-2935.

Capelli, L.P., Goncalves, M.R., Leite, C.C., Barbosa, E.R., Nitrini, R. and Vianna-Morgante, A.M. (2010) The fragile X-associated tremor and ataxia syndrome (FXTAS). *Arq. Neuropsiquiatr.*, **68**, 791-798.

Castel, S.E. and Martienssen, R.A. (2013) RNA interference in the nucleus: roles for small RNAs in transcription, epigenetics and beyond. *Nat. Rev. Genet.*, **14**, 100-112.

Chalasani, S.H., Kato, S., Albrecht, D.R., Nakagawa, T., Abbott, L.F. and Bargmann, C.I. (2010) Neuropeptide feedback modifies odor-evoked dynamics in *Caenorhabditis elegans* olfactory neurons. *Nat. Neurosci.*, **13**, 615-621.

Chen, L.S., Tassone, F., Sahota, P. and Hagerman, P.J. (2003) The (CGG)n repeat element within the 5' untranslated region of the *FMR1* message provides both positive and negative *cis* effects on *in vivo* translation of a downstream reporter. *Hum. Mol. Genet.*, **12**, 3067-3074.

Chen, Y., Tassone, F., Berman, R.F., Hagerman, P.J., Hagerman, R.J., Willemsen, R. and Pessah, I.N. (2010) Murine hippocampal neurons expressing *Fmr1* gene premutations show early developmental deficits and late degeneration. *Hum. Mol. Genet.*, **19**, 196-208.

Colbert, H.A. and Bargmann, C.I. (1995) Odorant-specific adaptation pathways generate olfactory plasticity in C. elegans. *Neuron*, **14**, 803-812.

D'Hulst, C., Heulens, I., Brouwer, J.R., Willemsen, R., De Geest, N., Reeve, S.P., De Deyn, P.P., Hassan, B.A. and Kooy, R.F. (2009) Expression of the GABAergic system in animal models for fragile X syndrome and fragile X associated tremor/ataxia syndrome (FXTAS). *Brain Res.*, **1253**, 176-183.

Denli, A.M., Tops, B.B., Plasterk, R.H., Ketting, R.F. and Hannon, G.J. (2004) Processing of primary microRNAs by the Microprocessor complex. *Nature*, **432**, 231-235.

Dernburg, A.F., Zalevsky, J., Colaiacovo, M.P. and Villeneuve, A.M. (2000) Transgene-mediated cosuppression in the *C. elegans* germ line. *Genes Dev.*, **14**, 1578-1583.

Ding, L., Spencer, A., Morita, K. and Han, M. (2005) The developmental timing regulator AIN-1 interacts with miRISCs and may target the argonaute protein ALG-1 to cytoplasmic P bodies in *C. elegans*. *Mol. Cell*, **19**, 437-447.

Duchaine, T.F., Wohlschlegel, J.A., Kennedy, S., Bei, Y., Conte, D., Jr., Pang, K., Brownell, D.R., Harding, S., Mitani, S., Ruvkun, G. *et al.* (2006) Functional proteomics reveals the biochemical niche of *C. elegans* DCR-1 in multiple small-RNA-mediated pathways. *Cell*, **124**, 343-354.

Entezam, A., Biacsi, R., Orrison, B., Saha, T., Hoffman, G.E., Grabczyk, E., Nussbaum, R.L. and Usdin, K. (2007) Regional FMRP deficits and large repeat expansions into the full mutation range in a new Fragile X premutation mouse model. *Gene*, **395**, 125-134.

Etchberger, J.F., Lorch, A., Sleumer, M.C., Zapf, R., Jones, S.J., Marra, M.A., Holt, R.A., Moerman, D.G. and Hobert, O. (2007) The molecular signature and cis-regulatory architecture of a *C. elegans* gustatory neuron. *Genes Dev.*, **21**, 1653-1674.

Fu, Y.H., Kuhl, D.P., Pizzuti, A., Pieretti, M., Sutcliffe, J.S., Richards, S., Verkerk, A.J., Holden, J.J., Fenwick, R.G., Jr., Warren, S.T. *et al.* (1991) Variation of the CGG repeat at the fragile X site results in genetic instability: resolution of the Sherman paradox. *Cell*, **67**, 1047-1058.

Grishok, A., Pasquinelli, A.E., Conte, D., Li, N., Parrish, S., Ha, I., Baillie, D.L., Fire, A., Ruvkun, G. and Mello, C.C. (2001) Genes and mechanisms related to RNA interference regulate expression of the small temporal RNAs that control *C. elegans* developmental timing. *Cell*, **106**, 23-34.

Guang, S., Bochner, A.F., Pavelec, D.M., Burkhart, K.B., Harding, S., Lachowiec, J. and Kennedy, S. (2008) An Argonaute transports siRNAs from the cytoplasm to the nucleus. *Science*, **321**, 537-541.

Hagerman, P. (2013) Fragile X-associated tremor/ataxia syndrome (FXTAS): pathology and mechanisms. *Acta Neuropathol.*, **126**, 1-19.

Hagerman, R. and Hagerman, P. (2013) Advances in clinical and molecular understanding of the *FMR1* premutation and fragile X-associated tremor/ataxia syndrome. *Lancet Neurol.*, **12**, 786-798.

Hammell, C.M., Lubin, I., Boag, P.R., Blackwell, T.K. and Ambros, V. (2009) nhl-2 Modulates microRNA activity in *Caenorhabditis elegans*. *Cell*, **136**, 926-938.

Hashem, V., Galloway, J.N., Mori, M., Willemsen, R., Oostra, B.A., Paylor, R. and Nelson, D.L. (2009) Ectopic expression of CGG containing mRNA is neurotoxic in mammals. *Hum. Mol. Genet.*, **18**, 2443-2451.

Hoem, G., Raske, C.R., Garcia-Arocena, D., Tassone, F., Sanchez, E., Ludwig, A.L., Iwahashi, C.K., Kumar, M., Yang, J.E. and Hagerman, P.J. (2011) CGG-repeat length threshold for *FMR1* RNA pathogenesis in a cellular model for FXTAS. *Hum. Mol. Genet.*, **20**, 2161-2170.

Hoffman, G.E., Le, W.W., Entezam, A., Otsuka, N., Tong, Z.B., Nelson, L., Flaws, J.A., McDonald, J.H., Jafar, S. and Usdin, K. (2012) Ovarian abnormalities in a mouse model of fragile X primary ovarian insufficiency. *J. Histochem. Cytochem.*, **60**, 439-456.

Huang, V. and Li, L.C. (2012) miRNA goes nuclear. *RNA Biol.*, **9**, 269-273.

Hunt-Newbury, R., Viveiros, R., Johnsen, R., Mah, A., Anastas, D., Fang, L., Halfnight, E., Lee, D., Lin, J., Lorch, A. *et al.* (2007) High-throughput *in vivo* analysis of gene expression in *Caenorhabditis elegans*. *PLoS Biol.*, **5**, e237.

Iwahashi, C.K., Yasui, D.H., An, H.J., Greco, C.M., Tassone, F., Nannen, K., Babineau, B., Lebrilla, C.B., Hagerman, R.J. and Hagerman, P.J. (2006) Protein composition of the intranuclear inclusions of FXTAS. *Brain*, **129**, 256-271.

Jacquemont, S., Hagerman, R.J., Leehey, M., Grigsby, J., Zhang, L., Brunberg, J.A., Greco, C., Des Portes, V., Jardini, T., Levine, R. *et al.* (2003) Fragile X premutation tremor/ataxia syndrome: molecular, clinical, and neuroimaging correlates. *Am. J. Hum. Genet.*, **72**, 869-878.

Juang, B.T., Gu, C., Starnes, L., Palladino, F., Goga, A., Kennedy, S. and L'Etoile N, D. (2013) Endogenous nuclear RNAi mediates behavioral adaptation to odor. *Cell*, **154**, 1010-1022.

Kaye, J.A., Rose, N.C., Goldsworthy, B., Goga, A. and L'Etoile, N.D. (2009) A 3'UTR pumilio- binding element directs translational activation in olfactory sensory neurons. *Neuron*, **61**, 57-70.

Kenneson, A., Zhang, F., Hagedorn, C.H. and Warren, S.T. (2001) Reduced FMRP and increased *FMR1* transcription is proportionally associated with CGG repeat number in intermediate-length and premutation carriers. *Hum. Mol. Genet.*, **10**, 1449-1454.

Ketting, R.F., Haverkamp, T.H., van Luenen, H.G. and Plasterk, R.H. (1999) Mut-7 of *C. elegans*, required for transposon silencing and RNA interference, is a homolog of Werner syndrome helicase and RNaseD. *Cell*, **99**, 133-141.

L'Etoile, N.D. and Bargmann, C.I. (2000) Olfaction and odor discrimination are mediated by the *C. elegans* guanylyl cyclase ODR-1. *Neuron*, **25**, 575-586.

L'Etoile, N.D., Coburn, C.M., Eastham, J., Kistler, A., Gallegos, G. and Bargmann, C.I. (2002) The cyclic GMP-dependent protein kinase EGL-4 regulates olfactory adaptation in *C. elegans*. *Neuron*, **36**, 1079-1089.

Lai, C.H., Chou, C.Y., Ch'ang, L.Y., Liu, C.S. and Lin, W. (2000) Identification of novel human genes evolutionarily conserved in *Caenorhabditis elegans* by comparative proteomics. *Genome Res.*, **10**, 703-713.

Lee, J.I., O'Halloran, D.M., Eastham-Anderson, J., Juang, B.T., Kaye, J.A., Scott Hamilton, O., Lesch, B., Goga, A. and L'Etoile, N.D. (2010) Nuclear entry of a

cGMP-dependent kinase converts transient into long-lasting olfactory adaptation. *Proc. Natl. Acad. Sci. U. S. A.*, **107**, 6016-6021.

Leehey, M.A. (2009) Fragile X-associated tremor/ataxia syndrome: clinical phenotype, diagnosis, and treatment. *J. Investig. Med.*, **57**, 830-836.

Leehey, M.A. and Hagerman, P.J. (2012) Fragile X-associated tremor/ataxia syndrome. *Handb. Clin. Neurol.*, **103**, 373-386.

Li, Y. and Jin, P. (2012) RNA-mediated neurodegeneration in fragile X-associated tremor/ataxia syndrome. *Brain Res.*, **1462**, 112-117.

Ludwig, A.L., Espinal, G.M., Pretto, D.I., Jamal, A.L., Arque, G., Tassone, F., Berman, R.F. and Hagerman, P.J. (2014) CNS expression of murine fragile X protein (FMRP) as a function of CGG-repeat size. *Hum. Mol. Genet.*, **Feb 11. [Epub ahead of print]**.

Ludwig, A.L., Hershey, J.W. and Hagerman, P.J. (2011) Initiation of translation of the *FMR1* mRNA Occurs predominantly through 5'-end-dependent ribosomal scanning. *J. Mol. Biol.*, **407**, 21-34.

McLennan, Y., Polussa, J., Tassone, F. and Hagerman, R. (2011) Fragile X syndrome. *Curr. Genomics*, **12**, 216-224.

McNeill, E. and Van Vactor, D. (2012) MicroRNAs shape the neuronal landscape. *Neuron*, **75**, 363-379.

O'Halloran, D.M., Altshuler-Keylin, S., Lee, J.I. and L'Etoile, N.D. (2009) Regulators of AWC- mediated olfactory plasticity in *Caenorhabditis elegans*. *PLoS Genet.*, **5**, e1000761.

Olde Loohuis, N.F., Kos, A., Martens, G.J., Van Bokhoven, H., Nadif Kasri, N. and Aschrafi, A. (2012) MicroRNA networks direct neuronal development and plasticity. *Cell. Mol. Life Sci.*, **69**, 89-102.

Qin, M., Entezam, A., Usdin, K., Huang, T., Liu, Z.H., Hoffman, G.E. and Smith, C.B. (2011) A mouse model of the fragile X premutation: effects on behavior, dendrite morphology, and regional rates of cerebral protein synthesis. *Neurobiol. Dis.*, **42**, 85-98.

Qin, M., Xia, Z., Huang, T. and Smith, C.B. (2011) Effects of chronic immobilization stress on anxiety-like behavior and basolateral amygdala morphology in *Fmr1* knockout mice. *Neuroscience*, **194**, 282-290.

Saluto, A., Brussino, A., Tassone, F., Arduino, C., Cagnoli, C., Pappi, P., Hagerman, P., Migone, N. and Brusco, A. (2005) An enhanced polymerase chain reaction assay to detect pre- and full mutation alleles of the fragile X mental retardation 1 gene. *J. Mol. Diagn.*, **7**, 605-612.

Scheckel, C., Gaidatzis, D., Wright, J.E. and Ciosk, R. (2012) Genome-wide analysis of GLD-1- mediated mRNA regulation suggests a role in mRNA storage. *PLoS Genet.*, **8**, e1002742.

Schneider, A., Ballinger, E., Chavez, A., Tassone, F., Hagerman, R.J. and Hessl, D. (2012) Prepulse inhibition in patients with fragile X-associated tremor ataxia syndrome. *Neurobiol. Aging*, **33**, 1045-1053.

Sellier, C., Freyermuth, F., Tabet, R., Tran, T., He, F., Ruffenach, F., Alunni, V., Moine, H., Thibault, C., Page, A. *et al.* (2013) Sequestration of DROSHA and DGCR8 by

expanded CGG RNA repeats alters microRNA processing in fragile X-associated tremor/ataxia syndrome. *Cell Rep*, **3**, 869-880.

Sellier, C., Rau, F., Liu, Y., Tassone, F., Hukema, R.K., Gattoni, R., Schneider, A., Richard, S., Willemsen, R., Elliott, D.J. *et al.* (2010) Sam68 sequestration and partial loss of function are associated with splicing alterations in FXTAS patients. *EMBO J.*, **29**, 1248-1261.

Sofola, O.A., Jin, P., Qin, Y., Duan, R., Liu, H., de Haro, M., Nelson, D.L. and Botas, J. (2007) RNA-binding proteins hnRNP A2/B1 and CUGBP1 suppress fragile X CGG premutation repeat-induced neurodegeneration in a *Drosophila* model of FXTAS. *Neuron*, **55**, 565-571.

Sullivan, S.D., Welt, C. and Sherman, S. (2011) *FMR1* and the continuum of primary ovarian insufficiency. *Semin. Reprod. Med.*, **29**, 299-307.

Tan, H., Poidevin, M., Li, H., Chen, D. and Jin, P. (2012) MicroRNA-277 modulates the neurodegeneration caused by Fragile X premutation rCGG repeats. *PLoS Genet.*, **8**, e1002681.

Tassone, F., Hagerman, R.J., Taylor, A.K., Gane, L.W., Godfrey, T.E. and Hagerman, P.J. (2000) Elevated levels of *FMR1* mRNA in carrier males: a new mechanism of involvement in the fragile-X syndrome. *Am. J. Hum. Genet.*, **66**, 6-15.

Tassone, F., Iwahashi, C. and Hagerman, P.J. (2004) *FMR1* RNA within the intranuclear inclusions of fragile X-associated tremor/ataxia syndrome (FXTAS). *RNA Biol.*, **1**, 103-105.

The C. elegans Sequencing Consortium (1998) Genome sequence of the nematode *C. elegans*: a platform for investigating biology. *Science*, **282**, 2012-2018.

Todd, P.K., Oh, S.Y., Krans, A., He, F., Sellier, C., Frazer, M., Renoux, A.J., Chen, K.C., Scaglione, K.M., Basrur, V. *et al.* (2013) CGG repeat-associated translation mediates neurodegeneration in fragile X tremor ataxia syndrome. *Neuron*, **78**, 440-455.

Tops, B.B., Plasterk, R.H. and Ketting, R.F. (2006) The *Caenorhabditis elegans* Argonautes ALG-1 and ALG-2: almost identical yet different. *Cold Spring Harb. Symp. Quant. Biol.*, **71**, 189-194.

Torayama, I., Ishihara, T. and Katsura, I. (2007) *Caenorhabditis elegans* integrates the signals of butanone and food to enhance chemotaxis to butanone. *J. Neurosci.*, **27**, 741-750.

Troemel, E.R., Sagasti, A. and Bargmann, C.I. (1999) Lateral signaling mediated by axon contact and calcium entry regulates asymmetric odorant receptor expression in *C. elegans*. *Cell*, **99**, 387-398.

Vasquez-Rifo, A., Jannot, G., Armisen, J., Labouesse, M., Bukhari, S.I., Rondeau, E.L., Miska, E.A. and Simard, M.J. (2012) Developmental characterization of the microRNA-specific *C. elegans* Argonautes alg-1 and alg-2. *PLoS One*, **7**, e33750.

Verkerk, A.J., Pieretti, M., Sutcliffe, J.S., Fu, Y.H., Kuhl, D.P., Pizzuti, A., Reiner, O., Richards, S., Victoria, M.F., Zhang, F.P. *et al.* (1991) Identification of a gene (*FMR-1*) containing a CGG repeat coincident with a breakpoint cluster region exhibiting length variation in fragile X syndrome. *Cell*, **65**, 905-914.

Wes, P.D. and Bargmann, C.I. (2001) *C. elegans* odour discrimination requires asymmetric diversity in olfactory neurons. *Nature*, **410**, 698-701.

Willemsen, R., Levenga, J. and Oostra, B.A. (2011) CGG repeat in the *FMR1* gene: size matters. *Clin. Genet.*, **80**, 214-225.

Wittenberger, M.D., Hagerman, R.J., Sherman, S.L., McConkie-Rosell, A., Welt, C.K., Rebar, R.W., Corrigan, E.C., Simpson, J.L. and Nelson, L.M. (2007) The *FMR1* premutation and reproduction. *Fertil. Steril.*, **87**, 456-465.

Yandell, M.D., Edgar, L.G. and Wood, W.B. (1994) Trimethylpsoralen induces small deletion mutations in *Caenorhabditis elegans*. *Proc. Natl. Acad. Sci. U. S. A.*, **91**, 1381-1385.

Zhang, L., Ding, L., Cheung, T.H., Dong, M.Q., Chen, J., Sewell, A.K., Liu, X., Yates, J.R., 3rd and Han, M. (2007) Systematic identification of *C. elegans* miRISC proteins, miRNAs, and mRNA targets by their interactions with GW182 proteins AIN-1 and AIN-2. *Mol. Cell*, **28**, 598-613.

Zongaro, S., Hukema, R., D'Antoni, S., Davidovic, L., Barbry, P., Catania, M.V., Willemsen, R., Mari, B. and Bardoni, B. (2013) The 3' UTR of *FMR1* mRNA is a target of miR-101, miR-129-5p and miR-221: implications for the molecular pathology of FXTAS at the synapse. *Hum. Mol. Genet.*, **22**, 1971-1982.

Publishing Agreement

It is the policy of the University to encourage the distribution of all theses, dissertations, and manuscripts. Copies of all UCSF theses, dissertations, and manuscripts will be routed to the library via the Graduate Division. The library will make all theses, dissertations, and manuscripts accessible to the public and will preserve these to the best of their abilities, in perpetuity.

Please sign the following statement:

I hereby grant permission to the Graduate Division of the University of California, San Francisco to release copies of my thesis, dissertation, or manuscript to the Campus Library to provide access and preservation, in whole or in part, in perpetuity.

Kelli Benedetti

Author Signature

08-08-19

Date